ISSN 1408-7073

RMZ – MATERIALS AND GEOENVIRONMENT

PERIODICAL FOR MINING, METALLURGY AND GEOLOGY

RMZ – MATERIALI IN GEOOKOLJE

REVIJA ZA RUDARSTVO, METALURGIJO IN GEOLOGIJO

RMZ-M&G, Vol. 56, No. 1 pp. 001–107 (2009)

Ljubljana, March 2009

Historical Review

More than 80 years have passed since in 1919 the University Ljubljana in Slovenia was founded. Technical fields were joint in the School of Engineering that included the Geologic and Mining Division while the Metallurgy Division was established in 1939 only. Today the Departments of Geology, Mining and Geotechnology, Materials and Metallurgy are part of the Faculty of Natural Sciences and Engineering, University of Ljubljana.

Before War II the members of the Mining Section together with the Association of Yugoslav Mining and Metallurgy Engineers began to publish the summaries of their research and studies in their technical periodical Rudarski zbornik (Mining Proceedings). Three volumes of Rudarski zbornik (1937, 1938 and 1939) were published. The War interrupted the publication and not until 1952 the first number of the new journal Rudarsko-metalurški zbornik - RMZ (Mining and Metallurgy Quarterly) has been published by the Division of Mining and Metallurgy, University of Ljubljana. Later the journal has been regularly published quarterly by the Departments of Geology, Mining and Geotechnology, Materials and Metallurgy, and the Institute for Mining, Geotechnology and Environment.

On the meeting of the Advisory and the Editorial Board on May 22nd 1998 Rudarsko-metalurški zbornik has been renamed into "RMZ - Materials and Geoenvironment (RMZ -Materiali in Geookolje)" or shortly RMZ - M&G.

RMZ - M&G is managed by an international advisory and editorial board and is exchanged with other world-known periodicals. All the papers are reviewed by the corresponding professionals and experts.

RMZ - M&G is the only scientific and professional periodical in Slovenia, which is published in the same form nearly 50 years. It incorporates the scientific and professional topics in geology, mining, and geotechnology, in materials and in metallurgy.

The wide range of topics inside the geosciences are welcome to be published in the RMZ -Materials and Geoenvironment. Research results in geology, hydrogeology, mining, geotechnology, materials, metallurgy, natural and antropogenic pollution of environment, biogeochemistry are proposed fields of work which the journal will handle. RMZ - M&G is co-issued and co-financed by the Faculty of Natural Sciences and Engineering Ljubljana, and the Institute for Mining, Geotechnology and Environment Ljubljana. In addition it is financially supported also by the Ministry of Higher Education, Science and Technology of Republic of Slovenia.

Editor in chief

Table of Contents – Kazalo

Original Scientific Papers – Izvirni znanstveni članki

Review Papers – Pregledni članki

The synthesis of a magneto-caloric $Gd_5(GeSi)_4$ alloy using arc melting procedure

B. Markoli[1], P. J. Mcguiness[2], B. Podmiljšak[2], I. Škulj[3], S. Kobe[2]

[1]University of Ljubljana, Faculty of Natural Sciences and Engineering, Department for Materials and Metallurgy, Aškerčeva cesta 12, SI-1000 Ljubljana, Slovenia; E-mail: bostjan.markoli@ntf.uni-lj.si
[2]Jožef Stefan Institute, SI-1000 Ljubljana, Slovenia; E-mail: paul.mcguiness@ijs.si, beno.podmiljsak@ijs.si
[3]Magneti Ljubljana, d. d., SI-1000 Ljubljana, Slovenia

Received: January 13, 2009 **Accepted:** February 10, 2009

Abstract: In this paper we report on the synthesis of a gadolinium-based magneto-caloric alloy using the technique of arc melting. This alloy belongs to the group of metallic materials that exhibit a considerable magneto-caloric effect, and which have the potential to be used for a range of refrigeration applications.

A series of five alloys weighing from 1 g to 5 g with the nominal composition $Gd_5Ge_2Si_2$ were prepared and examined using optical (LOM) and electron microscopy (SEM with EDS) and XRD in the as-cast and heat-treated conditions. The alloys in the as-cast state contain more than one phase, and only after the heat treatment at elevated temperature were we able to obtain a predominantly single-phase alloy with the required stoichiometry of $Gd_5Ge_2Si_2$.

Izvleček: V delu je predstavljena sinteza magnetokalorične zlitine na osnovi gadolinija z uporabo taljenja pod oblokom. Ta zlitina spada med tiste kovinske materiale, ki izkazujejo izrazit magnetokaloričen učinek in bi bila lahko primerna za različne načine hlajenja. Izdelanih je bilo skupaj pet zlitin z nominalno sestavo $Gd_5Ge_2Si_2$ in maso od 1 g do 5 g, ki so bile pregledane v izhodnem in toplotno obdelanem stanju z uporabo svetlobne in elektronske mikroskopije ter rentgenske fazne analize. Zlitine v izhodnem stanju vsebujejo več kot le eno fazo, kar smo dosegli šele s toplotno obdelavo pri povišanih temperaturah, kjer smo dobili pretežno enofazne zlitine z želeno stehiometrijo $Gd_5Ge_2Si_2$.

Keywords: magneto-caloric effect, gadolinium alloys, arc melting
Ključne besede: magnetokalorični učinek, zlitine na osnovi gadolinija, taljenje pod oblokom

Original scientific paper

INTRODUCTION

Contemporary cooling systems for domestic applications are usually based on compression techniques. Such systems, although cheap, are not particularly efficient, and as such alternative refrigeration techniques are always of interest to manufacturers of cooling devices. Additionally, conventional cooling techniques involve gases and coolants that are ecologically problematic. In the late 1990s Gschneidner and Pecharsky discovered alloys that exhibit the so-called giant magneto-caloric effect [1] (GMCE). Such alloys tend to warm up when subjected to a magnetic field and cool down when the magnetic field is being removed. The same principle is used in conventional compressor refrigeration and thus this can be used for a practical cooling system. Today there are several alloys known to exhibit this giant magnetocaloric effect, e.g., Fe-Zr-Y [2], Co-Al-Ni [3], Mn-Fe-P-Ge [4], and La-Si-Fe [5], but most of the research work has been focused on the $Gd_5(GeSi)_4$ [6,7] alloys, as the group of alloys with the great magneto-caloric potential (GMCE). These alloys, like many others, suffer from difficulties associated with their synthesis. This can result in a smaller magneto-caloric effect, which is related to the excessive heterogeneity and the presence of unwanted phases with low magneto-caloric effect. A heat treatment of the synthesised alloys based on gadolinium is usually required to achieve the desired or the best possible magneto-caloric effect. But first let us take a look at the basics of the cooling that results from the magneto-caloric effect.

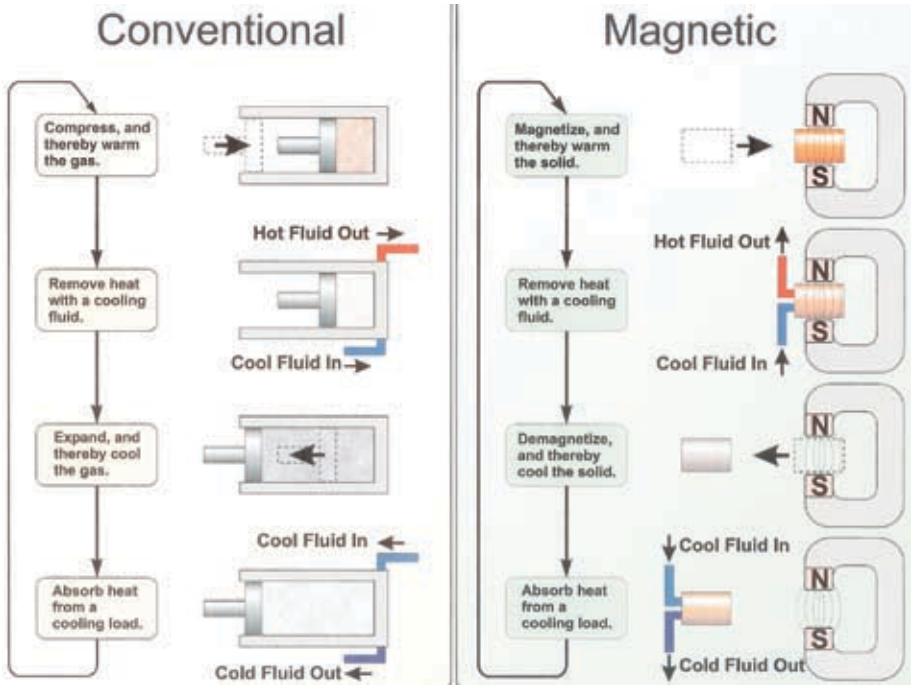

Figure 1. Schematic presentation of the principles of conventional and magnetic cooling

Principles of a "magnetic" refrigerator

The following scheme (Figure 1) shows a comparison between the basics of conventional cooling using standard gas compression and expansion, and the magnetic cooling, which is based on the magneto-caloric effect. As the cooling gas is compressed in a piston it heats up.

The coolant (e.g. water) then removes the excess heat generated due to the compression and cools down the cooling gas, which is then further cooled by the rapid expansion. The cycle can be repeated over and over again. In the case of the magneto-caloric effect the metallic magneto-caloric material is magnetized using magnets, which leads to the heating of the material in the magnetic field. The excess heat, that is, the heat generated because of the magnetization can be removed by the liquid coolant (e.g. water) as in the case of conventional cooling. The magneto-caloric material is then demagnetized right after the cooling with the liquid coolant and thus cooled down. So this cycle can be utilised for the everyday cooling of stored food in pretty much the same way as with conventional refrigerators. The major drawback to the mass production of magneto-caloric refrigerators is the cost and the shear size of the device that contains the magnets and the magneto-caloric material and the cooling system containing the liquid coolant. Namely, conventional refrigerators have the whole cooling system in the size of a typical shoebox, whilst the magnetic refrigerator would have a cooling unit the size of a conventional refrigerator itself.

Synthesis of magneto-caloric alloys

Among the different magneto-caloric alloys each alloy requires a specific synthesis route. In our research we focused ourselves on the synthesis of the most promising magneto-caloric alloy, containing gadolinium (Gd), germanium (Ge) and silicon (Si), so as to achieve a stochiometry of $Gd_5(Ge_2Si_2)$. In order to get the so-called giant magneto-caloric effect (GMCE) the alloy must have a stoichiometry of $Gd_5(Si_xGe_{1-x})_4$ where $0.24 \leq x \leq 0.5$, and the monoclinically distorted derivative of the orthorhombic Sm_5Ge_4-type structure are present. This is by no means an easy task, because the gadolinium itself is a very reactive element, so that conventional synthesis by melting in a crucible is not an option. Therefore, we employed arc melting in an inert atmosphere of argon using a pure copper hearth as the mould. This method proved to be very effective in terms of negligible mass losses of the charge material, but problematic due to the excessive heterogeneity in the microstructure of the synthesised alloys.

Experimental work

Pure gadolinium (99.99 %), silicon (99.9995 %) and germanium (99.9999 %) were used to produce fine pellets of Gd-Ge-Si alloys weighing from 1 g to 5 g. Each time the ratio between the alloy elements was kept at Gd5 : Ge2 : Si2 in atomic percent. An arc melting facility that allows the internal atmosphere to be removed and replaced by pure argon was used (see Figure 2).

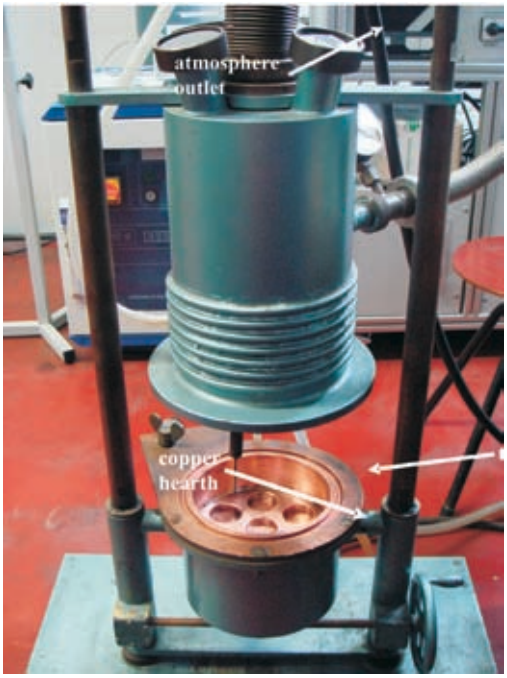

Figure 2. The melting facility with a water-cooled copper mould at the bottom and the tungsten tip used to produce the electric arc

Prior to introducing the argon into the arc-melter a small amount of pure titanium was ignited in order to remove any remaining oxygen. Each set of the charge material, weighing from 1g to 5 g, consisted of small pieces of gadolinium, germanium and silicon, and was placed on the water-cooled copper hearth. Each set of the charge material was then remelted for four times where DC electric current of 90 A was used. After each melting time the buttons were turned upside down and remelted in order to increase the homogeneity of the synthesised alloys. Weighing the synthesised alloys revealed that the mass losses during the synthesis process were of (0.4 ± 0.2) %, which is more than acceptable. The synthesised pellets were than cut in half and specimens were prepared for the optical (LOM; Reichert MeF2) and electron microscopy (SEM with EDS; JEOL JSM-5800). The remaining halves of the synthesised alloys were divided into two pieces, one of them being ground into a fine powder to be used for the XRD (Bruker AXS Endeavor D4) examination and the other one used for the heat treatment. The heat treatment of the synthesised alloys was carried out in an inert atmosphere of argon for 1 hour at 1300 ºC. The reason for varying the amount of charge material from 1 g up to 5 g was to effectively influence the cooling rate in order to see what effect this had on the crystallization path and therefore on the microstructure of synthesised alloys.

Results and discussion

The synthesised alloys were first examined using scanning electron microscopy to reveal the effect of the cooling rate on both the surface structure (Figure 3) and the microstructure (Figure 4).

It is obvious from Figure 3 that the cooling rate, which is higher in the case of the 1 g sample, has a profound effect on the surface structure with the formation of a “sinew” effect on the upper surface of the button (Figure 3 a) e.g. the flat plateaus on the alloy button tend to break up. This feature is all but absent with the 5 g sample (Figure 3 b). The 5 g sample has a smoother surface consisting of fairly regular pentagons and hexagons (reminiscent of the Fullerene

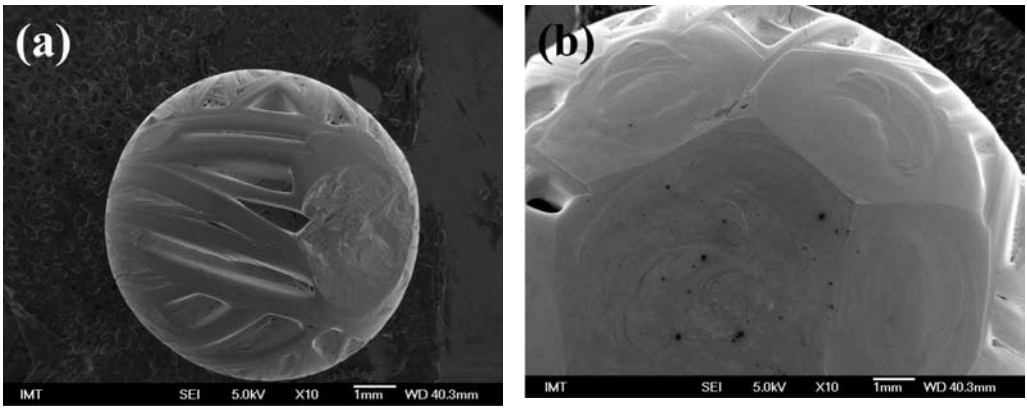

Figure 3. Surface structure of the $Gd_5Ge_2Si_2$ alloy button in the as-cast state: (a) 1 g of charge material and (b) 5 g of charge material

structure) that is typical for the crystallisation of semi-conducting elements, such as silicon and germanium (often also referred to as semi-metals) when moderate cooling rates are present. The metals, on the other hand, tend to form a curvaceous or uneven crystallisation front (on atomic scale) because of the small difference in the entropy of the solid and liquid state (melting entropy). This is not the case with silicon and germanium, both of which have large melting entropies (order of 30 J/(K mol), whilst order of 4–8 J/(K mol) for metals), leading to the formation of facets during the process of crystallisation. The comparison of the microstructure of the sample with the highest cooling rate (Figure 4 a) and the sample with the lowest cooling rate (Figure 4 b) reveals that in both cases the as-cast state provides us with at least three phases, with the dendritic-columnar phase being the dominant one.

This phase also contains small needle-like precipitates that lie within the dendritic columns at an angle of 90º and approx.

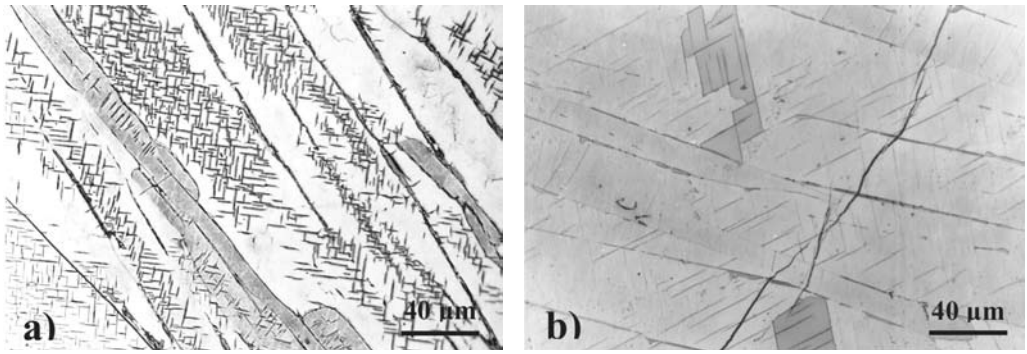

Figure 4. Optical micrographs of the microstructure of the $Gd_5Ge_2Si_2$ alloy in as-cast state: (a) 1 g of charge material and (b) 5 g of charge material

75º to each other. The intercolumnar space is filled with a third phase, which is rich in gadolinium and silicon. The columnar phase exhibits different shade effects because of the differences in the orientation of individual columns towards the sample surface, so that they produce the so-called orientation contrast. The number of phases revealed by the optical microscope is also confirmed by the SEM and EDS (Figure 5), which both show that the columnar phase has mole fractions of Si 22.9 %, Ge 21.0 % and Gd 56.1 %, the intercolumnar phase has mole fractions 31.6 % Si, 17.5 % Ge and 50.9 % Gd, and the precipitated phase has composition mole fractions of 17.3 % Si, 21.9 % Ge and 60.8 % Gd. The X-ray spectra of the as-cast samples weighing 1 g and 5 g are the same. Although there may be significant microstructural differences between the two samples the crystal structure of the main phase is the same for both samples. The X-ray diffraction pattern of the as-cast button weighing 5 g is shown in Figure 6a together with the calculated spectrum for the Gd_5Si_4-structure. This Gd_5Si_4-based solid solution allows germanium to substitute for silicon in the range $0.5 \leq x \leq 1.0$. On the other hand, the Gd_5Ge_4 solid solution extends from $0 \leq x \leq 0.2$. If we compare the two spectra, the experimentally obtained spectra and the calculated spectra, it is clear that they exhibit a good fit, albeit with a slight shift to higher angles, which is increasingly obvious to the right-hand side of the graph. This shift is due to the substitution of approximately 50 % of the silicon atoms by germanium atoms, and is inline with the observations of Pecharsky and Gschneidner [1]. However, after heat-treating the material at 1300 °C for one hour a change in the crystal structure is observed (Figure 6b). Here we observe the monoclinically distorted derivative of the orthorhombic Sm_5Ge_4-type phase, which we refer to in the figure as the $Gd_5Ge_2Si_2$ structure. It is believed that the heat treatment for 1 h at 1300 °C results in some phase purification and homogenisation of the arc-melted buttons, leading to a partial ordering of the crystal structure via a redistribution of silicon and germanium atoms among the various crystallographic sites. The annealing causes an enrichment

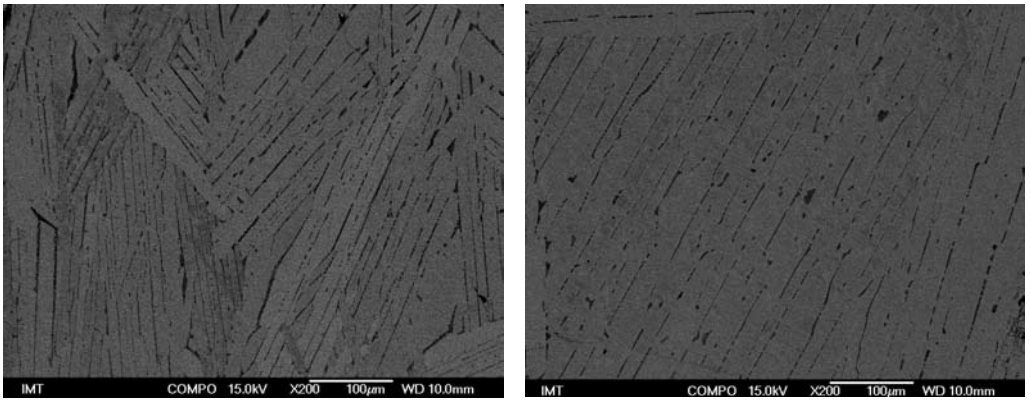

Figure 5. SEM micrographs of the microstructure of the $Gd_5Ge_2Si_2$ alloy in as synthesised state: (a) 1 g of charge material and (b) 5 g of charge material

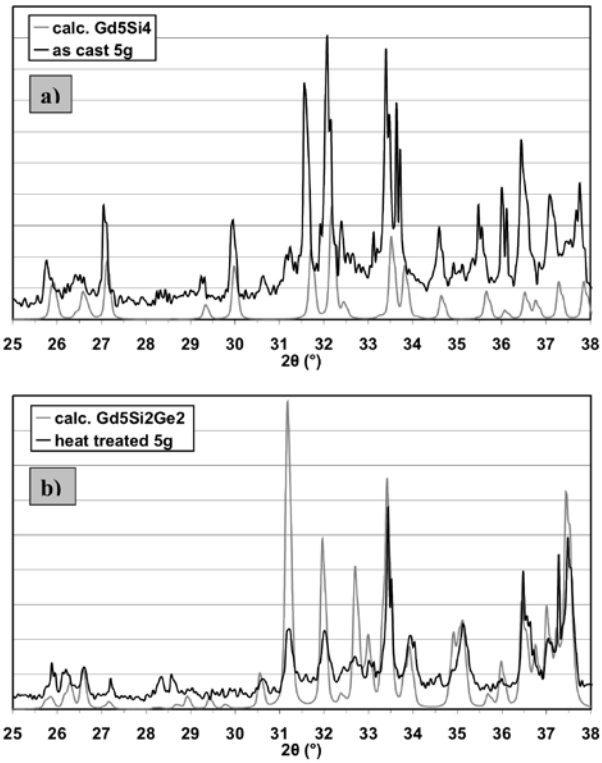

Figure 6. XRD analysis of the $Gd_5Ge_2Si_2$: (a) as-cast state and (b) heat treated state

of germanium for the sites responsible for the interslab bonding, thereby resulting in a considerable enhancement of the giant magneto-caloric effect.

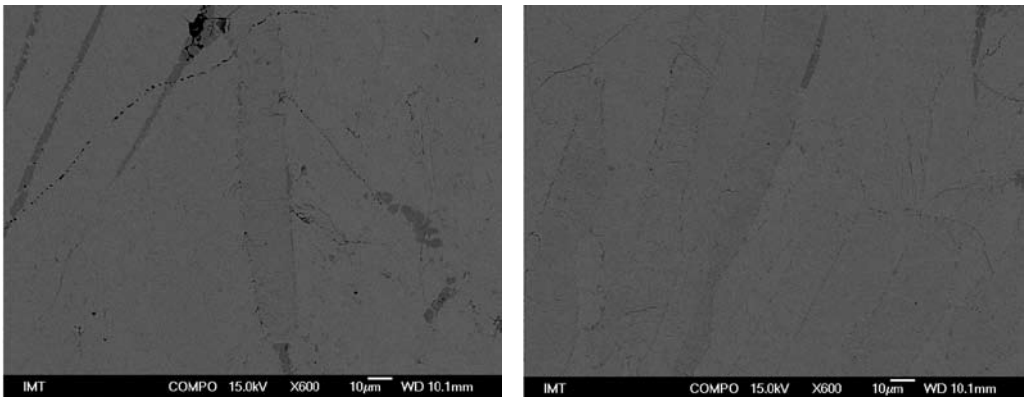

Figure 7. SEM micrograph of the microstructure of the $Gd_5Ge_2Si_2$ alloy in heat-treated state: (a) 1 g of charge material and (b) 5 g of charge material

From Figure 7 we can see that after the heat treatment at 1300 ºC we get a largely single-phased alloy with the composition very close to that of $Gd_5Si_2Ge_2$. This combination of the right chemistry and the right crystal structure should give us a material with a large magneto-caloric effect (GMCE) with an entropy effect of about –35 J/(kg K).

Conclusions

A series of five alloys with the composition close to $Gd_5Ge_2Si_2$ weighing from 1 g to 5 g were prepared by arc melting. This synthesis route provided alloys with a significant heterogeneity in their microstructures and at least three different phases.

However, a heat treatment at 1300 ºC for an hour initiated the transformation of these phases into the desired $Gd_5Ge_2Si_2$ phase, which exhibits a pronounced magneto-caloric effect and could potentially be used for the cooling applications.

The variations in the mass of the initial charge of material effectively influenced the cooling rate, causing marked effects on the surface of the buttons, producing a sinew appearance at fast cooling rates, which disappears as the mass of buttons increases towards 5 g.

The crystal structures of the main phases in the buttons were found to be largely independent of mass, and therefore of cooling rate, and a heat treatment at 1300 °C for one hour was sufficient to produce a single-phased material with the desired crystal structure.

References

[1] Pecharsky, V. K. & Gschneidner, K. A., Jr. (1997): Giant magnetocaloric effect in $Gd_5(Si_2Ge_2)$. *Phys. Rev. Lett.*, No. 78, pp. 4494–4499.

[2] Kim, K. S., Min, S. G., Yu, S. C., Oh, S. K., Kim, Y. C., Kim, K. Y. (2006): J Magn., *Magn. Mat.*; No. 304, pp. 642–644.

[3] Saito T. (2006): Magnetic properties of Co-Al-Ni melt-spun ribbon. *J. Appl. Phys.*; Vol. 100, No. 5, pp. 053916–053921.

[4] Yan, A., Muller, K. H., Schultz, L. & Gutfleisch, O. (2006): Magnetic entropy change in melt-spun MnFePGe. *J. Appl. Phys.*; Vol. 99, No. 8, pp. 08K903–08K908.

[5] Hu, F. X., Shen, B. G., Sun, J. R., Cheng, Z. H., Rau, G. H. & Zhang, X. X. (2001): Influence of negative lattice expansion and metamagnetic transition on magnetic entropy change in the compound $LaFe_{11.4}Si_{1.6}$. *Appl. Phys. Lett.*; Vol. 78, No. 23, pp. 3675–3681.

[6] Pecharsky, A. O., Gschneidner, K. A., Jr. & Pecharsky, V. K. (2003): The giant magnetocaloric effect of optimally prepared $Gd_5Si_2Ge_2$. *J. Appl. Phys.*; Vol. 93, No. 8, pp. 4722–4726.

[7] Pecharsky, V. K. & Gschneidner, K. A., Jr. (1997): Effect of alloying on the giant magnetocaloric effect of $Gd_5(Si_2Ge_2)$. *J. Alloys and Comps.*; Vol. 260, pp. 98–102.

The influence of elevated temperatures on microstructure of cast irons for automotive engine thermo-mechanical loaded parts

Faruk Unkić[1], Zoran Glavaš[1], Katarina Terzić[1]

[1]University of Zagreb, Faculty of Metallurgy, Aleja narodnih heroja 3, 44103 Sisak, Croatia;
E-mail: unkic@simet.hr, glavaszo@simet.hr, terzicka@simet.hr

Received: December 18, 2009 **Accepted:** January 13, 2009

Abstract: The influence of elevated temperatures (550 °C and 850 °C) on microstructure and resistance to oxidation of gray iron quality EN-GJL-250 and ductile irons qualities: EN-GJS-400-18, EN-GJS-500-7, EN-GJS-SiMo4-1 and EN-GJS-AXNiCr20-2 were analyzed in this paper. The highest resistance to oxidation and microstructure changes at 550 °C and 850 °C shows austenitic ductile iron quality EN-GJS-AXNiCr20-2, followed by ferritic ductile iron quality EN-GJS-SiMo4-1. During oxidation of those cast irons at elevated temperatures two oxide layers over the surface of samples were occurred. Outward layer is easy detachable and consists of iron oxide. Inward layer is tightly connected with metal matrix and prevents progression of oxidation to the samples inside. This oxide layer consists of Fe_2SiO_4 (fayalite) or complex oxides (Fe, Cr, Ni, Si, and O). Due to favorable high-temperatures properties, those materials are suitable for construction of thermo-mechanical loaded parts of automotive engine, such as turbocharger housings and exhaust manifolds. Ferritic ductile iron quality EN-GJS-400-18, pearlitic ductile iron quality EN-GJS-500-7 and pearlitic gray iron quality EN-GJL-250 did not show an adequate resistance to oxidation and microstructure changes at 550 °C and 850 °C.

Key words: cast irons, elevated temperatures, microstructure

Introduction

Automotive industry absorbs about 1/3 of total produced castings in the industrial developed countries. Increased use of cars is not only facing with the energy problems, but also with ecological problems, which include global warming, air pollution, acid rains, ozone destruction, greenhouse effect and waste disposal. Cars manufacturers must increase efficiency of the engines, i.e. reduce the emission of harmful gases and fuel consumption and also increase engine performance and comfort. In order to achieve these demands, new systems of fuel injection and treatment of exhaust gases have been developed, turbochargers are used more, as well as the modern concepts of cars production (downsizing, light weight constructions etc.)[1, 2].

Original scientific paper

Higher temperatures of combustion and higher pressures in the cylinders result in higher thermal and mechanical loads of individual components of automotive engine (engine block and cylinder head, turbocharger housing, exhaust manifold etc.). Therefore, modern concepts of automotive engines production require the application of high quality materials, i.e. materials that have adequate high-temperatures properties.

Cast irons with graphite, i.e. gray cast irons which apply for automotive engine components production which are exposed to elevated temperatures (engine blocks, cylinder heads, turbocharger housing, exhaust manifolds etc.) must have adequate resistance to oxidation and growth, resistance to thermal fatigue and sudden temperature changes and adequate mechanical properties[3–9]. Therefore, engine blocks are made more and more of vermicular cast iron instead of gray cast iron, while turbocharger housings and exhaust manifolds are made of ferritic ductile irons (alloyed with 4,0–6,0 % Si) or austenitic ductile irons (alloyed with 18,0–36,0 % Ni)[4, 10–13]. For the same structure of metal matrix, ductile iron has better properties at elevated temperatures than gray iron.
The influence of elevated temperatures on microstructure and resistance to oxidation of pearlitic gray iron and ferritic, pearlitic and austenitic ductile irons was analyzed in this paper.

MATERIALS AND METHODS

The samples of pearlitic gray iron quality EN-GJL-250, pearlitic ductile iron quality EN-GJS-500-7, ferritic ductile iron quality EN-GJS-400-18, ferritic ductile iron alloyed with Si and Mo quality EN-GJS-SiMo4-1 and austenitic ductile iron quality EN-GJS-AXNiCr20-2 were heated at 550 °C and 850 °C in the furnace for annealing without protective atmosphere. Test samples were held at the mentioned temperatures for 5 h, and then cooled in furnace until the room temperature. For each temperature of examination, a new series of samples were used. The samples were put into the furnace in porcelain cups, which were previously annealed to constant mass at 850 °C. Cups and samples were weighted before and after the heating.

Metallographic examinations were performed by light microscope with digital camera and image analysis system before and after the heating at 550 °C and 850 °C. Shape of graphite, structure of metal matrix and thickness of the oxide layers on the surface of the samples were determined by metallographic examinations. Oxide layers on the samples of ferritic ductile iron quality EN-GJS-SiMo4-1 and austenitic ductile iron quality EN-GJS-AXNiCr20-2 were analyzed by scanning electron microscope with energy dispersive spectrometer (SEM + EDS).

RESULTS AND DISCUSSION

Chemical composition of test samples

Table 1 shows chemical composition of cast irons test samples. Chemical composition of gray iron is usual for quality EN-GJL-250. Higher content of pearlite

Table 1. Chemical composition of test samples

Content of element, *w*/%	Quality				
	EN-GJL-250	EN-GJS-500-7	EN-GJS-400-18	EN-GJS-SiMo4-1	EN-GJS-AXNiCr20-2
C	3,43	3,71	3,60	2,90	2,38
Si	2,15	2,79	2,01	4,61	2,74
Mn	0,61	0,16	0,17	0,41	0,56
S	0,090	0,005	0,020	0,015	0,003
P	0,031	0,044	0,027	0,045	0,016
Cu	0,12	0,57	0,03	0,02	0,12
Sn	0,010	0,014	0,008	0,005	0,006
Cr	0,07	0,06	0,07	0,09	2,08
Ni	0,05	0,06	0,02	0,01	21,73
Mo	0,006	0,009	0,003	1,27	0,019
Mg	-	0,026	0,054	0,047	0,058

in metal matrix was achieved by using a higher content of Mn and Cu.

High content of pearlite in metal matrix of pearlitic ductile iron quality EN-GJS-500-7 was achieved by using higher content of Cu (0,57 %). The content of the carbide-forming elements was low.

Chemical composition of ferritic ductile iron quality EN-GJS-400-18 is usual for this quality. The content of elements which promote the formation of pearlite and carbides was low.

From the chemical composition of ductile iron quality EN-GJS-SiMo4-1 it could be seen that the melt was alloyed with Si (4,61 %) and Mo (1,27 %). By high content of Si it has been tried to achieve full ferritic metal matrix in as-cast condition. Moreover, a high content of Si results in moving of eutectoid transformation temperature toward higher values. In this way phase transformation to austenite moves toward higher temperatures and avoids volume changes which accompany this phase transformation. Moreover, higher Si content improves the resistance to oxidation. Addition of Mo improves the tensile properties and resistance to creep at elevated temperatures. The Mn content was relatively high (0,41 %), which is harmful because Mn segregates during solidification at grain boundaries and promotes the creation of pearlite and carbides. Content of other carbide-forming elements and elements which promote formation of pearlite was low.

Ductile iron quality EN-GJS-AXNiCr20-2 was highly alloyed with Ni (21,73 %), which resulted in creation of austenitic metal matrix in as-cast condition. Addition of Cr improves resistance to oxidation and tensile strength at elevated temperatures.

Results of mass examination of the samples before and after the heating

Table 2 shows results of mass examination of the test samples before and after the heating at 550 °C for 5 h.

Table 2. Mass of samples before and after the heating at 550 °C for 5 h

Quality	Mass of sample, m/g	Mass (sample + cup) before heating, m_{bh}/g	Mass (sample + cup) after heating, m_{ah}/g	Δm/g
EN-GJL-250	18,1254	28,5151	28,5285	0,0134
EN-GJS-500-7	7,4301	17,7772	17,7797	0,0025
EN-GJS-400-18	8,6252	18,8286	18,8309	0,0023
EN-GJS-SiMo4-1	15,3985	22,9902	22,9914	0,0012
EN-GJS-AXNiCr20-2	21,6868	31,0594	31,0594	0,0000

Table 3. Mass of samples before and after the heating at 850 °C for 5 h

Quality	Mass of sample, m/g	Mass (sample + cup) before heating, m_{bh}/g	Mass (sample + cup) after heating, m_{ah}/g	Δm/g
EN-GJL-250	16,3504	26,5537	26,9066	0,3529
EN-GJS-500-7	8,1970	15,7898	15,9146	0,1248
EN-GJS-400-18	8,3403	18,0365	18,1406	0,1041
EN-GJS-SiMo4-1	15,5324	24,8985	24,9052	0,0067
EN-GJS-AXNiCr20-2	10,2913	20,6811	20,6830	0,0019

From Table 2 it could be seen that all the test samples, except austenitic ductile iron (EN-GJS-AXNiCr20-2), show increasing of mass after heating at 550 °C, which is an indicator of oxidation, i.e. formation of oxide layer. Gray iron shows the largest increase of mass. Ferritic ductile irons (EN-GJS-400-18, EN-GJS-SiMo4-1) have a smaller increase of mass than pearlitc ductile iron (EN-GJS-500-7).

Table 3 shows results of mass examination of the test samples before and after the heating at 850 °C for 5 h.

From Table 3 it could be seen that all the test samples show increasing of mass after the heating at 850 °C, which is an indicator of oxidation, i.e. formation of oxide layer. Gray iron shows highest increase of mass. Austenitic ductile iron shows lowest increase of mass. Ferritic ductile irons have a smaller increase of mass than pearlitc ductile iron.

Microstructure analysis of the samples before and after the heating

From Figure 1 it could be seen that oxidation occurred during the heating of samples of gray iron quality EN-GJL-250 at 550 °C and 850 °C for 5 h. Formed oxide layers do not have the protective effect because they were not compact and tightly connected with metal matrix, which allows progression of oxidation to the samples inside.

During the heating at 550 °C, the changes in the metal matrix did not occurred. The partial decomposition of pearlite and the accompanying growth occurred during the heating at 850 °C.

From Figure 2 it could be seen that oxidation occurred during the heating of samples of ductile iron quality EN-GJS-500-7 at 550 °C and 850 °C for 5 h. Oxide layer formed on the surface of the sample during the heating at 550 °C was relatively

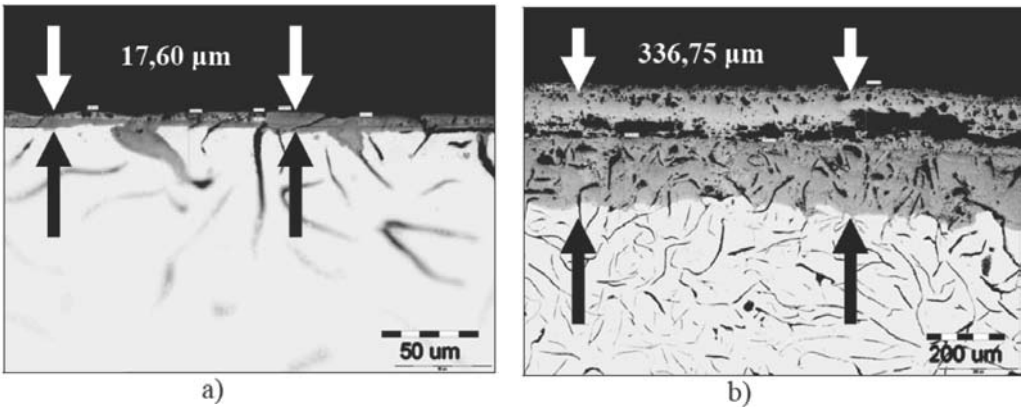

Figure 1. Optical micrographs of the oxide layers on the surface of the samples of pearlitic gray iron quality EN-GJL-250: a) after the heating at 550 °C, b) after the heating at 850 °C

thin and tightly connected with metal matrix. Oxide layer formed on the surface of sample during the heating at 850 °C was significantly thicker than oxide layer formed during the heating at 550 °C and was not tightly connected with metal matrix, which allows progression of oxidation to the sample inside.

During the heating at 550 °C, because of partial decomposition of pearlite, increasing of ferrite content in metal matrix occurred in relation to the state before heating. Further increase of ferrite content in metal matrix occurred during the heating at 850 °C.

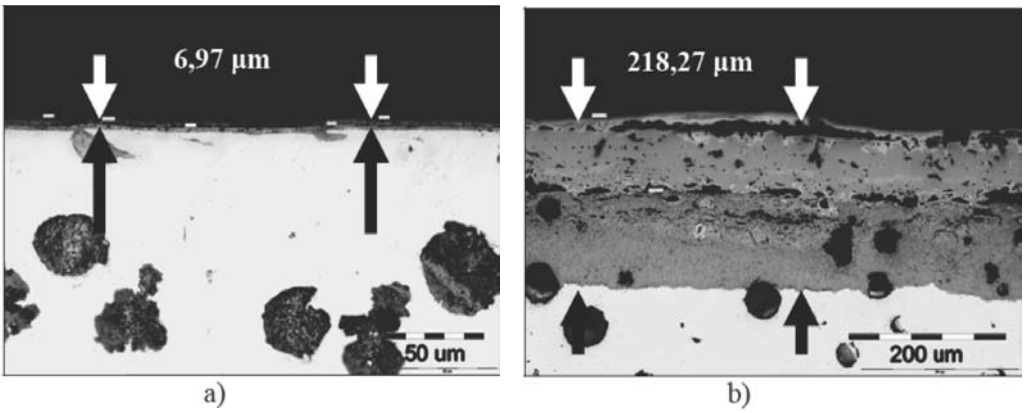

Figure 2. Optical micrographs of the oxide layers on the surface of the samples of pearlitic ductile iron quality EN-GJS-500-7: a) after the heating at 550 °C, b) after the heating at 850 °C

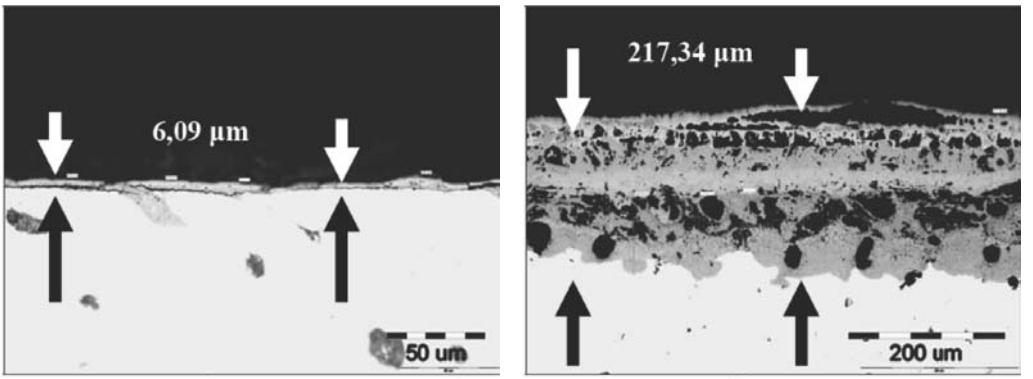

Figure 3. Optical micrographs of the oxide layers on the surface of the samples of ferritic ductile iron quality EN-GJS-400-18: a) after the heating at 550 °C, b) after the heating at 850 °C

From Figure 3 it could be seen that oxidation occurred during the heating of samples of ductile iron quality EN-GJS-400-18 at 550 °C and 850 °C for 5 h.

Figure 3 a shows that oxide layer formed on the surface of the sample during the heating at 550 °C was relatively thin and tightly connected with metal matrix. Oxide layer formed on the surface of the sample during the heating at 850 °C was significantly thicker than oxide layer formed during the heating at 550 °C and was not tightly connected with metal matrix, which allows progression of oxidation to the sample inside (Figure 3 b).

Because of partial decomposition of pearlite during the heating at 550 °C, increasing of ferrite content in metal matrix occurred in relation to the state before heating. Decomposition of pearlite occurred in a greater extent during the heating at 850 °C.

From Figure 4 it could be seen that oxidation occurred during the heating of samples of ductile iron quality EN-GJS-SiMo4-1-at 550 °C and 850 °C for 5 h.

The average thickness of oxide layer formed during the heating at 550 °C was 4,33 µm, i.e. 77,72 µm during the heating at 850 °C. This means that the alloyed ferritic ductile iron quality EN-GJS-SiMo4-1 has a much better resistance to oxidation than gray iron and non-alloyed ferritic and pearlitic ductile iron. Oxide layers were tightly connected with metal matrix and prevent progression of oxidation to the sample inside.

From Figure 5 it could be seen the layered structure of oxide layer. Outward layer consisted of iron oxide (Figure 6). Inward layer, i.e. the layer alongside the base (non-oxidized) material consisted of iron silicate (fayalite) (Figure 7). This oxide layer prevents progression of oxidation to the sample inside. In this way resistance to high-temperature oxidation was improved.

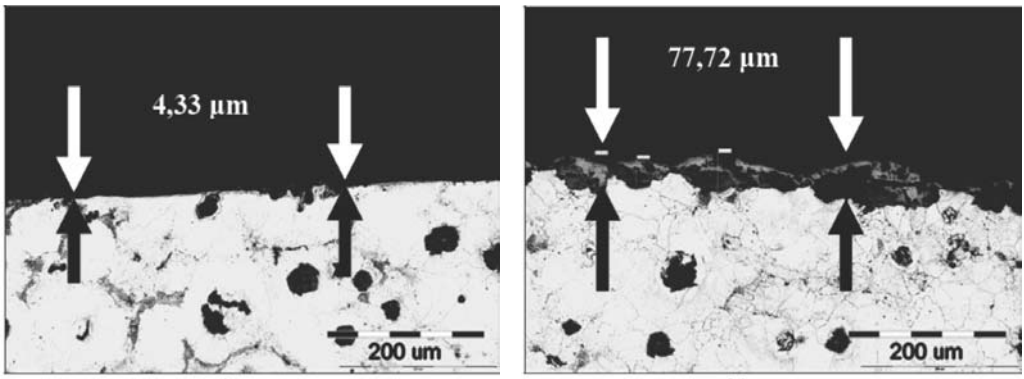

Figure 4. Optical micrographs of the oxide layers on the surface of the samples of ferritic ductile iron quality EN-GJS-SiMo4-1: a) after the heating at 550 °C, b) after the heating at 850 °C

During the heating at 550 °C and 850 °C increasing of ferrite content in metal matrix occurred in relation to the state before heating. Decomposition of pearlite occurred in a greater extent during the heating at 850 °C. Higher content of Mn (0,41 %) is a potential cause of the presence of pearlite in metal matrix before the heating.

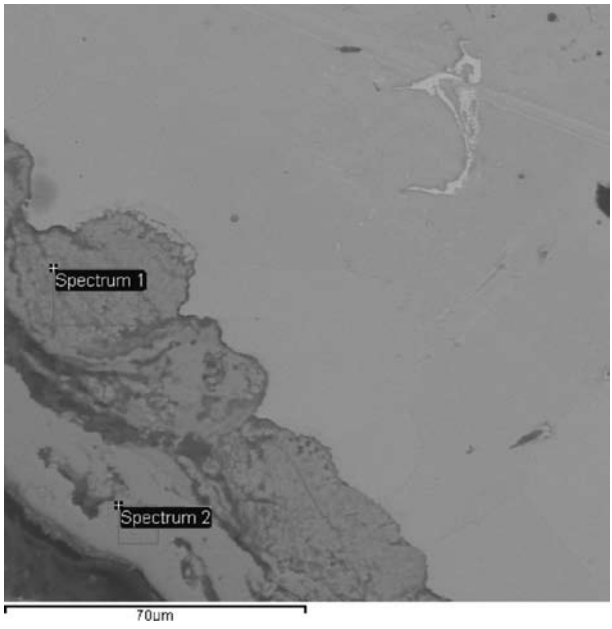

Figure 5. SEM micrograph of oxide layer formed on the surface of the sample of ductile iron quality EN-GJS-SiMo4-1 during the heating at 850 °C for 5 h. Places analyzed by the use of EDS are marked in the picture.

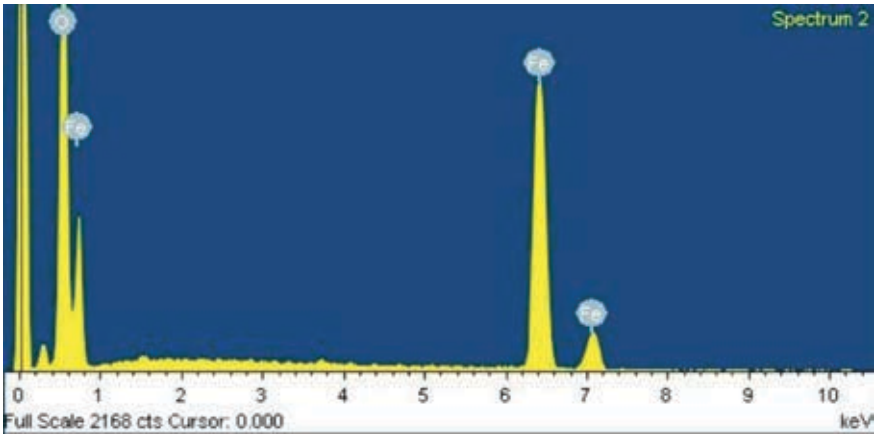

Figure 6. EDS spectrum of outward oxide layer formed on the surface of the sample of alloyed ferritic ductile iron quality EN-GJS-SiMo4-1 during the heating at 850 °C for 5 h. Place where analysis was performed is marked in the figure 5

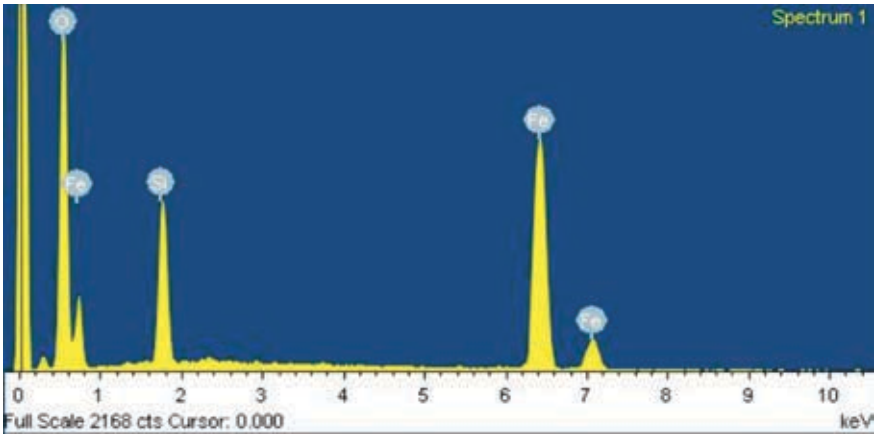

Figure 7. EDS spectrum of inward oxide layer formed on the surface of the sample of alloyed ferritic ductile iron quality EN-GJS-SiMo4-1 during the heating at 850 °C for 5 h. Place where analysis was performed is marked in the figure 5

Because of higher Mo content (1,27 %), in ferritic ductile iron quality EN-GJS-SiMo4-1 precipitation of primary carbides at grain boundaries and secondary carbides in ferrite occurred (Figure 8). At low magnification, carbides precipitated at grain boundaries are similar to pearlite. A clear difference can be seen at higher magnification (Figure 8). In both cases these are complex carbides, which are composed of iron, molybdenum, silicon and carbon (Figure 9).

During the heating at 550 °C and 850 °C, increasing of amount of fine secondary carbides in ferrite occurred. Higher increase in the amount of carbides was present after the heating at 850 °C.

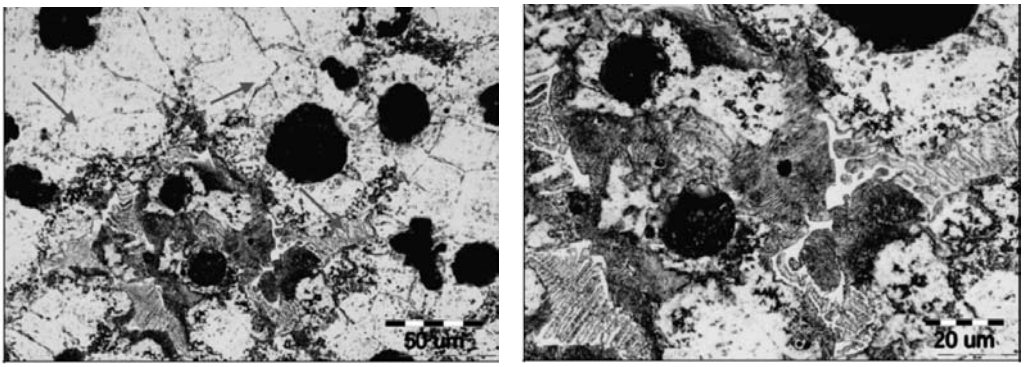

Figure 8. Optical micrographs of microstructure of ductile iron quality EN-GJS-SiMo4-1 before the heating, etched. From the figure it could be seen primary carbides at grain boundaries and fine secondary carbides in ferrite

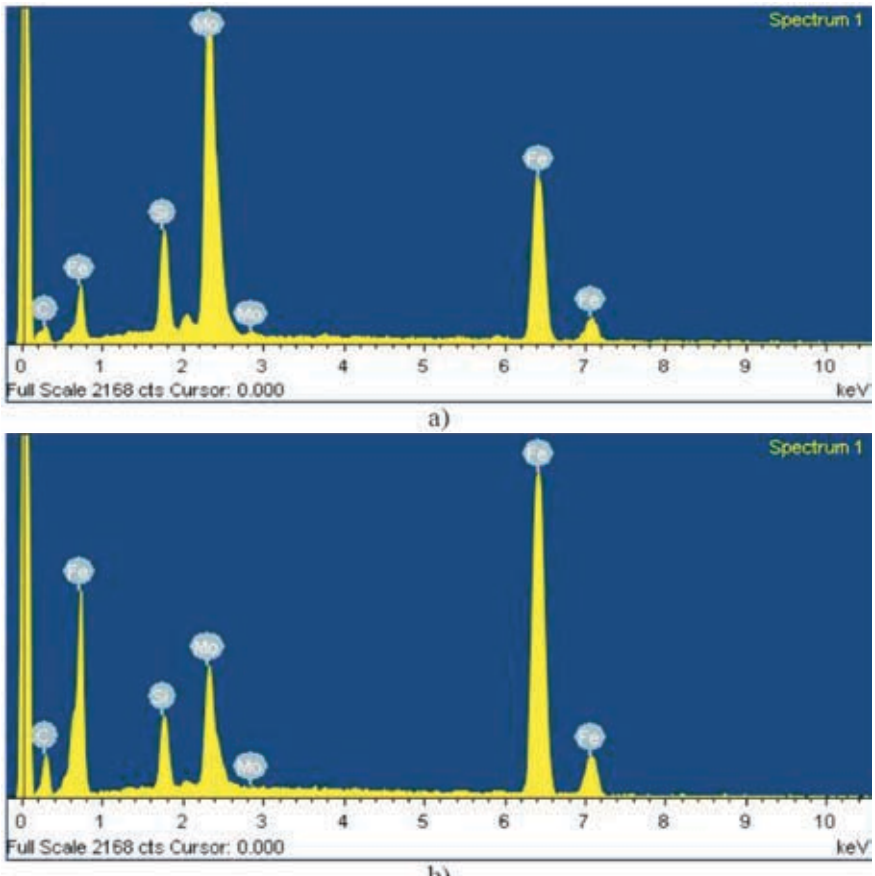

Figure 9. EDS spectum of primary (a) and secondary (b) carbides in ferritic ductile iron quality EN-GJS-SiMo4-1

The presence of complex primary and secondary carbides in the microstructure of alloyed ferritic ductile iron quality EN-GJS-SiMo4-1 results in increasing of tensile strength at elevated temperatures and resistance to creep and thermal fatigue.

From Figure 10 a it could be seen that oxidation occurred in a very small extent during the heating of samples of austenitic

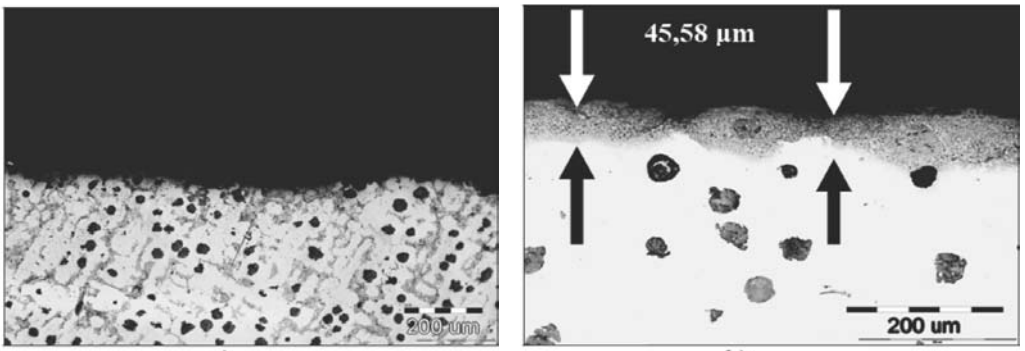

Figure 10. Optical micrographs of the oxide layers formed on the surface of the samples of austenitic ductile iron quality EN-GJS-AXNiCr20-1: a) after the heating at 550 °C, b) after the heating at 850 °C

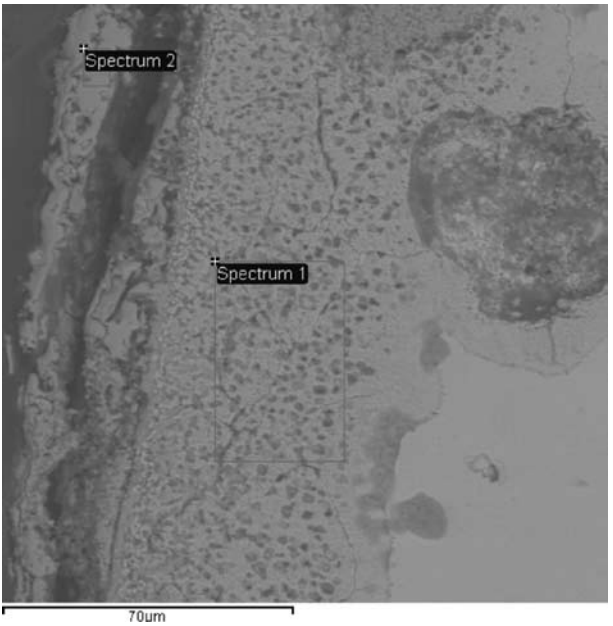

Figure 11. SEM micrograph of oxide layer formed on the surface of the sample of austenitic ductile iron quality EN-GJS-AXNiCr20-1 during the heating at 850 °C for 5 h. Places analyzed by the use of EDS are marked in the picture.

ductile iron quality EN-GJS-AXNiCr20-2 at 550 °C. This resulted in the formation almost negligible oxide layer on certain places. Oxide layer formed on the surface of the sample during the heating at 850 °C was tightly connected with metal matrix (Figure 10 b). The average thickness of oxide layer was 45,58 μm. Oxide layer formed during the heating austenitic ductile iron at 850 °C was thinner than oxide layers formed during the heating other analyzed materials at 850 °C. This shows the superiority of austenitic ductile iron in comparison to other analyzed materials.

From Figure 11 it could be seen the layered structure of oxide layer formed during the heating at 850 °C.

Inward oxide layer, i.e. the layer alongside the base (non-oxidized) material was complex oxide which consisted of Fe, Cr,

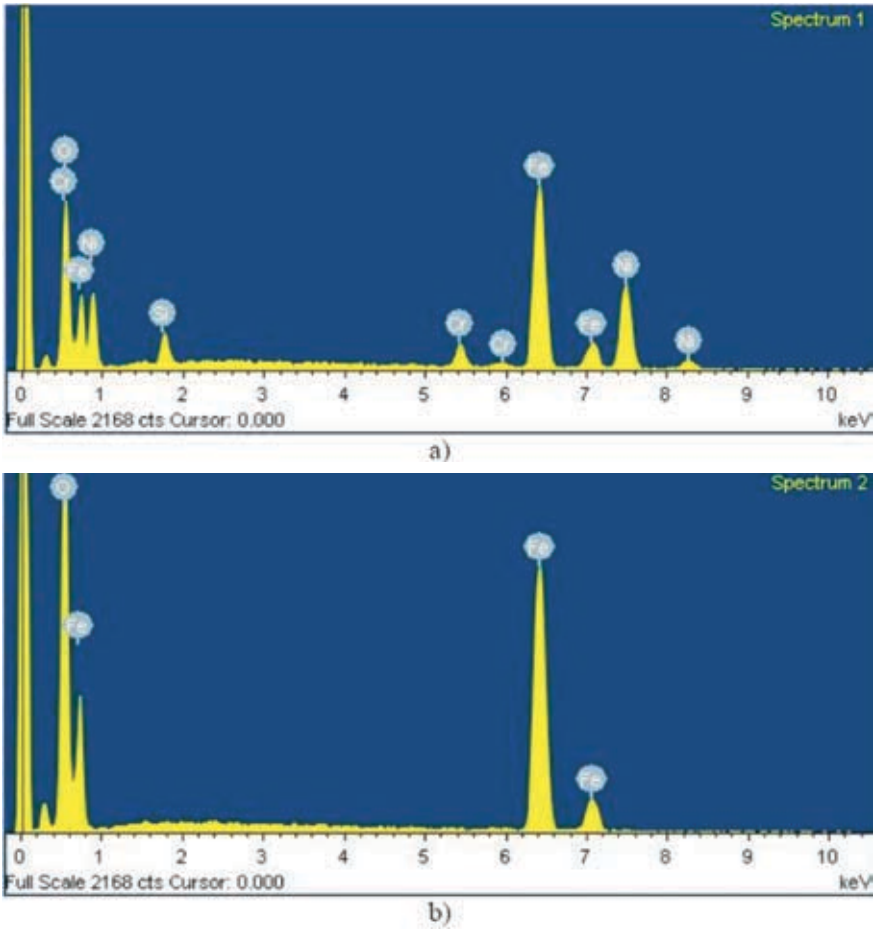

Figure 12. EDS spectra of oxide layer formed on the surface of the sample of austenitic ductile iron quality EN-GJS-AXNiCr20-1 during the heating at 850 °C for 5 h: a) inward oxide layer, b) outward oxide layer. Places where analysis were performed are marked in the figure 11

Ni, Si and O (Figure 12 a). Outward layer consisted of Fe and O (Figure 12 b). Complex oxide layer alongside the base material prevents progression of oxidation to the sample inside. In this way resistance to high-temperature oxidation was improved.

During the heating at 550 °C and 850°C, the changes in the metal matrix did not occurred. Because there are no phase transformations, it could be concluded that the volume changes and the accompanying growth will not occur during the application of austenitic ductile iron at 550 °C and

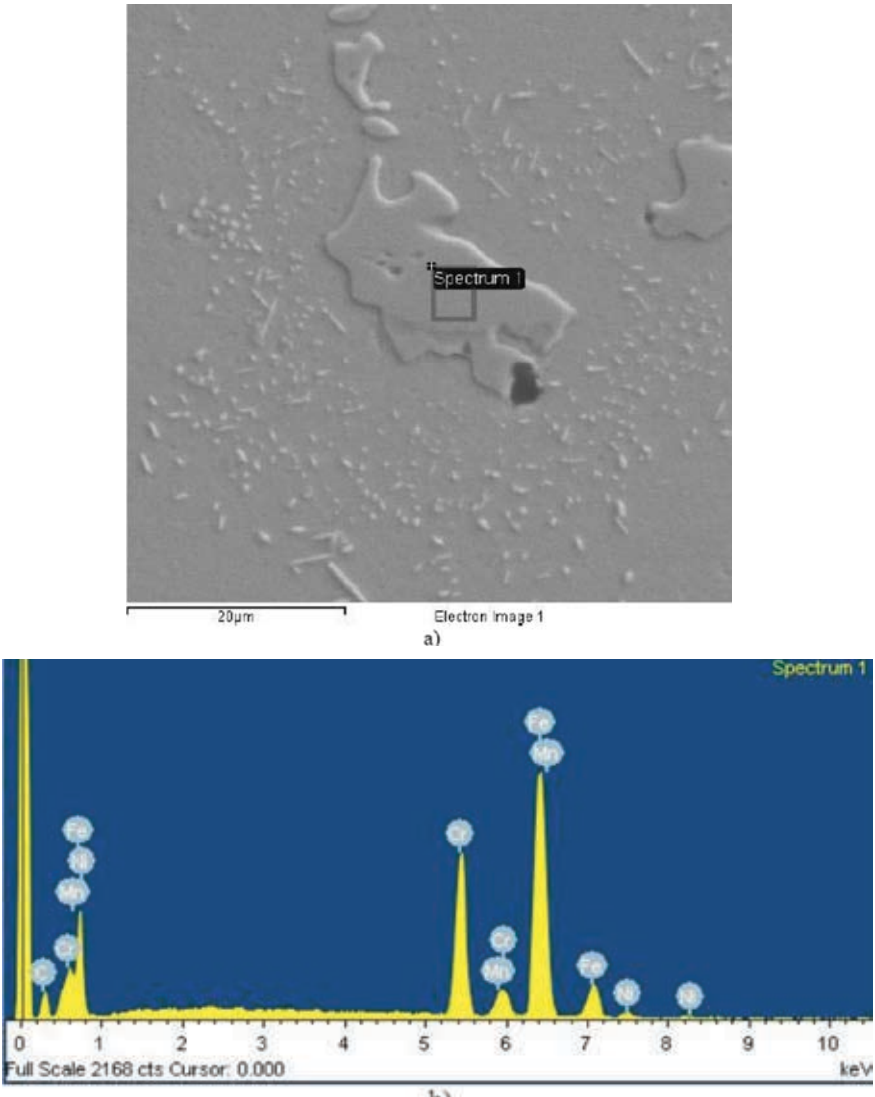

Figure 13. a) SEM micrograph of primary carbides in austenitic ductile iron quality EN-GJS-AXNiCr20-1, b) EDS spectum of primary carbides in austenitic ductile iron quality EN-GJS-AXNiCr20-1

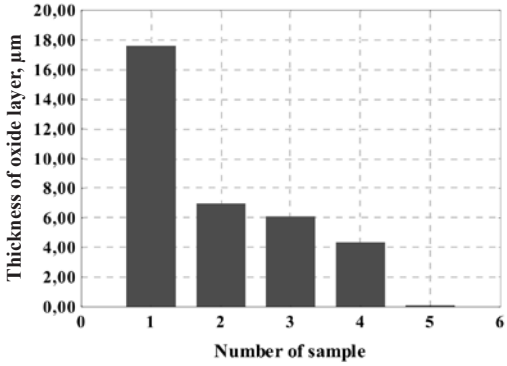

Figure 14. Thickness of oxide layers formed on the surface of the samples during the heating at 550 °C for 5 h: 1 - gray iron quality EN-GJL-250; 2 - ductile iron quality EN-GJS-500-7; 3 - ductile iron quality EN-GJS-400-18; 4 - ductile iron quality EN-GJS-SiMo4-1; 5 - ductile iron quality EN-GJS-AXNiCr20-2

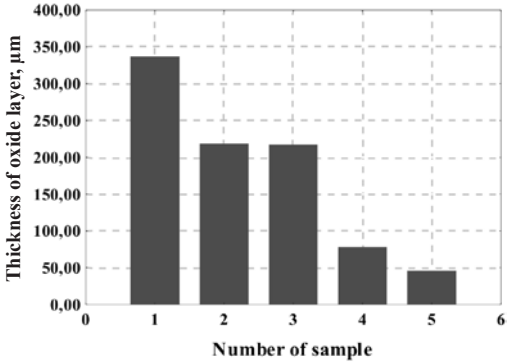

Figure 15. Thickness of oxide layers formed on the surface of the samples during the heating at 850 °C for 5 h: 1 - gray iron quality EN-GJL-250; 2 - ductile iron quality EN-GJS-500-7; 3 - ductile iron quality EN-GJS-400-18; 4 - ductile iron quality EN-GJS-SiMo4-1; 5 - ductile iron quality EN-GJS-AXNiCr20-2

850 °C. This shows the superiority of austenitic ductile iron in comparison to other analyzed materials.

During the solidification of ductile iron quality EN-GJS-AXNiCr20-1 precipitation of primary carbides at grain boundaries occurred (Figure 13a). These are complex carbides, which are composed of iron, chromium, manganese and carbon (Figure 13b).

Figures 14 and 15 summarily show results of measurements of oxide layers thickness formed during the heating at 550 °C and 850 °C for 5 h.

From the Figures 14 and 15 it could be seen that austenitic ductile iron quality EN-GJS-AXNiCr20-2 is the most suitable for construction of castings which will be applied at elevated temperatures. Gray iron quality EN-GJL-250 is not suitable material for castings which will be applied at elevated and high temperatures.

Conclusions

From the examination of microstructure properties and oxide layers and measurements of mass before and after the heating of gray and ductile irons samples at 550 °C and 850 °C for 5 h the following conclusions could be performed:

- during the heating at 550 °C and 850 °C for 5 h in the samples of pearlitic gray iron quality EN-GJL-250, pearlitic ductile iron quality EN-GJS-500-7, ferritic ductile iron quality EN-GJS-400-18, ferritic ductile iron quality EN-GJS-SiMo4-1 and austenitic ductile iron quality EN EN-GJS-AXNiCr20-2 oxidation, increasing of

mass and microstructure changes occur,

- the highest resistance to oxidation, i.e. smallest thickness of oxide layer and smallest increasing of mass during the heating at 550 °C and 850°C was determined at austenitic ductile iron quality EN-GJS-AXNiCr20-2, followed by ferritic ductile iron quality EN-GJS-SiMo4-1, thereafter ferritic ductile iron quality EN-GJS-400-18 and pearlitic ductile iron quality EN-GJS-500-7. Pearlitic gray iron quality EN-GJL-250 shows the worst resistance to oxidation,
- during oxidation at elevated temperatures two oxide layers over the surface of the samples of ductile iron qualities EN-GJS-SiMo4-1 and EN-GJS-AXNiCr20-2 occur. Outward layer is easy detachable and consists of iron oxide. Inward layer is tightly connected with metal matrix and prevents progression of oxidation to the samples inside. This oxide layer consists of Fe_2SiO_4 (fayalite) or complex oxides (Fe, Cr, Ni, Si, and O),
- for all analyzed materials, thickness of oxide layer formed during the heating at 850 °C for 5 h is greater than thickness of oxide layer formed during the heating at 550 °C for 5 h,
- if oxide layer is compact and tightly connected with metal matrix it has a protective effect and prevents progreassion of oxidation to the sample inside,
- during the heating at 550 °C and 850 °C for 5 h in the samples of pearlitic gray iron quality EN-GJL-250, pearlitic ductile iron quality EN-GJS-500-7, ferritic ductile iron quality EN-GJS-400-18 and ferritic ductile iron quality EN-GJS-SiMo4-1 decomposition of pearlite occur and increasing of ferrite content in metal matrix. This phase transformation occur in a greater extent during the heating at 850 °C and results in growth of cast irons,
- ductile iron has higher resistance to elevated temperatures than gray iron due to discontinuous nature of graphite nodules. Continuous nature of graphite lamellas in gray iron allows quick progression of oxidation to the sample inside,
- to achieve a high resistance to oxidation, formation of scale and growth during the application of cast irons at elevated temperatures it is necessary to perform appropriate alloying to obtain full ferritic (alloying with 4,0 – 6,0 % Si) or austenitic (alloying with min. 18,0 % Ni) metal matrix, i.e. avoid formation of pearlite in metal matrix and accompanying phase transformations. For the same graphite shape, austenitic metal matrix gives superior properties than ferritic metal matrix, i.e. allows the application of casting at higher temperatures,
- regarding to severe requests toward automotive industry in regard of increasing of engine efficiency and accompanying increasing of exhaust temperatures, it is obviously that demand for ferritic ductile irons which are alloyed with Si and Mo (SiMo) and austenitic ductile iron which are high-alloyed with Ni will increase. Because of suitable properties of these materials at elevated temperatures, applica-

tion of low-alloyed and high-alloyed gray irons for production turbocharger housings and exhaust manifolds, i.e. automotive engine thermo-mechanical loaded parts will be reduced.

References

[1] Röhrig, K. (2003): Gießtechnik in Motorenbau – Anfoderung der Automobilindustrie, Teil 1. *Gisserei-Praxis*, No. 5, pp. 191–197.

[2] Röhrig, K. (2003): Gießtechnik in Motorenbau – Anfoderung der Automobilindustrie, Teil 2. *Gisserei-Praxis*, No. 5, pp. 255–262.

[3] Röhrig, K. (1987): Temperaturwechselnverhalten von Gußeisenwerkstoffen. *Giesserei-Praxis*, No. 23 - 24, pp. 375–392.

[4] ASM Handbook (1997): *Alloy Cast Iron*, chapter in the book: ASM Handbook Volume Special, Heat-Resistant Materials. ASM International, Metals Park, Ohio.

[5] The Castings Development Centre (1997): Data Handbook for Grey Irons. The Castings Development Centre, England.

[6] Birks, N., Meier, G. H. (1983): *Introduction to High Temperature Oxidation of Metals*. Edward Arnold Ltd, London.

[7] Rio Tinto Iron & Titanium (2004): *The Sorelmetal Book of Ductile Iron*. Rio Tinto Iron & Titanium, Montreal.

[8] Rio Tinto Iron & Titanium (1998): *Ductile Iron Data for Design Engineers*, Rio Tinto Iron & Titanium, Montreal.

[9] Unkić, F., Glavaš, Z., Terzić, K., Bakić, M. (2008): Utjecaj povišenih temperatura na mikrostrukturu željeznih ljevova. *Proceedings Book of 8th International Foundrymen Conference, Development of Foundry Management and Technology.* Metalurški fakultet, Opatija, Paper No. 09.

[10] Weber, G., Faubert, G., Rothwell, M., Tagg, A., Wirth, D. J. (1998): High Si-Mo Ductile Iron: Views from Users and Producers. *Modern Casting*, Vol. 88, No. 3, pp. 48–51.

[11] Li, D., Perrin, R., Burger, G., McFarlan, D., Black, B., Logan, R., Williams, R. (2004): Solidification Behavior, Microstructure, Mechanical Properties, Hot Oxidation and Thermal Fatigue Resistance of High Silicon SiMo Nodular Cast Irons, *2004 SAE World Congress*, Detroit, Paper No. 2004-01-0792.

[12] Black, B., Burger, G., Logan, R., Perrin, R. (2002): Microstructure and Dimensional Stability in Si-Mo Ductile Irons for Elevated Temperature Applications, *SAE International*, Paper No. 2002-01-2115.

[13] Hasse, S. (2008): *Structure of Cast Iron Alloys*, Schiele& Schön GmbH, Berlin.

Crack presence modeling after rolling by genetic programming

Modeliranje prisotnosti razpok z genetskim programiranjem

Miha Kovačič[1, 2], Katja Mačkošek[1, 3], Andrej Mihevc[1, 3], Tomaž Marolt[1]

[1]ŠTORE STEEL d. o. o., Štore, Slovenia
[2]University of Nova Gorica, Laboratory for Multiphase Processes, Nova Gorica, Slovenia
[3]University of Ljubljana, Faculty of Natural Science and Engineering,
Department of Materials and Metallurgy, Ljubljana, Slovenia

Received: December 18, 2009 **Accepted:** January 20, 2009

Abstract: The optimal material processing in steel industry is difficult because of the multi-constituent and multiphase character of the commercial steels, variety of the possible processing paths, and plant specific equipment characteristics. This paper shows implementation of the genetic programming approach for crack presence modeling after rolling. The data (110 samples covering 7 different steel grades) on diffusive annealing, last pass rolling temperature, chemical composition of steel (weight percent of Mn, Cr, Mo and V), steel bar dimensions (width and thickness), heating time of the first and the last batch billet were collected during daily production. The manual ultrasound method was used for crack detection. On the basis of the monitored data a mathematical model for crack presence was developed by genetic programming. For the modeling it was adopt that after the rolling the material was treated equally. According the modeling results it is possible to assume that the material processing after rolling is probably very influential on crack occurrence.

Izvleček: Optimalna obdelava materiala v jeklarstvu je v splošnem otežena zaradi raznolikosti komercialnih jekel, možnih obdelovalnih procesov in specifične obdelovalne in procesne opreme. V članku je opisana uporaba metode genetskega programiranja za modeliranje prisotnosti razpok v jeklu po valjanju. Podatki (110 primerov, 7 različnih kvalitet) so zbrani med dnevno proizvodnjo: kemijska sestava (masni procenti Mn, Cr, Mo in V), širina in debelina palice ter čas ogrevanja prve in zadnje gredice. Prisotnost napak smo ugotavljali z ročnim ultrazvokom. Na podlagi monitoringa podatkov je bil razvit matematični model za ugotavljanje prisotnosti razpok v jeklu. Pri modeliranju smo predpostavili, da je bil postopek po valjanju (ohlajevanje) za ves material enak. Rezultati modeliranja kažejo na to, da je rokovanje po valjanju izredno pomembno za pojav razpok.

Key words: steel, cracks, modeling, genetic programming
Ključne besede: jeklo, razpoke, modeliranje, genetsko programiranje

Original scientific paper

Introduction

The processes in steel industry are often specific and hardly defined according to different production linings and used technologies. There is a strong trend in steel industry for enhanced productivity, safety, and environmental friendliness of the involved processes, in parallel with the enhanced product variety and quality. In the last two decades, the thermo-mechanical physical models are increasingly developed for casting, rolling, and heat treatment operations[1].

The aim of the research was to find out possibilities to control cracks after rolling which occur between cooling process on the cooling bed. Several attempts for cracks control after rolling have been made[2] with also included artificial intelligence approach[4, 5].

According to obscure data on crack presence after rolling and lack of teorethical background in the paper the genetic modeling method for crack presence is proposed. Genetic programming has been successfully implemented into several manufacturing processes[6, 7].

Genetic programming is one of the methods of the evolutionary computation[7]. In the genetic programming, organisms which are more or less complicated computer programs, are subject to adaptation. The computer programs are in fact models for prediction of the hardness after the soft annealing in the present study. Many different prediction models, differing in the quality of prediction and the complexity of the structure, were obtained during the simulated evolution. Only one model out of many is presented in the paper.

Experimental setup

The experiment was performed in the factory Štore Steel Ltd. In the research rolling process was monitored. Rolling process consists of heating, rolling and cooling. The Figure 1 shows rolling mill layout. The number of each steel grade specimens and the average chemical composition (content of Mn, Cr, Mo, and V) is presented in Table 1.

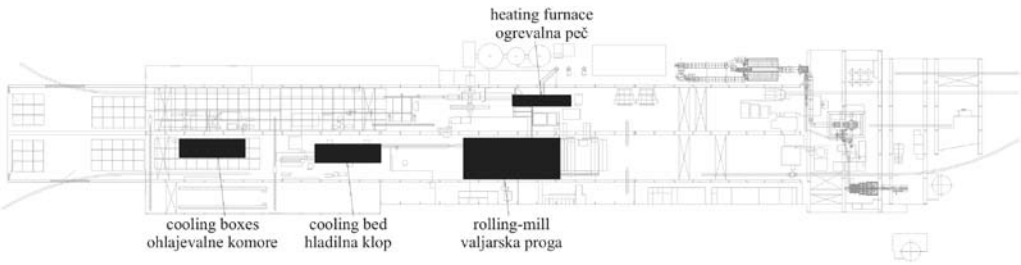

Figure 1. Štore Steel Ltd. rolling mill layout
Slika 1. Tloris Štore Steel d.o.o.

Table 1. The number of each steel grade specimens and average chemical composition and standard deviation
Tabela 1. Število kvalitet vzorcev in povprečna kemijska sestava s standardno deviacijo

Composition			*w*(Mn)/%	*w*(Cr)/%	*w*(Mo)/%	*w*(V)/%
#	Steel grade	Number of specimens				
1	16MnCrS5	1	1,17	0,96	0,01	0
2	20MnCr5	1	1,21	1,16	0,03	0
3	50CrV4	38	1,045 (±0,058)	1,139 (± 0,031)	0,046 (± 0,014)	0,130 (± 0,020)
4	51CrMoV4	66	0,942 (±0,037)	1,071 (± 0,022)	0,177 (± 0,019)	0,118 (± 0,010)
5	51CrV4	2	1,045 (±0,007)	1,130 (± 0,0141)	0,050 (± 0,014)	0,165 (± 0,021)
6	55Si7	1	0,71	0,24	0,04	0
7	ČSN 15230.3	1	0,54	2,27	0,04	0,12
SUM		110				

Before rolling some of the batches were diffusive annealed. Monitored heating parameters were time of the first and the last batch billet heating. The temperature regime in the heating furnace was the same in all cases. The only rolling parameter was the last rolling pass temperature.

The cooling was carried out on the cooling bad and at last in cooling boxes. In the cooling boxes the bars were in general isolative covered. The exact data on covering the bars could not be obtained. The cooling is also dimension dependent, so the bar width and thickness were also recorded.

After the cooling the manual ultrasound method (Krautkrämer USM-22 ultrasound device) for each bar was used for crack detection. That bar was taken from the bond

Table 2. Experimental data
Tabela 2. Eksperimentalni podatki

#	Diffusive annealing	Last rolling pass temperature, T/°C	*w*(Mn) /%	*w*(Cr) /%	*w*(Mo) /%	*w*(V) /%	Width, *a*/mm	Thickness, *d*/mm	First batch billet heating time t_{fb}/min	Last batch billet heating time t_{lb}/min	Crack presence
1	1	960.0	0.920	1.060	0.200	0.130	11.0	44.0	134.0	134.0	1
2	0	817.0	0.940	1.080	0.170	0.120	100.0	77.0	172.0	184.0	1
3	0	862.0	1.040	1.140	0.040	0.180	100.0	35.0	258.0	258.0	1
4	0	887.0	0.970	1.110	0.040	0.150	100.0	40.0	163.0	164.0	1
5	0	869.0	0.920	1.080	0.020	0.180	100.0	42.0	106.0	152.0	1
	…	…	…	…	…	…	…	…	…	…	…
106	1	942.0	0.910	1.040	0.170	0.120	100.8	56.0	118.0	120.0	0
107	0	850.0	1.060	1.150	0.040	0.120	99.6	50.0	127.0	127.0	0
108	0	833.0	1.040	1.120	0.050	0.140	100.1	51.0	129.0	126.0	0
109	1	935.0	0.990	1.080	0.180	0.110	100.0	60.0	124.0	124.0	0
110	0	897.0	0.880	1.010	0.190	0.110	75.0	32.0	98.0	95.0	0

from the cooling box. Whole bond was inspected. The Table 2 shows collected experimental data. Each bond was identified by its identification number from 1 to 110. If the crack in any bar from the bond was found the crack presence in the Table 2 was marked with value 1 and absence with 0, respectively. Also the diffusive annealing treated material before heating process is marked with value 1.

Crack presence modeling

Genetic programming is probably the most general evolutionary optimization method[[7]]. The organisms that undergo adaptation are in fact mathematical expressions (models) for hardness after soft annealing prediction consisting of the available function genes (i.e., basic arithmetical functions) and terminal genes (i.e., independent input parameters, and random floating-point constants). In our case the models consist of: function genes of addition (+), subtraction (-), multiplication (*) and division (/), terminal genes of diffusive annealing (*DA*), last pass rolling temperature (*T*), chemical composition of steel (Mn, Cr, Mo and V), steel bar dimensions width (*width*) and thickness (*thick*), heating time of the first (t_{fb}) and the last batch billet (t_{lb}).

Random computer programs of various forms and lengths are generated by means of selected genes at the beginning of simulated evolution. Afterwards, the varying of computer programs during several iterations, known as generations, by means of genetic operations is performed. After completion of varying of computer programs a new generation is obtained that is evaluated and compared with the experimental data, too.

The result of models for crack presence prediction more than zero predicted crack presence (value 1), otherwise crack absence (value 0). Evaluation of models were determined by Bayesian analysis (true positive *TP*, true negative *TN*, false positive *FP*, false negative *FN*) applying sensitivity $SENS = TP/(TP+FN)$, specificity $SPEC = TN/(FP+TN)$, positive predictive value $PPV = TP/(TP+FP)$ and negative predictive value $NPV = TN/(FN+TN)$. Models with higher *SPEC*, *SENS*, *PPV*, *NPV* have higher probability to contribute in operations of reproduction and crossover.

The process of changing and evaluating of organisms is repeated until the termination criterion of the process is fulfilled. This was the prescribed maximum number of generations.

For the process of simulated evolutions the following evolutionary parameters were selected: size of population of organisms 500, the greatest number of generation 200, reproduction probability 0.4, crossover probability 0.6, the greatest permissible depth in creation of population 6, the greatest permissible depth after the operation of crossover of two organisms 10 and the smallest permissible depth of organisms in generating new organisms 2. Genetic operations of reproduction and crossover were used. For selection of organisms the tournament method with tournament size 7 was used.

We have developed 100 independent civilizations of mathematical models for prediction of the crack presence. Only the best one out of 100 is presented here:

$$\frac{\left(DA+\frac{-tfb+tlb}{Cr}+Cr\left(Cr+DA-DA^2+\frac{tfb-tlb}{-MoT+DA\cdot tfb+thick}\right)+\frac{-tfb+tlb}{DA^2-MoT+thick+Mo\left(DA^2+\frac{-tfb+tlb}{DA\cdot T-Mo\cdot T+thick}\right)+width}\right)}{\left(\left(Cr+Cr\cdot Mn\left(DA+\frac{-tlb+(DA+Mn)tlb}{T}\right)\right)\cdot\left(T+Cr^2(7.6572+D+Mn-DA\cdot Mo\cdot T+Mo\cdot tfb+thick-Mo\cdot tlb)\cdot\left(\left(DA^2+\frac{-tfb+Cr\cdot tlb}{T}\right)\cdot\left(-Mo\cdot T+thick+width\left(DA^3+\frac{-tfb+tlb}{DA\cdot T-Mo\cdot T+thick}\right)+width\right)\right)\right)\right)}$$

with sensibility of 0.8545, specificity 0.8182, positive predictive value 0.8246, negative predictive value 0.8491 and test efficiency 0.8363.

The results about the best models in 100 civilizations are collected in Table 3.

Table 3. The best models in civilizations results
Tabela 3. Rezultati najboljših modelov civilizacij

	Test efficiency	Sensibility	Specificity	Positive predictive value	Negative predictive value
AVERAGE	0,746	0,703	0,789	0,776	0,732
STDEV	0,0398	0,093	0,0824	0,0547	0,0523
MAX	0,836	0,891	0,909	0,878	0,867
MIN	0,663	0,491	0,564	0,636	0,632

CONCLUSIONS

In this study genetic programming approach was applied for crack presence prediction. In genetic programming mathematical expressions (models for crack presence prediction) undergo adaptation. During simulated evolution models gradually improve. Experimental data set (110 samples) was used to obtain the model for crack presence prediction. Evaluation of models was determined by Bayesian analysis. Average values of all 100 models were: sensibility 0.7033, specificity 0.7898, positive predictive value 0.7764, negative predictive value 0.7321 and test efficiency 0.7466. The best model values are: sensibility of 0.8545, specificity 0.8182, positive predictive value 0.8246, negative predictive value 0.8491 and test efficiency 0.8363.

According to the results of the modeling it is possible to conclude that there are some more influential parameters, witch were not monitored during research, or that the experimental data, especially on cooling process, is obscure. So further researches

will be based on cooling parameters precise analysis and their mutual dependence. In addition, parameters optimization could be possible.

Povzetek

V tej študiji smo uporabili genetsko programiranje za napovedovanje prisotnosti razpok. Pri genetskem programiranju so matematični izrazi (modeli za napovedovanje prisotnosti razpok) izpostavljeni prilagajnju. Med simulirano evolucijo modeli postopoma napredujejo. Modeliranje je bilo izvedeno na podlagi 110 primerov. Modele smo ovrednotili z Bayesovo analizo. Povprečne vrednosti vseh 100 modelov so: občutljivost 0.7033, specifičnost 0.7898, pozitivna sposobnost napovedovanja 0.7764, negativna sposobnost napovedovanja 0.7321 in učinkovitost modela 0.7466. Vrednosti najboljšega modela pa so: občutljivost 0.8545, specifičnost 0.8182, pozitivna sposobnost napovedovanja 0.8246, negativna sposobnost napovedovanja 0.8491 in učinkovitost modela 0.8363.

Glede na rezultate modeliranja je možno zaključiti, da obstajajao vplivni parametri, ki jih med raziskavo nismo spremljali ali pa da so obstoječi podatki, vsaj pri ohlajevanju na hladilni klopi in hladilnih komorah, pomanjkljivi. Zato bi bilo potrebno podrobneje analizirati parametre ohlajevanja in njihovo soodvisnost. Dodatno bi lahko izvedli tudi optimizacijo le-teh.

References

[1] Verlinden, B., Driver, J., Samajdar, I., Doherty, R. D. (2007): T*hermo-mechanical Processing of Metallic Materials*; Elsevier, Amsterdam.

[2] Sekhar, A. S. (2008): Multiple cracks effects and identification. *Mechanical Systems and Signal Processing*; Vol. 22, 845–878.

[3] Perera, R., Ruiz. A. (2008): A multistage FE updating procedure for damage identification in large-scale structures based on multiobjective evolutionary optimization. *Mechanical Systems and Signal Processing*; Vol. 22, 845–878.

[4] Sterjovski, Z., Pitrun, M., Nolan, D., Dunne, D., Norrish, J. (2007): Artificial neural networks for predicting diffusible hydrogen content and cracking susceptibility in rutile flux-cored arc welds. *Journal of Materials Processing Technology*; Vol. 184, 420–427.

[5] Kovačič, M., Brezočnik, M., Turk, R. (2005): Modeling of hot yield stress curves for carbon silicion steel by genetic programming. *Materials and manufacturing processes*; Vol. 20, 1–10.

[6] Kovačič, M., Uratnik, P., Brezočnik, M., Turk, R. (2007): Prediction of the bending capability of rolled metal sheet by genetic programming. *Materials and manufacturing processes*; Vol. 22, 634–640.

[7] Koza, J. R. (1999): Genetic programming III. *Morgan Kaufmann*, *San Francisco*, 1154 p.

Calculation of thermodynamic properties for ternary Ag–Cu–Sn system

Saša Marjanović[1], Dragan Manasijević[1], Dragana Živković[1], Dragoslav Gusković[1], Duško Minić[2]

[1]University of Belgrade, Technical Faculty, Dept. of Metallurgy, VJ 12, 19210 Bor, Serbia;
E-mail: smarjanovic@tf.bor.ac.yu
[2]University of Pristina, Faculty of Technical Sciences, 38220 Kosovska Mitrovica, Serbia

Received: January 13, 2009 **Accepted:** February 17, 2009

Abstract: Results of thermodynamic properties calculations for the liquid alloys in ternary Ag–Cu–Sn system are presented in this paper. The general solution model has been used for the thermodynamic prediction in the sections from each component corner, with the molar ratio of the other two components 1:9, 3:7, 1:1, 7:3, 9:1, for which characteristic thermodynamic quantities have been obtained at temperature 1473 K.

Key words: Ag–Cu–Sn alloys, thermodynamics, general solution model

Introduction

The Ag–Cu–Sn system is fundamental to the development of technology of lead-free solder alloys. Recent legislations in many countries to eliminate the use of lead containing solder alloys have created renewed interest in this system, especially in the Sn rich region.

This system has rather already been investigated. Thus, Yen and Chen[1] have determined phase equilibria of the Ag–Sn–Cu ternary system experimentally as well as using the calculation of phase diagram (CALPHAD) method. Ohnuma et al.[2] have presented the phase equilibria and the related thermodynamic properties of the Sn–Ag–Cu alloys using a thermodynamic database for micro-soldering alloys that consists of the elements Pb, Bi, Sn, Sb, Cu, Ag, Zn and In. Hirose et al.[3] have investigated joint strength and interfacial microstructure between Sn–Ag–Cu and Sn–Zn–Bi solders and Cu substrate. Dutkiewicz et al.[4] have investigated rapid quenching and mechanical alloying of eutectic Ag–Cu–Sn alloys. He and Ding[5] have investigated Ag–Cu–Sn brazing filler metals. Also, Moon et al.[6] have investigated experimentally and made thermodynamic assessment of Sn–Ag–Cu solder alloys.

The latest thermodynamic assessment of Ag–Cu–Sn ternary system is work of Gisby and Dinsdale[7] carried out prior the COST 531 Action[8] and included in COST 531 Database for Lead Free Solders[9] and

Original scientific paper

in COST 531 Atlas of Phase Diagrams for Lead-Free Soldering[10]. The calculated binary systems and liquidus projection of ternary Ag–Cu–Sn system according to Reference[10] are shown in Figure 1. The phase diagram of the Ag–Cu binary system is rather simple without intermediate phases and the phase diagrams of the Ag–Sn and Cu–Sn are complex with appearance of many intermediate phases.

In this paper, in order to investigate thermodynamic behavior of liquid Ag–Cu–Sn alloys and its relationship with phase structure of solidified alloys, several integral and partial thermodynamic functions were calculated using Chou's general solution model. Obtained results were discussed in connection with a mutual reactivity of the components in investigated ternary system.

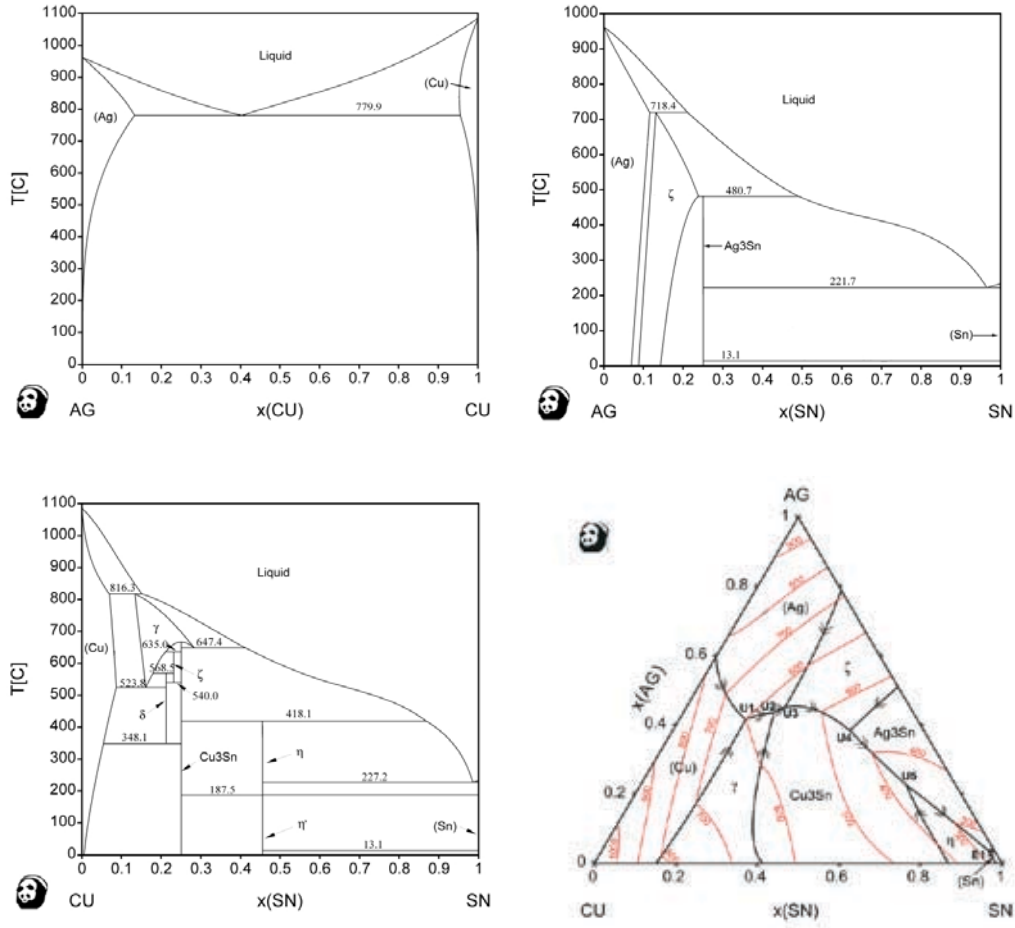

Figure 1. Phase diagrams of the boundary binary systems, and the liquidus projection of the ternary Ag–Cu–Sn system[10]

THEORETICAL FUNDAMENTALS

There are several traditional models to extrapolate thermodynamic properties of the ternary system based on the three constitutive binary systems, which are classified, according to HILLERT[11], into two categories: symmetrical (KOHLER[12], MUGGIANU[13]) and asymmetrical (TOOP[14], HILLERT[11]).

The use of a symmetrical model when an asymmetrical model is more appropriate can often give rise to errors. Categorization of the investigated ternary system in the one of these two categories is, in some cases and in the lacking of the adequate experimental data, uncertain task. Also, a different choice of an arrangement of the three components to the three apexes of triangle in the case of the asymmetric model application will lead to a different result of the ternary Gibbs energy of mixing. From this reasons CHOU[15,16] proposed a new model, based on the "similarity coefficient concept", which advantage is that its application does not require predetermination if a system is symmetrical or not, neither choice of the symmetric and asymmetric components in the particular ternary system. The correctness of this model has already been confirmed in some practical examples[17–19]. Therefore this model is applied for the calculation of the thermodynamic properties of the liquid Ag–Cu–Sn ternary system.

The basic equation of general solution model developed by CHOU is given as follows (in detail see References[15,16]):

$$\Delta G^E = x_1x_2\,(A^o_{12} + A^1_{12}\,(x_1\text{-}x_2) + A^2_{12}\,(x_1\text{-}x_2)^2) + x_2x_3\,(A^o_{23} + A^1_{23}\,(x_2\text{-}x_3) + A^2_{23}\,(x_2\text{-}x_3)^2) + x_3x_1\,(A^o_{31} + A^1_{31}\,(x_3\text{-}x_1) + A^2_{31}\,(x_3\text{-}x_1)^2) + f x_1x_2x_3 \quad (1)$$

where ΔG^E is an integral excess Gibbs energy for a ternary system, x_1, x_2, x_3 are the mole fractions of a ternary alloy, A^o_{ij}, A^1_{ij}, A^2_{ij} are regular-solution type parameters for binary system "ij" and can be temperature dependent.

The function f is the ternary interaction coefficient expressed by:

$$f = (2\xi_{12} -1)\{A^2_{12}\,((2\xi_{12} -1)x_3 + 2(x_1\text{-}x_2)) + A^1_{12}\} + (2\xi_{23} -1)\{A^2_{23}\,((2\xi_{23} -1)x_1 + 2(x_2\text{-}x_3)) + A^1_{23}\} + (2\xi_{31} -1)\{A^2_{31}\,((2\xi_{31} -1)x_2 + 2(x_3\text{-}x_1)) + A^1_{31}\} \quad (2)$$

where ξ_{ij} are the similarity coefficients defined by η_i called the deviation sum of squares:

$$\xi_{ij}=\eta_i/(\eta_i+\eta_j) \quad (3)$$

where are:

$$\eta_I = \int_0^1 (\Delta G^E_{12} - \Delta G^E_{13})^2\,dX_1$$

$$\eta_{II} = \int_0^1 (\Delta G^E_{21} - \Delta G^E_{23})^2\,dX_2$$

$$\eta_{III} = \int_0^1 (\Delta G^E_{31} - \Delta G^E_{32})^2\,dX_3 \quad (4)$$

and

$$X_{1(12)} = x_1 + x_3\xi_{12}$$
$$X_{2(23)} = x_2 + x_1\xi_{23}$$
$$X_{3(31)} = x_3 + x_2\xi_{31} \quad (5)$$

Results and discussion

The thermodynamic calculation were performed using general solution model, in the sections from each component corner with the molar ratio of the other two components 1:9, 3:7, 1:1, 7:3, 9:1 at chosen temperature 1473 K. This temperature is appropriate for analysis of atomic interaction in liquid phase because it is not too high. The starting data values of Redlich-Kister parameters of the liquid phases of the binary systems Ag–Cu, Ag–Sn, and Cu–Sn are shown in Table 1.

For the calculation of integral excess Gibbs energy using Chou's model we arbitrary adopted following settings of components: Ag-component 1, Cu-component 2 and Sn-component 3. Therefore the Redlich-Kister parameters (named with L_{ij} in Table 1) for the Ag(1) – Cu(2) and Cu(2) – Sn(3) binary systems are identical to regular-solution type parameters appearing in Chou's model (named with A_{ij} in Eqs. 1,2). Only for the second parameter in the Sn(3) – Ag(1) binary system stands following relation $A_{ij} = -L_{ij}$. Calculated regular-solution type parameters for constitutive binaries, deviation sum of squares and similarity coefficients for the ternary Ag–Cu–Sn system at 1473 K are presented in Table 2.

Using the values from Table 1 and Equation 1 ΔG^E functions for boundary binary systems and chosen ternary sections at 1473 K were calculated and shown in Figure 2.

Table 1. The Redlich-Kister parameters for boundary binary systems

Parameter	Ag–Cu[20,21]	Ag–Sn[22]	Cu–Sn[23]
L^0_{ij}	+ 17384.37 – 4.46438 T	– 5146.7 – 5.0103T	– 9002.8 – 5.8381 T
L^1_{ij}	+ 1660.74 – 2.31516T	– 15799.3 + 3.3208 T	– 20100.4 + 3.6366 T
L^2_{ij}	-	– 6687.5	– 10528.4

Table 2. Regular-solution type parameters for Ag–Cu, Cu–Sn and Sn–Ag binaries, deviation sum of squares and similarity coefficients for the ternary Ag–Cu–Sn system at 1473 K (Ag–Cu–Sn set in 1–2–3 order).

A^0_{AgCu}	A^1_{AgCu}	A^2_{AgCu}	η_I	$\xi_{Ag\text{-}Cu}$
10808.34	1749.491	0	2.01E+07	0.391709
A^0_{CuSn}	A^1_{CuSn}	A^2_{CuSn}	η_{II}	$\xi_{Cu\text{-}Sn}$
– 17602.3	– 14743.29	– 10528.4	3.12E + 07	0.881417
A^0_{SnAg}	A^1_{SnAg}	A^2_{SnAg}	η_{III}	$\xi_{Sn\text{-}Ag}$
– 12526.9	10907.76	– 6687.5	4200970	0.172818

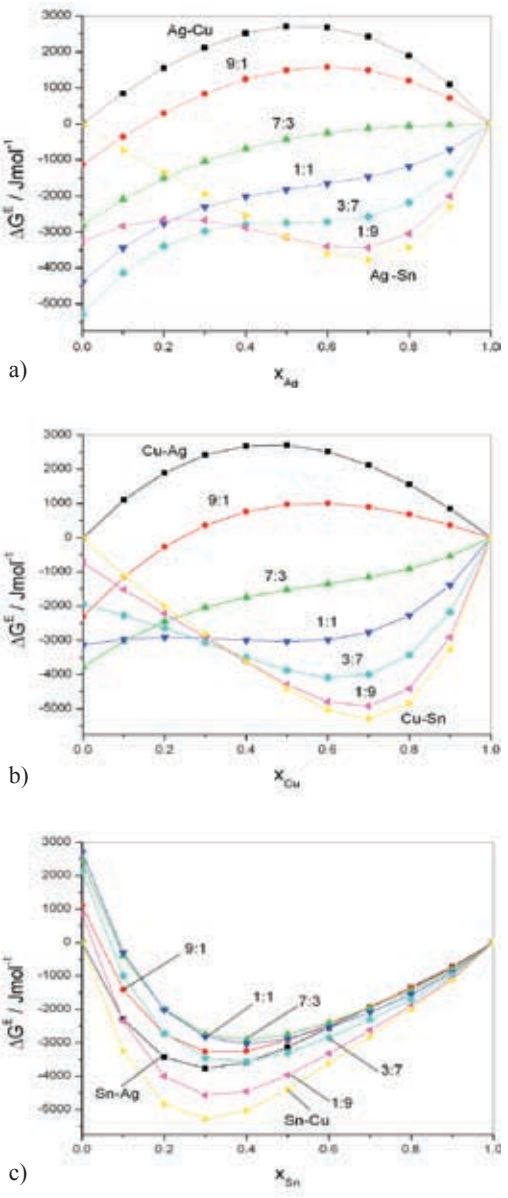

Figure 2. Dependence of ΔGE on molar fraction of Xi for three binary systems and chosen ternary sections at 1473 K (a – Ag-corner, b – Cu-corner, c – Sn-corner)

In Figure 2 it can be observed that Cu–Ag binary system has positive values ΔG^E in whole concentration range, while the other two constitutive binary systems have negative values ΔG^E. According to this, chemical interaction between atoms Sn on one side and atoms Cu and Ag on the other side is much stronger than chemical interaction between atoms Cu and Ag. This causes that in solid state Ag and Cu do not make any new intermediate phases while Sn with both Cu and Ag forms a series of intermediate phases. This tendency is held in ternary system. According to the liquidus projection of the Ag–Cu–Sn system, shown in Figure 1, for the alloys with low concentration of Sn, primary crystallization phases are solid solutions based on Ag and Cu and for alloys with moderately and high concentration of Sn primary crystallization phases are intermediate phases based on Sn.

According to calculated dependence of G^{xs} of composition, and using equations (4) and (5), partial thermodynamic quantities have been obtained.

$$G^{xs}_i = G^{xs} + (1 - x_i)\,(\partial G^{xs}/\partial x_i) \qquad (6)$$

$$G^{xs}_i = RT \ln(a_i / x_i) \qquad (7)$$

Dependence of the partial molar Gibbs free energies on composition of each component at 1473K is shown in Figure 3.

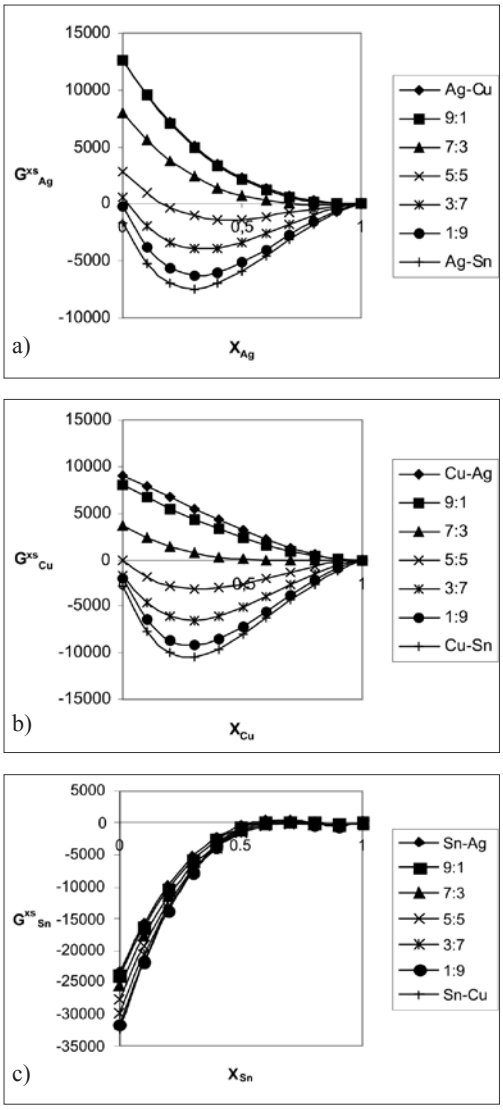

Figure 3. Dependence Gxsi on composition of components for all observed sections in Cu–Ag–Sn system at 1473 K(a – Ag-corner, b – Cu-corner, c – Sn-corner)

Further calculation involves determining the dependence of activity of components of composition in the observed sections of the ternary Cu–Ag–Sn system.

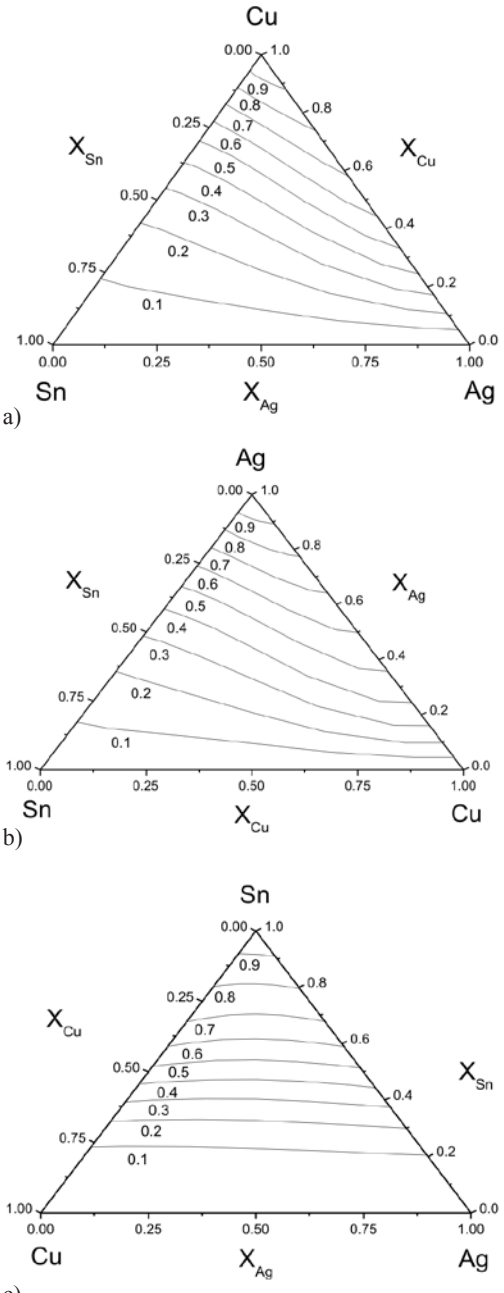

Figure 4. Iso-activity lines for Cu (a), Ag (b), and Sn (c) in ternary Cu–Ag–Sn system at 1473 K

The calculated activities of the components in Cu–Ag–Sn system at 1473K indicate that activities of Ag and Cu decrease rapidly with increase of Sn content in ternary alloys. Minimum of thermodynamic activity Ag and Cu achieve in boundary Ag–Sn and Cu–Sn systems which is in agreement with their strong chemical affinity toward Sn. Variation of Ag and Cu concentration in ternary Ag–Cu–Sn alloys has much less influence on Sn activity.

Iso-activity lines for Cu, Ag, and Sn at 1473 K that illustrate previously mentioned facts are shown in Figure 4.

Conclusions

Thermodynamic analysis of the liquid Cu–Ag–Sn alloys has been carried out with geometrical Chou's general solution model for predicting the thermodynamic quantities of ternary alloys according to known thermodynamic quantities of the constituting binary systems. Integral excess Gibbs free energies for fifteen distinguished sections at 1473 K have been calculated. Further calculation has involved obtaining of the partial molar Gibbs free energies, and diagrams of iso-activity lines for all three components have been constructed.

It has been determined that thermodynamic properties of the constituting binary systems define thermodynamic behavior of the ternary system alloys, and that chemical affinities between the elements in binary systems remain in ternary alloys, as well.

Presented results can be used for comparison with future experimental results in order to determine the deviation and to define ternary interaction parameters.

Acknowledgement

The authors are grateful to the Ministry of Science of the Republic of Serbia (Project N^{0}142043) for financial support.

References

[1] Yen, Y., Chen, S. (2004): *Journal of Materials Research* 19 (8), pp. 2298–2305.

[2] Ohnuma, I., Miyashita, M., Anzai, K., Liu, X. J., Ohtani, H., Kainuma, R., Ishida, K. (2000): *J. Electron. Mater.*, 2000, 29 (10), pp. 1137–1144.

[3] Hirose, A., Yanagawa, H., Ide, E., Kobayashi, K. F. (2004): *Science and Technology of Advanced Materials*, 5 (1-2), pp. 267–276.

[4] Dutkiewicz, J., Lityfiska, L., Swiatek, R. (1995): *Journal of Materials Processing Technology*, 53, pp. 131–138.

[5] He, Z., Ding, L. (1997): *Materials Chemistry and Physics*, 49, pp. 1–6.

[6] Moon, K. W., Boettinger, W. J., Kattner, U. R., Biancaniello, F. S., Handwerker, C. A. (2000): *Journal of Electronic Materials*, 29 (10), pp. 1122–1136.

[7] Gisby, J. A., Dinsdale, A. T. *unpublished research*.

[8] Lead-free Solder Materials-COST Action 531 (http://www.univie.ac.at/cost531/)

[9] Dinsdale, A. T., Kroupa, A., Vízdal, J., Vrestal, J., Watson, A., Zemano-

va, A. (2008): *COST531 Database for Lead-free Solders, Ver. 3.0*, unpublished research.

[10] Dinsdale, A. T., Watson, A., Kroupa, A., Vrestal, J., Zemanova, A., Vizdal J. (Eds.) (2008): *COST Action 531-Atlas of Phase Diagrams for Lead-free Solders*, Vol. 1, Brno, Czech Republic.

[11] Hillert, M. (1980): *Calphad* 4, p. 1.

[12] Kohler, F. (1960): *Monatsh. Chem.* 91, p.738.

[13] Muggianu, Y. M., Gambino, M., Bross, J. P. (1975): *J. Chimie Physique* 72, p.83.

[14] Toop, G. W. (1965): *Trans. Met. Soc.* AIME 233, p.850.

[15] Chou, K. C. (1995): *Calphad*, 19 (3), pp. 315–325.

[16] Chou, K. C., Li, W. C., Li, F., He, M. (1996): *Calphad*, 20, p. 395.

[17] Katayama, I., Yamazaki, K., Nakano, M., Iida, T. (2003): *Scan. J. Metall*., 32.

[18] Živković, D., Katayama, I., Kostov, A., Živković, Ž. (2003): *J. Thermal Analysis and Calorimetry*, 71, p. 567.

[19] Živković, D., Živković, Ž., Šestak, J. (1999): *Calphad,* 23, p. 113.

[20] Hayes, F. H., Lukas, H. L., Effenberg, G., Petzow, G. (1986): *Z. Metallkde.* 77, pp. 749–754.

[21] Lukas, H. L. (1998): *Unpublished work.*

[22] Shim, J. H., Oh, C. S., Lee, B. J., Lee, D. N. (1996): *J. Alloys and Compounds*, 238, pp.155–166.

[23] Liu, X. J., Liu, H. S., Ohnuma, I., Kainuma, R., Ishida, K., Itabashi, S., Kameda, K., Yamaguchi, K. (2001): *J. Electron. Mater*., 30(9), p. 1093.

Compositional trends and rare metal (Ta-Nb) mineralization potential of pegmatite and associated lithologies of Igbeti area, Southwestern Nigeria

Olugbenga A. Okunlola[1], Matthew O. Oyedokun[1]

[1]University of Ibadan, Department of Geology, Ibadan, Nigeria

Received: December 07, 2008 **Accepted:** February 03, 2009

Abstract: The increase in global demand for rare metal Ta-Nb deposits has created the need for renewed search for economically viable deposits. This study therefore, involves petrographic and geochemical evaluation of near flat lying pegmatite veins intruding gneisses, schists and granitic rocks around Igbeti area, southwestern Nigeria. This is with a view to determine their compositional characteristics and rare metal Ta-Nb potential.

A total of 24 samples comprising whole rock pegmatites and mineral extracts of albite, mica and tourmaline were analysed for major, trace and rare earth elements using Inductively Coupled Plasma-Mass Spectrometry technique (ICP-MS). From the results, the whole rock pegmatite is considerably siliceous, but with noticeable depletion of silica in the tourmaline extract. Average Fe_2O_3, MgO and MnO values are low in all the samples. Trace element analysis also reveal Ta-Nb enrichment in all the samples (>246 μg/g) with highest values in the tourmaline phase and lowest values in the whole rock pegmatite. Similarly, Cs values are highest in the tourmaline extracts, but Ti, Ba and Zr values are generally low. All samples analysed reveal that the pegmatites are magmatic with evidence of late metasomatic alterations with appreciable degree of fractionation and mineralization as indicated in the low K/Cs (0.04) Th/U (0.08) and K/Rb (0.001) values. Also, from plots of Ta/(Ta+Nb)/Mn/(Mn+Fe), and other bulk geochemical features, the pegmatite is complex, of the rare element class and belongs to the Lithium, Ceasium Tantalum (LCT) petrogenetic family. Furthermore, variation plots involving K, Rb, Ta, Ga, Cs, and W show enhanced Ta-Nb mineralization potential comparable to world class Tanco and Noumas deposits.

Compositional trends within the various mineral phases analysed indicate preffered enrichment in the tourmaline, mica, and albite phases in that order respectively.

Key words: pegmatite, Ta-Nb, mineralization, fractionation, tourmaline

Original scientific paper

Introduction

Pegmatites are known to host many metallic and non-metallic (industrial) minerals that are of great economic benefits. Consequently, the increase in global demand for these minerals especially the rare metals (Ta-Nb-Sn), has led to the renewed interest in the search for economically viable deposits in Nigeria (Okunlola, 1998; Adekoya et. al., 2003; Ajayi and Ogedengbe, 2003; Garba, 2003; Okunlola and Ogedengbe, 2003; Okunlola, 2005; Okunlola and Jimba, 2006; Okunlola and Ofonime, 2006; Okunlola and Somorin, 2006). In Nigeria, Precambrian pegmatites occur mostly in the western half of Nigeria along a NNE – SSW trending belt (Jacobson and Webb, 1964). However, recent studies such as those of Garba, (2003) and Okunlola, (2005), have shown that they also occur on a minor scale in the southeast and northeastern parts. The pegmatite bodies and associated rocks of this study area which is part of the Iseyin Oyan schist belt (one of the prominent belts of the metasedimentary belt of Nigeria) and the Oke-Ogun Ta-Nb field (Okunlola, 2005) were thus studied with a view to elucidate their compositional features and rare metal Ta-Nb economic potentials. This, it is hoped will add to the inventory of data of productive rare metal pegmatites. Okunlola, (2005) earlier had defined the metallogeny of the Nigerian rare metal bearing pegmatites outlining seven broad fields namely; Kabba-Isanlu, Ijero-Aramoko, Keffi-Nassarawa, Lema-Ndeji, Oke-Ogun, Ibadan–Osogbo and the Kushaka-Birnin Gwari fields.

Materials and methods

The study involves systematic geological mapping, and thin section examinations of 10 pegmatite samples. Also, geochemical analysis of schists, gneiss, the whole rock pegmatite and extracts of mineral components albite, muscovite and tourmaline extracted from the pegmatites were carried out for major, trace and rare earth elements at the Activation laboratories, Ontario, Canada using the ICP-AES instrumentation method. All the samples were dried at 60 ^{o}C, crushed and dried to –80 mesh (–177 μm). The analytical procedure involves a sample weight of 0.5 g put in a platinum crucible. 5 mL of perchloric acid ($HClO_3$), trioxonitrate (V) (HNO_3) and 15 mL of hydrofluoric acid (HF) are added. The solution is stirred properly and allowed to evaporate as it is heated at a lower temperature for some hours. Four ml of hydrochloric acid (HCl) was then added to the cooled solution and warmed to dissolve the salts. On cooling, the solution was diluted to 50 ml with distilled water. The solution is then introduced into the ICP torch as an aqueous aerosol. The emitted light by the ions in the ICP was converted to an electric signal by a photomultiplier in the spectrometer. The intensity of the electrical signal produced by emitted light from the ions was compared to a standard or control (a previously measured intensity of a known concentration of the elements) This quality control incorporates a sample prep blank as the first sample and a pulp duplicate to monitor analytical precision which is carried through all the stages of preparation to analysis.

A total of 30 samples were analyzed comprising 3 samples each of granite and schist and 6 samples each of whole rock pegmatite, mica, tourmaline and albite extracted from the pegmatite. Care was taken to ensure that the mineral extracts were obtained from only fresh coarse grained pegmatite samples containing grains >2 cm of each of these mineral components. Initial diasaggregation was done by a hand held hammer with the final separation into the different mineral components done by hand.

RESULTS AND DISCUSSION

The study area, lies within the southwestern part of the reactivated Pre Cambrian basement complex of Nigeria. The Nigeria basement complex forms part of the Pan-African mobile belt, which lies to the east of the West African Craton (Figure 1). Despite contrasting documentation of the evolution of the basement complex of Nigeria, they could be loosely categorized into three major groups namely: Gneiss Quartzite Complex: comprising biotite and biotite hornblende gneisses, quartzites and quartz schist. Schist Belts: comprising paraschists and meta-igneous rocks, which include phyllitic schists, amphibole schists, amphibolites, talcose rocks, and marble and calc-silicate rocks. They are mainly N-S to NNE-SSW trending belts of low grade supracrustal and minor volcanic assemblages. The Older granites include granite, granodiorite, diorite, charnockite, pegmatites and aplites. In the study area, as revealed from systematic mapping on

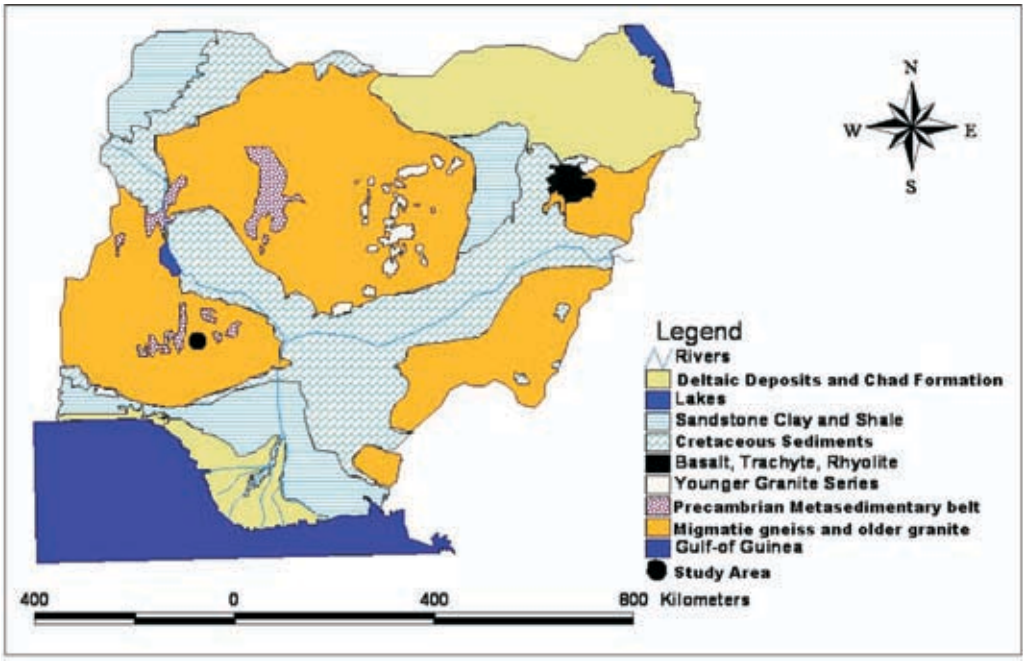

Figure 1. Geological Map of Nigeria Showing Location of the Study Area

a scale of 1 : 20000, biotite schists, augen gneiss, granites and semi discordant intrusive dykes of pegmatite veins which intrude other rock units especially in the northern parts are the main rock units (Figure 2). Schistose rocks are more prominent in the central and the northern parts of the study area. They are low lying, with schistose quartzites and biotite schists predominating. Mineralogically, they are mostly made up of quartz, garnet, biotite, muscovite, microcline, and accessory opaques. The granites also occur as coarse grained to porphyritic sometimes extensively weathered rock with biotite, microcline, and quartz being the main minerals.

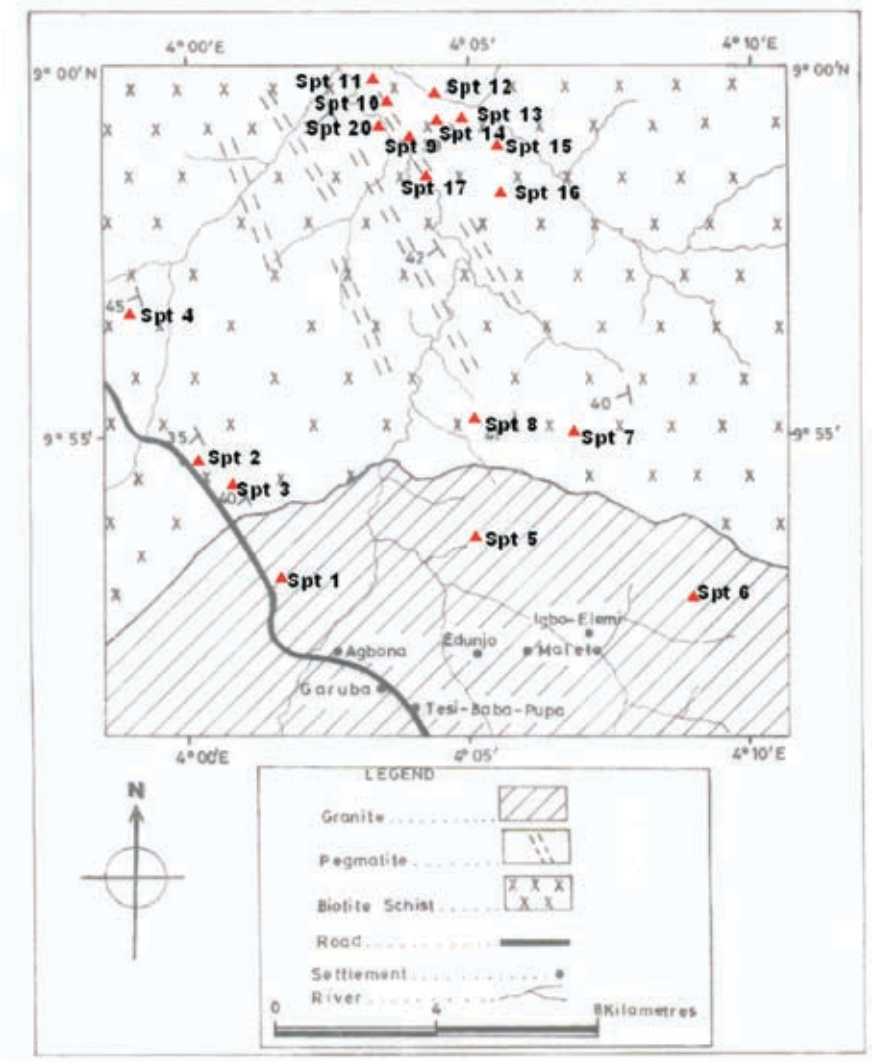

Figure 2. The location map of study area showing geology, drainage pattern and sampling points

Pegmatites occur as leucocratic tabular veins trending mostly NNW-SSE and ranging from medium to coarse grained texturally. They are more predominant in the northern parts intruding the schistose rocks (Figure 2). They range in size from about 50–200 m long and about 10–50 m wide in places. Petrographic studies reveal a mineral assemblage of mainly quartz, albite, microcline, muscovite, and tourmaline with accessory opaques mainly columbotantalite, rutiles, and magnetite. Garnets and zircon make up the accessory composition. Quartz exhibits euhedral shape, cloudy to colourless with evidence of poikilitic intergrowth of feldspar. Albite exhibits characteristic albite twinning with grains showing some stretching (Figure 3). Crosshatched twinning is also displayed in the microcline with perthitic texture common in the feldspars. Muscovite occurs as elongated tiny plates mostly interstitial between the quartz and the albite, it also exhibits perfect cleavage in one direction and strong birefringence colors. The modal composition of 10 samples of whole rock from 5 sample points each on the thin section of the pegmatite is shown in Table 1.

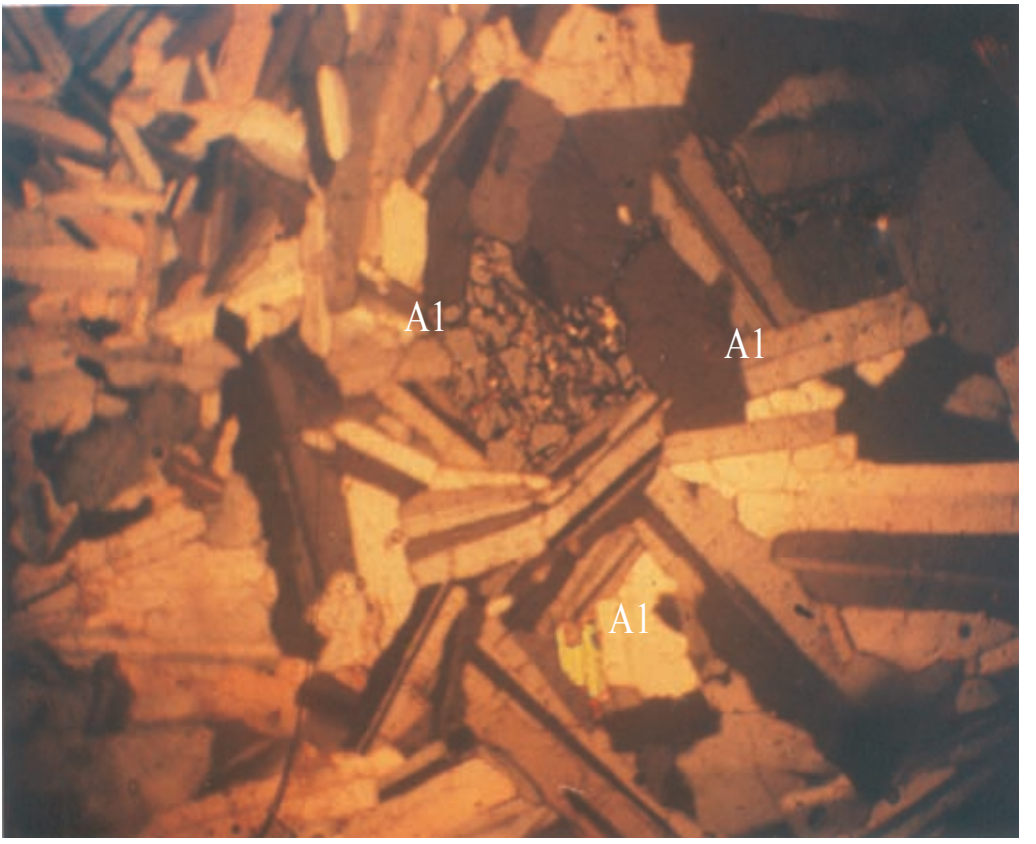

Figure 3. Photomicrograph of pegmatite in transmitted light, showing predominance of albite (Al) and interstitial muscovite (M) minerals

Table 1. Modal composition of minerals of the pegmatite from the study area

Minerals	Composition (%) (n = 10)	
	Range	Average
Quartz	15–25	20
Albite	26–45	35
Microcline	10–18	15
Tourmaline	6–12	10
Muscovite	8–18	15
Accessories	1–6	5
Total		100

The analytical results of major, trace and rare elements which are presented in Tables 2 and 3 show average SiO_2 values of 63.02 %, 69.88 %, and 69.61 % in the whole rock, albite and muscovite samples respectively. However there is a noticeable depletion in the tourmaline extracts with minimal variation in their values. The SiO_2 values of the whole rock and mica values are slightly lower than average for Nigeria's Ta-Nb pegmatite (Okunlola, 2005) but compares with those of Komu area, also within the Oke-Ogun field (Okunlola and Ofonime, 2006). Al_2O_3 value is greater than 14 % in all the samples with noticeably high values (37.25–37.42 %) in the tourmaline extracts. Al_2O_3 values, for the other mineral samples compare with those for other Ta-Nb pegmatite fields within Nigeria. In contrast to these elevated values, Fe_2O_3, MgO, TiO_2 and MnO values are lower than 0.4 % especially in the mica and albite extracts except for the Fe_2O_3 values of 2.14 % in the tourmaline and 5.58 % in the whole rock samples. P_2O_5 values also are generally low in all the samples with highest values of 1.98 % recorded for the albite samples and lowest values in the tourmaline extracts (0.25 %). Trace element data (Tables 3) show appreciable content of rare metals in all the samples. For example, Ta values in the albite samples range from 140–500 μg/g while in the mica (muscovite) samples range of values is between 135–402 μg/g. The tourmaline samples have the highest mean Ta values of 330 μg/g and a range of 295–388 μg/g, while the lowest Ta values are recorded for the whole rock pegmatites (160–175 μg/g). Nb values are relatively lower with the range of 48–130 μg/g, 56–150 μg/g in the albite and muscovite samples respectively (Table 3). Tourmaline and whole rock samples contain much lower Nb with average content of 16.33 μg/g and 19.17 μg/g respectively. The Ta and Nb values in the mica extracts are comparable with those of the richer Nasarawa-Keffi and Kushaka Ta-Nb fields of Nigeria respectively (Okunlola, 2005). Rb values are enhanced in all the samples (452–1000 μg/g) while Sr samples are highest (420–515 μg/g) in the whole rock samples and albite samples (41–138 μg/g) respectively. Average elemental ratio Na/K, is expectedly highest in the albite samples with values as high as 82.8 and lowest in the tourmaline (1.25) (Table 5). The Rb/Sr ratio show non varability in all the samples with average of 11.5. The Ta/Nb ratio clearly shows that the Ta is preferred relative to Nb, in all the samples with highest values of about 20 in the tourmaline samples compared with about 3 in the whole rock samples (Table 5). This also indicates preferred tantalite enrichment in the tourmaline extracts of the Igbeti pegmatite.

Table 2. Range and average values of major elements in the albite, mica, tourmaline and whole rock samples in mass fractions (*w*/%)

Oxides	Albite N = 6		Mica N = 6		Tourmaline N = 6		Whole rock Pegmatite N = 6	
	Range	Average (%)	Range	Average (%)	Range	Average (%)	Range	Average (%)
SiO_2	64.98–74.69	69.88	66.54–72.76	69.61	42.92–42.96	42.94	62.03–63.61	63.02
Al_2O_3	15.66–20.15	17.85	14.82–19.75	17.99	37.07–37.42	37.27	14.74–15.30	15.03
Fe_2O_3	0.04–0.31	0.19	0.12–0.44	0.33	2.13–2.16	2.14	4.99–6.56	5.58
MnO	0.01–0.31	0.10	0.02–0.25	0.12	0.73–0.74	0.74	0.13–0.22	0.18
MgO	0.01–0.21	0.05	0.02–0.09	0.06	0.13–0.15	0.14	2.54–2.99	2.75
CaO	0.01–0.11	1.24	0.26–3.44	1.42	0.80–0.96	0.90	3.62–4.92	4.25
Na_2O	0.64–2.46	7.76	6.29–7.47	6.88	1.62–1.66	1.64	2.63–3.05	2.93
K_2O	0.09–2.95	1.10	0.85–2.01	1.52	1.13–1.17	1.15	1.13–6.54	4.10
TiO_2	0.01–0.05	0.03	0.01–0.04	0.03	0.04–0.05	0.05	0.74–0.76	0.75
P_2O_5	0.13–2.05	0.97	0.28–2.70	1.20	0.24–0.26	0.25	0.28–0.32	0.30

Table 3. Range and averages of some of trace elements in Albites, Mica, tourmaline and whole rock samples

Element	Albite		Mica		Toumaline		Whole rock Pegmatite	
	Range	Average	Range	Average	Range	Average	Range	Average
Bas	23–59	35	13.00–91.00	49.83	47.00–51.00	48.67	1070–1487	1289.00
Sr	41–138	92.17	34.00–170.00	92.00	89.00–91.00	89.83	420–575	483.33
Y	1.50–2.00	1.58	1.50–4.00	2.50	2.00–3.00	2.33	24–28	26.33
Zr	31–155	68.83	71.00–169.00	102.67	14.00–16.00	14.83	203–334	276.67
Zn	30–890	210.00	60.00–410.00	276.67	2040.00–2210.00	2110.00	60–90	77.00
Ga	23–75	46.67	37.00–68.00	56.00	203.00–210.00	206.17	22– 25	23.00
Rb	52–1000	710.50	958–1000	826.33	1000–1000	1000.00	133–290	219.33
Nb	48–130	79.67	56.00–150.00	121.33	15.00–18.00	16.33	13–24	19.17
Sn	0.50–5.00	2.75	2.00–9.00	5.17	2.00–3.00	2.50	10–25	18.50
Cs	84.60–401	214.28	125.00–335.00	235.83	1000–1000	1000.00	8.60–12.40	10.72
Ta	140–500	246.33	135.00–402.00	264.50	295.00–388.00	330.50	160–175.00	168.33
W	0.50–2.00	1.17	0.50–3.00	1.08	3.00–4.00	3.50	1.00–3.00	1.83
Ti	0.70–25.60	9.30	5.40–20.20	13.72	57.50–60.80	59.3	0.90–1.80	1.45

Table 4. Rare earth element composition of pegmatite and associated minerals from Igbeti area (ppm); 1–6 ALBITE SAMPLES, 7–12 MICA SAMPLES, 13–18 TOURMALINE SAMPLES, 19–24 WHOLE PEGMATITE SAMPLES

Elements	1	2	3	4	5	6	7	8	9	10	11	12
La	2.4	2	4.8	200	3.8	1.7	3	14.4	3	1.6	1.8	2.9
Ce	3.5	3.1	7.9	1.4	4.2	1.9	4.3	25.4	4.3	1.5	1.7	4.1
Pr	0.42	0.41	0.83	0.17	0.67	0.46	0.68	2.77	0.69	0.28	0.33	0.68
Nd	1.4	1.6	2.8	0.7	2.7	2.1	2.7	9.4	2.8	1.1	1.3	2.8
Sm	0.2	0.3	0.4	0.1	0.5	0.5	0.6	1.5	0.6	0.2	0.3	0.6
Eu	0.09	0.09	0.1	0.08	0.11	0.16	0.19	0.27	0.17	0.06	0.06	0.17
Gd	0.2	0.3	0.3	0.1	0.5	0.6	0.6	1	0.6	0.2	0.2	0.6
Tb	< 0.1	0.1	0.1	0.1	0.1	0.1	0.1	0.2	0.1	0.1	0.1	0.1
Dy	0.1	0.3	0.2	0.1	0.4	0.6	0.6	0.8	0.5	0.2	0.2	0.5
Ho	0.1	0.1	0.1	0.1	0.1	0.1	0.1	0.2	0.1	0.1	0.1	0.1
Er	0.1	0.1	0.1	0.1	0.2	0.3	0.3	0.4	0.3	0.1	0.1	0.3
Yb	0.1	0.1	0.1	0.1	0.2	0.3	0.3	0.4	0.3	0.1	0.1	0.3
Lu	0.04	0.04	0.04	0.04	0.04	0.04	0.04	0.06	0.04	0.04	0.04	0.04
Hf	8	5.6	9.1	15.8	27.8	19.7	13.8	9.9	14.3	18.7	20.6	13.4
Ta	140	165	190	500	171	312	369	164	402	135	214	303
W	1	1	1	2	1	2	3	1	2	1	1	3
Th	4.4	2.1	5.2	2.2	6.1	36.4	20.1	9.3	20.4	4.1	2.3	18.6
U	12.6	4.2	13.4	6.3	3.7	22.8	19.3	13	27.8	2.1	2.7	18.4

Elements	13	14	15	16	17	18	19	20	21	22	23	24
La	2.3	2.6	2.4	2.5	24	2.3	40	82.8	55	60	75	72
Ce	4.8	5.6	4.9	5	5.2	5.4	85.6	179	150	163	99	170
Pr	0.58	0.67	0.59	0.66	0.62	0.6	9.72	19.7	10.5	13.5	18	16.7
Nd	2.3	2.6	2.4	2.35	2.5	2.4	37.6	72.1	45.1	58.3	70.9	39
Sm	0.5	0.5	0.5	0.45	0.55	0.5	7.6	12.1	12.2	11.3	8.5	9.6
Eu	0.12	0.13	0.12	0.13	0.12	0.13	1.68	2.43	2.41	1.89	2.38	2.4
Gd	0.4	0.5	0.4	0.4	0.5	0.5	5.9	7.8	6.2	6.5	7.4	7.1
Tb	0.1	0.1	0.1	0.1	0.1	0.1	1	1.1	1	1.2	1.1	1
Dy	0.4	0.5	0.4	0.42	0.46	0.5	5.3	5.3	5.5	5.6	5.3	5.2
Ho	0.1	0.1	0.1	0.1	0.1	<0.1	1	0.9	0.95	0.9	1	1.1
Er	0.3	0.3	0.4	0.4	0.4	0.3	2.8	2.5	2.9	2.85	2.8	2.7
Yb	0.2	0.3	0.2	0.25	0.28	0.3	2.6	2.2	2.7	2.6	2.4	2.2
Lu	0.04	0.04	0.04	0.04	0.04	0.04	0.37	0.32	0.38	0.37	0.35	0.35
Hf	1.7	1.5	1.6	1.5	1.7	1.6	5.5	8.8	6.7	7.2	7.9	8.5
Ta	295	388	300	310	350	340	160	170	175	164	172	169
W	3	4	3	3	4	4	1	3	2	3	1	1
Th	1.1	1.2	1.1	1.3	1.1	1.2	12.3	37.8	20.6	15.7	35	32.5
U	6.5	8.3	7.2	6.7	8.1	7.5	2	4.2	3.5	3.7	2.7	2.3

Table 5. Ratios of selected major and trace elements from whole rock pegmatite and associated minerals from Igbeti area; 1–6 ALBITE SAMPLES, 7–12 MICA SAMPLES, 13–18 TOURMALINE SAMPLES, 19–24 WHOLE PEGMATITE SAMPLES

Element ratio	1	2	3	4	5	6	7	8	9	10	11	12
Th/U	0.35	0.5	0.39	0.35	1.65	1. 6	1.04	0.72	0.73	1.95	0.85	1.01
Ta/W	140	165	0.39	250	171	156	123	164	201	135	214	101
Rb/Sr	7.75	9.02	7.25	0.59	11.3	13.5	9.62	5.64	9.35	29.4	29.4	9.71
Ba/Rb	0.04	0.06	0.06	0.44	0.05	0.02	0.06	0.1	0.06	0.02	0.01	0.06
Zr/Hf	5	5.89	4.84	1.96	5.58	5.58	5.15	17. 1	5.46	5.56	5.63	5.82
Sr/Rb	0.13	0.11	0.14	1.69	0.09	0.07	0.10	0.18	0.11	0.03	0.03	0.10
Rb/Cs	3.546	3.22	2.49	0.26	5.43	11.8	3.00	7.66	2.99	6.99	6.62	3.05
K/Rb	0.001	0.001	0.002	0.001	0.001	0.001	0.002	0.001	0.002	0.001	0.001	0.002
K/Cs	0.005	0.002	0.006	0	0.004	0.007	0.005	0.006	0.005	0.007	0.006	0.005
Ta/Nb	2.85	2.57	2.43	10.4	1.56	2.4	2.58	2.92	2.95	1.19	1.42	2.33
Na/K	0.18	11.5	1.67	82.82	16.9	12.1	3.19	6.61	2.95	5.80	5.71	2.95

Element Ratio	13	14	15	16	17	18	19	20	21	22	23	24
Th/U	0.17	0.145	0.15	0.19	0.14	0.16	1.52	0.10	0.37	0.39	1.11	0.40
Ta/W	98.3	97	100	**103.3**	87.5	85	68	250	58. 7	66. 7	128	210
Rb/Sr	11.2	11.0	11.2	11.1	11.0	11.2	7.27	14.5	9.22	8.84	8.89	11.3
Ba/Rb	0.05	0.05	0.05	0.05	0.05	0.05	0.09	0.03	1.19	1.18	0.89	0.70
Zr/Hf	8.24	10. 7	8.75	9.33	8.82	10	8.21	5.39	7	6.67	4.8	5.63
Sr/Rb	0.09	0.09	0.09	0.09	0.09	0.09	0.14	0.07	0.18	0.11	0.11	0.09
Rb/Cs	1.01	1.01	1.01	1.01	1..03	1.02	5.36	6.65	10.7	6.92	8	8.84
K/Rb	0.001	0.001	0.001	0.001	0.001	0.001	0.001	0.001	0.001	0.001	0.001	0.001
K/Cs	0.001	0.001	0.001	0.001	0.001	0.001	0.004	0.004	0.008	0.006	0.006	0.005
Ta/Nb	16.3	22.5	18.7	19.3	23.3	18.8	12.3	7.08	9.21	10.9	8.6	7.04
Na/K	1.25	1.28	1.27	1.27	1.26	1.28	0.89	8.87	8.87	6.82	8.21	11.5

From field evidence and bulk chemistry signatures, the Igbeti pegmatite is a complex pegmatite, of the rare element class and displays typical characteristic of the Lithium, Ceasium, and Tantalite (LCT) family. Apart from the typical minor element content of Li, Rb, Cs, Ga, Sn, Ta > N, (B, P, F) their silicic and per aluminous (A/CNK > 1) character supports this assertion (Cerny, 1991b; London, 2005). LCT pegmatites as in this study, are also known to contain moderate to abundant Ta-Nb mineralization,) gemstones and industrial minerals (Cerny, 1989). The metamorphic environment in this study area which is a low pressure upper green schist facies to lower amphibolite facies (Okunlola and Ofonime, 2006) with quasi conformable to cross cutting structural feature is also typical of LCT pegmatites of the rare element class (Beus and Sitnin, 1968; Cerny, 1982; Mentzer, 1987). Also, Solodov (1971) and Cerny, (1982, 1991a) had observed that schists, gneisses and early intrusions are the hosts of this family of pegmatites. In addition, the fracture filling dyke like configuration of the pegmatitic bodies seems to have been largely contributed by the ductility of the schistose host rocks which according to Cerny (1991b) is also typical of LCT pegmatites. This characteristic coupled with the Rb, Sr, content of the Igbeti pegmatites, suggests that the pegmatites could have been derived from the remelting (anatexis) of supracrustals. However, the Rb /Y + Nb plot (Figure 4) shows that the pegmatite are within plate granite while the Sr/Rb plot also reveals their mixed ancestry with some samples plotting completely out of the magmatic "M" field (Figure 5) These petrogenetic signatures seem incongruous. Cerny (1991b) had noted that metapelites sequences have been traditionally suspected to be the main or sole protoliths of the LCT suites because of their enrichment in LCT elements and an overall character. Veizeuf and Holloway (1998) also demonstrated that fluid absent melting of metapelites produces peraluminous melts, but also a number of rare metal pegmatites have been identified as derived from mixed basement plus supracrustal protoliths having homogenous chemistry. In some cases, undepleted basement lithologies such as paragneisses and metatonalites seem to be the sole source leading to both I and S characteristics (Meintzer, 1987; Walker, et. al., 1986; Wright and Haxell, 1982). The K/Rb/Rb plot (Figure 6) clearly indicates their rare metal bearing affinity, while the low K/Rb ratio shows progressive fractionation and mineralization (Kuster, 1990). This, combined with the low Mg, Ti, Ba, Zr and attendant enhanced values of Rb, Li, Cs and Y composition also indicate high fractionation of the pegmatite, while the Cs values indicate moderately high alkali metal fractionation (Cerny, 1991a). Evidence of possible metasomatism being involved in the mineralization process is seen in the presence of sacharroidal albitic, micaceous units and tourmalinisation. Although, Manning (1984), Henderson and Manning (1984), Henderson and Martin, (1985) and Cerny (1991b) believe that such association could still be explained by late but primary crystallization from residual melt in situ.

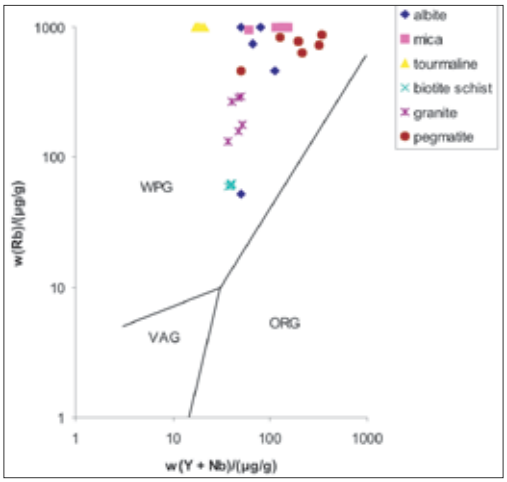

Figure 4. Graph of Rb against Y + Nb for samples from Igbeti area (after PEARCE et al., 1984)

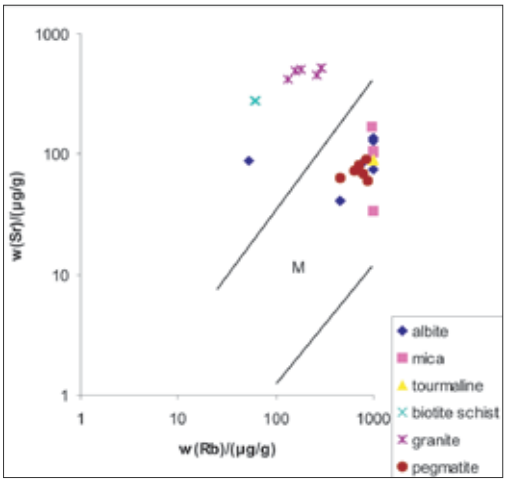

Figure 5. Graph of Sr against Rb for samples from Igbeti area

However, from the works of CHRISTIANSEN, et.al., (1993) and LONDON (1990, 2005) it is believed that this association coupled with the boron effect as shown from the preffered Ta-Nb mineralization in the tourmaline extract is an evidence of the role of metasomatism in the mineralization.

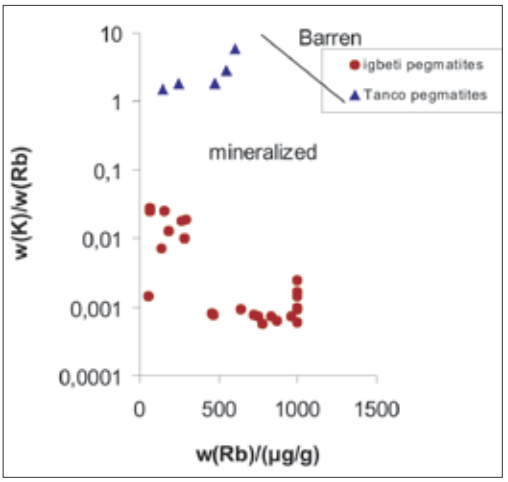

Figure 6. Graph of K/Rb against Rb for pegmatite samples from Igbeti area compared to those of Tanco (after STRAUROV et al., 1966)

Compared to the more endowed Tanco (Canada) pegmatite, the mineralization level is lower. On the plot of Ta against Ga, (Figure 7), Ta versus K/Cs (Figure 8) the samples of the whole rock and mineral extracts plot well above the mineralized GORDIYENKO (1971) line, but the mineralization level in the pegmatite samples is still lower compared to those for Tanco and Noumas pegmatite (Figures 8 and 10). The gneissic and schistose samples plot far below the BEUS (1966) line thus confirming clearly their barren nature. Significantly, however the tourmaline samples are clearly discriminated on these diagrams, plotting clearly away from the other samples indicating greater rare metal Ta enrichment. Similarly, the Ta, Rb, Cs (Figure 10) plots indicate the same trend of mineralization.

In the pegmatites of this study area, Rare earth elements (REE) abundances are low (Table 4). The chondrite normalized plot

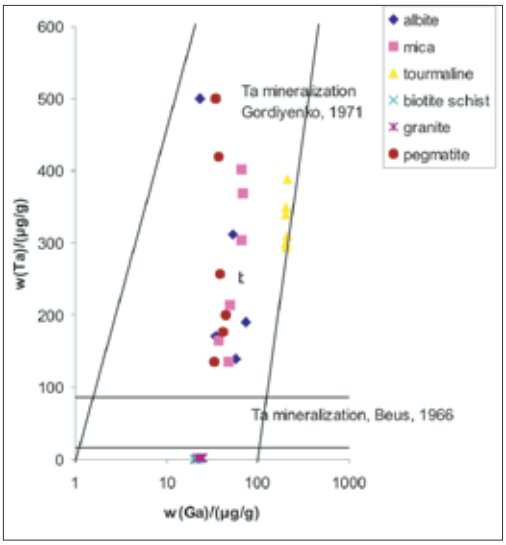

Figure 7. Graph of Ta against Ga for pegmatite samples from Igbeti area

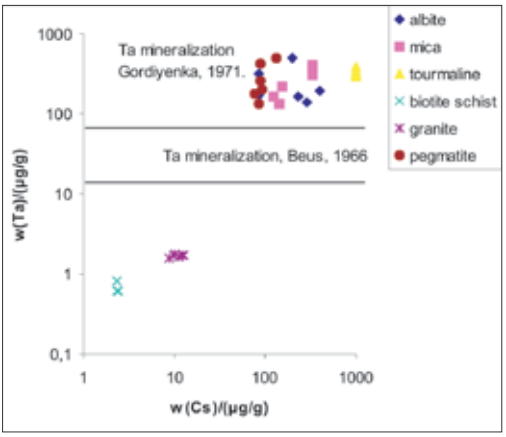

Figure 9. Graph of Ta against Cs for samples from Igbeti area

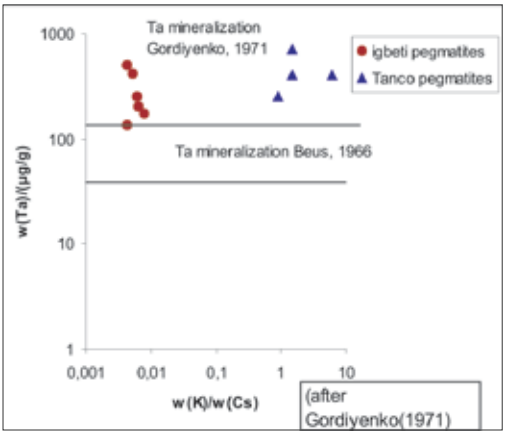

Figure 8. Graph of Ta against K/Cs for pegmatite samples from Igbeti area compared to those of Tanco (After Gaupp et.al, 1984)

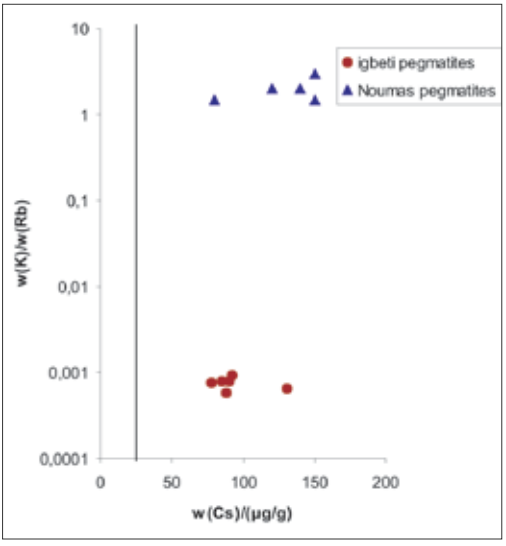

Figure 10. Graph of K/Rb against Cs for pegmatite samples of Igbeti area compared to those for Noumas

(Figure 11) shows high LREE La, Ce, Pr values and lower HREE values. Also, there are extensive negative Eu anomalies and kinking is dominant. This is especially characteristic of LCT pegmatites with attendant high fractionation. (Cerny, 1991b; Fourcade and Allegre, 1981; Lee and Christansen, 1983). Christiansen, et.al, (1993) have highlighted the difficulty of using REE for pegmatite petrogenetic in-

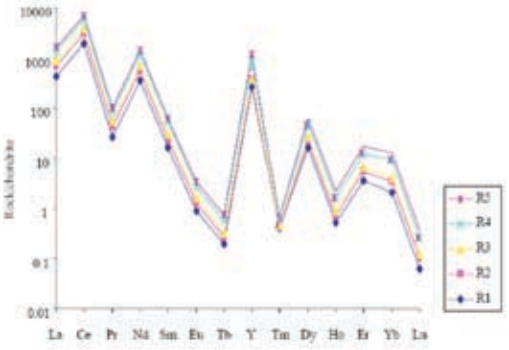

Figure 11. REE chondrite normalized plots of Igbeti pegmatite samples

terpretation because of their occurrence in accessory phases. However, TAYLOR (1965) had suggested earlier that where there is a weak negative Ce anomaly and a strong negative Eu anomaly as in this case of Igbeti pegmatite samples it is an evidence of considerable fractionation and metasomatism. Also, PIPER, (1974) and GARBA, (2003) believe that Negative Ce anomaly of rare metal pegmatite is taken to indicate oxidising condition during mineralization and interaction between magmatic, melt fluids and host rocks over long distance sometimes.

CONCLUSIONS

Pegmatite rock bodies trending mainly in the NNW–SSE direction intrude older lithologies of schists, and gneisses in the Igbeti area south western Nigeria. Thin section studies show they contain mainly quartz, albite, mica and tourmaline. They are coarse grained complex pegmatite. Geochemical analysis of the whole rock, mica, albite and tourmaline samples show they are LCT tourmaline sub type pegmatite. They are clearly enriched in tantalum compared to niobum and the trend of enrichment as clearly Ta >> Nb >> Sn. Variation plots shows they are within plate granites, possibly magmatic but with evidence of anatexis of depleted supracrustals Compared to other Ta-Nb fields in Nigeria, they compare favourably with the richest Ta-Nb mineralized pegmatite but still less endowed compared to those of Tanco (Canada) and Noumas deposit. Negative Europeum anomaly signatures indicate appreciable level metasomatic effect in the pegmatite. The high level of rare metal (Ta), mineralization in the tourmaline compared to other mineral extracts shows possibly a high influence of boron metasomatism in the mineralization process.

REFERENCES

[1] ADEKOYA, J. A., KEHINDE-PHILLIPS, O. O., ODUKOYA, A. M. (2003): Geological distribution of mineral resources in Southwestern Nigeria. Prospects for investment in mineral resources of Southwestern Nigeria, A. A. Elueze (ed), *Nigerian Mining and Geosciences Society* (NMGS); pp. 1–13.

[2] AJAYI, T. R., & OGEDENGBE, O. (2003): Opportunities for the exploitation of precious and rare metals in Nigeria. Prospects for investment in mineral resources of Southwestern Nigeria, A. A. Elueze (ed), *Nigerian Mining and Geosciences Society (NMGS)*; pp. 15–56.

[3] BEUS, A. A. (1966): Distribution of tantalum and niobium in muscovites

of granitic pegmatites. *Geokhimiya*; Vol. 1966, No. 10, pp. 1216–1220.

[4] Beus A. A. & Sitnin, A. A. (1968): Geochemical features of the distribution of tantalum in Granitoids. *Geochmiya*;Vol. 1968, pp 579–585.

[5] Cerny, P. (1982): Petrogenesis of granitic pegmatites, in Cerny, P., ed., granitic pegmatites in science and industry. *Mineralogical association of Canada Short course Hand book*; Vol. 8, pp. 405–461.

[6] Cerny, P. (1989): Characteristics of pegmatite deposits of tantalum, In Moller, P., Cerny, P. and Saupe., F., eds., Lanthanides, Tantalum and Niobium. *Society for Geology Applied to Mineral Deposits*, *Special publication 7*; Springer Verlag, pp. 192–236.

[7] Cerny, P. (1991a): Geochemical and petrogenetic features of mineralization in rare element granitic pegmatites in the light of current research. *Applied geochemistry*; Vol. 18, pp. 48–68.

[8] Cerny, P. (1991b): Rare element granitic pegmatites – regional to global environments and petrogenesis. *Geoscience Canada*; Vol. 18, pp. 49–62.

[9] Christiansen, E. H., Stuckless, J. S., Funkhouser–Marolf, M. J. & Howell, K. H. (1993): Petrogenesis of rare metal granites from depleted sources: an example from the Cenozoic of western Utah. *Recent Advances in the Geology of Granite-related Mineral deposits*; pp. 307–321.

[10] Fourcade, S. & Allegre, C. J. (1981): Trace element behaviour in granite gneiss. A case study. *The calc. alkaline plutonic association. Contrib. Mineral. Petrol*; Vol. 17, pp.177–195.

[11] Garba, I. (2003): Geochemical discrimination of newly discovered rare metal bearing and barren pegmatites in the Pan African 600 ± 150 Ma basement of northern Nigeria. *Applied earth science transaction institute of mining and metallurgy 13*; Vol. 112, pp. 287–292.

[12] Gordiyenko, V. V. (1971): Concentration of Li, Rb, and Cs in potash feldspar and muscovite as criteria for assessing the rare metal mineralization in granitic pegmatites. *International Geological Review*; Vol. 13, pp. 134–142.

[13] Harris, N. B. W., Pearce, J. A. & Tindle A. G. (1986):Geochemical characteristics of collision-zone magmatism, In Corward, M. P. and Ries, A. C. eds., Collission Tectonics. *Geological Society of London . Special Publication*; No. 19, pp. 67–81.

[14] Henderson, C. M. B. & Manning, D. A. C. (1984): The effect of Cs on phase relations in the granite systems; stability of pollucite. In Henderson C. M. B., eds, 6th progress report of research supported by NERC. *Progress in Experimental petrology*. Vol. 6, p. 41–42.

[15] Henderson, C. M. B. & Martin, J. (1985): Continuity of magmatic and hydrothermal processes in the granite systems: 2nd International symposium on hydrothermal reactions, Penn State University, Program with abstracts.

[16] Jacobson, R. E. E. & Webb, J. S. (1964): The Pegmatite of central Nigeria. *Geological Survey of Nigeria*;

Bulletin 17, 61p.

[17] KUSTER, D. (1990): Rare metal pegmatites of Wamba, central Nigeria - Their formation in relationship to late Pan-African granites. *Mineral Deposita*; Vol. 25, pp. 25–28.

[18] LEE, D. E. & CHRISTIANSEN, E. H. (1993): The granite problem as exposed in the southern snake range, Nevada. *Contrib. Miner. Petrol.*; Vol. 83, pp. 99–116.

[19] LONDON, D. (1990): Internal differentiation of rare metal pegmatites: a synthesis of recent research. In Stein, H. J., Hannah, J. L., eds. Ore bearing granite systems; Petrogenesis and Mineralising processes. *Geological Society of America Special Paper*; Vol. 46, pp. 35–50.

[20] LONDON, D. (2005): Granitic pegmatites: An assessment of current concepts and directions for the future LITHOS. Vol. 8, pp. 281–303.

[21] MANNING, D. A. C. (1984): The effect of fluorine on liquidus phase relationships in the system Qz-Ab-Or with excess water at 1kb. *Contrib. Mineral. Petrol.*; Vol. 71, pp. 193–209.

[22] MEINTZER, R. E. (1987): *The mineralogical and geochemistry of the granitoid rocks and related pegmatites of the Yellowknife pegmatite field. North- west territories*. Unpublished Ph. D. thesis, University of Manitoba, Winnipeg, p. 708.

[23] OKUNLOLA, O. A. (1998): Specialty metal potentials of Nigeria. *Proceedings of 1st mining in Nigeria Conference*; Federal Ministry of Solid Minerals, Abuja.

[24] OKUNLOLA, O. A. (2005): Metallogeny of Tantalum-niobium mineralisation of Precambrian pegmatites of Nigeria. *Mineral Wealth*; 104/2, pp. 38–50.

[25] OKUNLOLA, O. A. & JIMBA, S. (2006): Compositional trends in relation to Ta-Nb mineralization in Precambrian pegmatites of Aramoko – Ara – Ijero area, south western Nigeria. *Journal of Mining and Geology*; Vol. 42(2), pp. 113–126.

[26] OKUNLOLA, O. A. & OFONIME, B. E. (2006): Geological setting, petrographical features and age of raremetal (Ta-Nb) mineralization of pegmatites of Komu area, Southwestern Nigeria. *African Journal of Science and Technology (AJST)*; *Science and Engineering Series*; Vol. 7, No. 1, pp. 96–110.

[27] OKUNLOLA, O. A. & OGEDENGBE, O. (2003): Investment Potential of Gemstone Occurrences in Southwestern Nigeria. In: Prospects for investment in mineral resources of Southwestern Nigeria, A. A. Elueze (ed). *Nigerian Mining and Geosciences Society (NMGS)*; pp. 41–45.

[28] OKUNLOLA, O. A. & SOMORIN, E. B. (2006): Compositional features of Precambrian pegmatites of Itakpe area, Central Nigeria. *Global Journal of Geological Science*; Vol. 4, No. 2, pp. 221–230.

[29] PIPER, D. Z. (1974): Rare earth elements in sedimentary cycle: A summary. *Chem. Geol.*; Vol. 14., pp. 285–304.

[30] *Gaupp, R., Moller, P. & Morteani,* G. (1984): Tantalum pegmatite: geologische, petrologische und geoche-

mische unterschungen. Monograph series min dep. 23 Borntreger Berlin Struttggart.

[31] Pearce, J. A., Harris, N. B. W., Tindle, A. G. (1984): Trace element discrimination diagram for the tectonic interpretation of granitic rocks. *Journal of Petrology*; Vol. 22, pp. 956–983.

[32] Solodov, N. A. (1971): Scientific principles of perspective evaluation of rare element pegmatite, Nauka, Moscow; p.292.

[33] Straurov, O. D., Stolyarov, I. S. & Iocheva, E. I. (1966): Geochemistry and origin of Verkh-Iset granitoid massif in central Ural. *Geochem. Intern.*; Vol. 6, pp. 1138–1146.

[34] Taylor, S. R. (1965): The Application of trace element data to problems of petrology. In: L.Ahrens, F. Press, S. K. Runcorn and C. Urey (eds.). *Physics and Chemistry of the Earth*, Pergamon Press, Oxford; Vol. 6, pp.133–214.

[35] Vieizeuf. D. & Holloway, J. R. (1988): Experimental determination of the fluid absent melting relationship in the pelitic system. *Contributions to Minearlogy and petrology*; Vol. 98, pp. 257–276.

[36] Walker, R. J. Hanson, G. N., Papike, J. J., O'Neill, J. R. & Laul, J. C. (1986): Internal evolution of the Tin Mountain Pegmatite, Black hills, South Dakota: *Geochimica et Cosmochimical Acta*; Vol. 50, 2833–2846.

[37] Wright, J. E. & Haxell, G. (1982): A garnet two mica granite, Coyote Mountains, southern Arizona. Geologic setting, uranium lead isotopic systematics of Zircon, and nature of the granite source region. *Geological Society of America Bulletin*; Vol. 93, pp. 1176–1188.

Correlation relationship between drilling bit endurance and the most important parameters of the rock mass

Ljubinko Savić[1], Ivica Ristović[2], Ljiljana Savić[1]

[1]University of Pristina, Faculty of Technical Sciences, Kneza Milosa 7, 38220 Kosovska Mitrovica, Serbia
[2]University of Belgrade, Faculty of Mining and Geology, Djusina 7, 11000 Belgrade, Serbia; E-mail: ivica@rgf.bg.ac.yu

Received: January 13, 2009 **Accepted:** February 17, 2009

Abstract: The paper presents the possibility of correlation relationships between the drilling bit endurance and the most important parameters of a rock mass. The correlation relationships were determined between the drilling bit endurance and the rock strength, separately for all examined rocks. The endurance of the drilling bit is monitored in a wider area, with the rock strength coefficient from 23–160 MPa (f = 2.3–16). The drilling was carried out using hammer drill RK-28, where the borehole diameter was 32 mm. The analysis of the obtained data identified a graphical and analytical dependence between the drilling bit endurance and the most important parameters of rock mass. The graphic dependence is shown on diagrams 1, 2, 3 and 4, while the analytical dependence is shown in equations 1, 2, 3, 4, 5, 6, 7, 8, 9 and 10.

Key words: drilling, rock mass, correlation

Introduction

Operating elements of drilling tools and machines in contact with rocks are exposed not only to mechanical stress but to the friction between the surfaces of operating elements and rocks. The same applies to percussive rotary drilling bits, rotary drilling heads, toothed roller for deep rotary drilling etc. When the friction between surfaces is intensified, particles are swept away from the bit, operating element, and thus cause the change in the shape and dimensions of the operating element.

Drilling bit endurance depends on several main natural factors, where the most eminent are: abrasive characteristics, rock mass strength, elasticity, crushing resistance, quartz and other hard material content in the rock, rock mass weight level and others. In addition to natural characteristics, drilling bit endurance is also affected by technical factors including the steel quality of the drilling bit, the shape and geometry of the bore-crown, reinforcement and technological solution, and the quality of the joint between hard alloy and the crown matrix, as well as by the disciplined main-

Original scientific paper

tenance of the crown and the drilling bit shank head.

All these factors, both separately and collectively, affect the drilling bit endurance. Such research works enable one to determine how many linear meters could be drilled by a drilling bit before it becomes useless.

Table 1 presents the total bore length that a single drilling bit can achieve. From a scientific and practical viewpoint, it is of great interest to find out the correlation between the drilling bit's useful life and one of the mechanical rock parameters. To this effect, the analysis was made in relation to:

- Rock mass strength coefficient,
- Elasticity module,
- Strength coefficient determined by a crushing method and the rock mass quality index *RQD* established by Dir method.

Testing conditions

Rock mass and ore in the Kopaonik region were examined. Rocks and ores of different strength, and with a compression strength ranging from 23–160 MPa (f = 2.3–16), were examined. For such rock masses, the following main mechanical properties were also examined:

- Compression strength *R*p, on the basis of which (*f*) is determined according to Protodjakonov;
- Elasticity module (*E*);
- Crushability coefficient (f_1);
- Quality index of the rock mass according to Dir.

The obtained results of examining 17 different rock types are shown in Table 1.

Blast holes were always drilled by means of a hammer drill (RK 28) and the same type of drilling bit (manufacturer Sandvik Coromant, length 1.6 m, diameter of the bore-crown blade 32 mm, with the constant air pressure of 0.6 MPa).

Analysis of the obtained results

The obtained results enable an analysis of the correlation between each single parameter of the rock mass and the drilling bit endurance, as well as that the drilling bit endurance is expressed through all of the examined rock mass' mechanical characteristics. The software adapted to PC operations was used with this purpose in mind.

Correlation Relationship Between the Drilling Bit Endurance and the Rock Mass Strength Coefficient

Using the data about the length that a drilling bit can drill before it becomes useless, and the data about the rock mass strength coefficient (Table 1), it was possible to define their relationships analytically and graphically. The relationship between these two characteristics is graphically shown in Figure 1. We can see in the Figure that the regularity in behavior concerning their relationships has the correct development in rocks of medium hardness and hard rocks, for $f > 5$, and can be expressed with the equation:

$$L_f = 238{,}54 - 7{,}8\,f - 0{,}18\,f^2 \qquad (1)$$

Table 1. Overview of Rock mass parameters (f, E, f_d and RQD) and drilling bit endurance achieved in each examined rock mass

Rock type code	1	2	3	1	5	6
Rock mass strength coefficient (f)	3.1	4.0	6.7	3.2	5.7	4.3
Elasticity module E/(MPa × 10)	25.0	33.9	60.1	29.6	35.5	62.1
Crushability coefficient (f_d)	2.1	3.4	8.6	4.2	4.9	5.6
Quality index (RQD)	37.0	64.0	58.0	41.0	68.0	83.0
Optimum angle of sharpening αopt for achieving the maximum drilling speed	110.0	105.0	110.0	100.0	105.0	90.0
Total meters drilled (m)	186.6	203.8	186.0	325.0	153.0	211.2

Table 1. Overview of Rock mass parameters (f, E, f_d and RQD) and drilling bit endurance achieved in each examined rock mass; continuation of Table 1

7	8	9	10	11	12	13	14	15	16	17
5.6	15.9	4.8	2.3	2.7	2.3	3.0	12.7	10.4	8.4	12.0
47.9	96.1	73.0	61.0	17.4	47.0	19.9	94.1	65.6	51.4	81.0
3.6	16.8	4.6	3.4	3.2	2.8	2.5	12.4	9.2	7.4	14.2
87.0	65.0	47.0	49.0	43.0	45.0	39.0	79.0	72.0	64.0	68.0
105.0	110.0	90.0	90.0	110.0	90.0	100.0	110.0	105.0	105.0	110.0
229.1	66.4	100.6	127.0	219.8	294.2	313.2	118.0	135.6	152.2	120.2

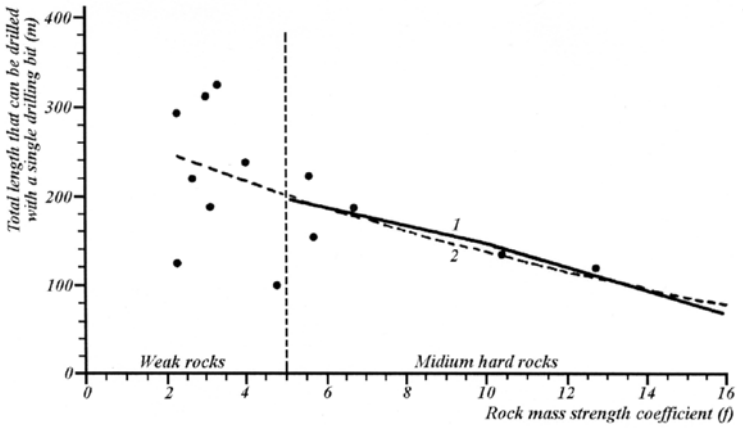

Figure 1. Correlation between the rock mass elasticity module and the total length that can be drilled by a single drilling bit with an optimum sharpening angle. 1. Curve for medium hard and hard rocks; 2. Curve for all examined rocks.

However, with regard to weak rocks ($f < 5$), such regularity cannot be guaranteed considering the great attenuation of results. The final analytical expression of this dependence is given in the equation below:

$$L_f(\text{general}) = 279{,}96 - 17{,}47\,f + 0{,}29\,f^2 \quad (2)$$

Correlation Relationship Between the Drilling Bit Endurance and the Elasticity Module

The correlation relationship between the elasticity module and the drilling bit endurance was established in the same way as in the previous case. The data shown in Table 1 enabled making a diagram of this relationship and thereby obtaining a visualisation of the phenomenon's behaviour. Also, it is possible to define this phenomenon analytically on the basis of the available data.

Based on the mathematical analysis of the available data, the following correlation relationship was obtained:

- For medium hard and hard rocks:

$$L_e = -158{,}27 + 15{,}22\,E - 0{,}205\,E^2 + 7{,}58\cdot 10^{-4}\,E^3 \quad (3)$$

- For all other examined rocks:

$$L_e = 223{,}62 + 3\cdot 10\,E - 0{,}10\,E^2 + 5{,}2\cdot 10^{-4}\,E^3 \quad (4)$$

Correlation Relationship Between the Drilling Bit Endurance and the Strength Coefficient Determined by Crushing Method

In the same way that it was done in the previous two examples, in this case the correlation relationship between the drilling bit endurance and the strength coefficient was also determined via the crushing method. A diagram of relationship between these two parameters is shown in Figure 3. While the analytical dependence between the drilling bit endurance and the strength coefficient was defined with the crushing method, such a relationship for medium hard and hard rocks was given as follows:

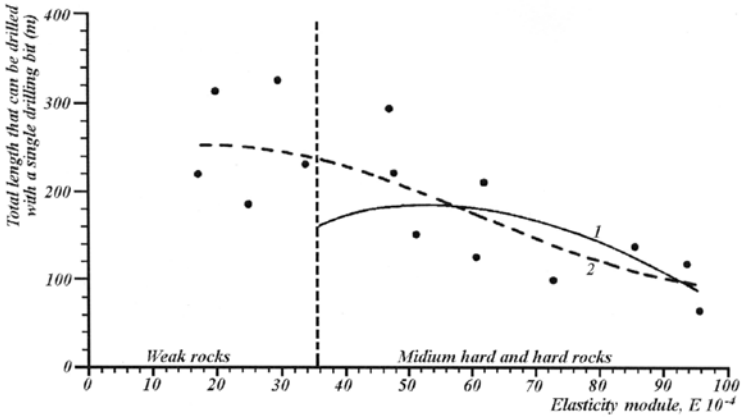

Figure 2. Correlation between the rock mass strength coefficient and the total length that can be drilled by the drilling bit with an optimum blade angle. 1. Curve for medium hard and hard rocks; 2. Curve for all examined rocks.

$$L_f = 176{,}97 + 2{,}81\, f_d - 0{,}55\, f^2 \quad (5)$$

- And for the whole locality:

$$L_f(\text{general}) = 277{,}11 - 17{,}49\, f - 0{,}35\, f^2 \quad (6)$$

Correlation Relationship Between the Drilling Bit Endurance and the Rock Quality Index *RQD* According to Dir

As it was done in previous cases, in this case the correlation between the drilling bit endurance and the rock quality index according to DIR was determined. A diagram of the relationship between these two parameters is shown in Figure 4. While the analytical dependence between the drilling bit endurance and the rock quality index was determined according to Dir, the cor-

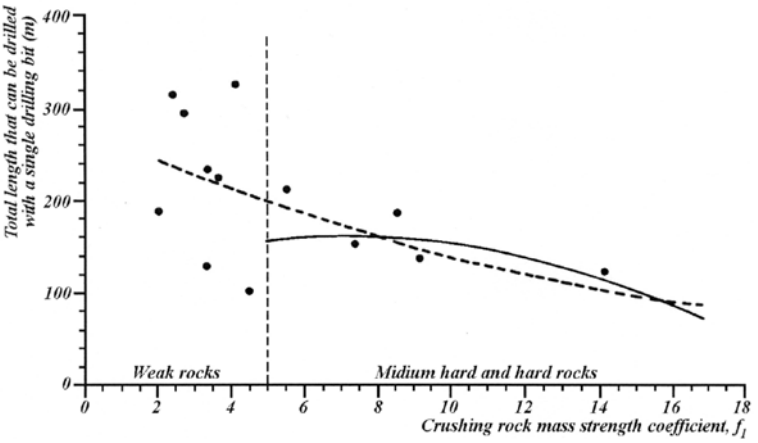

Figure 3. Correlation between the crushing rock coefficient (f_1) and the total length that can be drilled by the drilling bit with the optimum sharpening angle. 1. Curve for medium hard and hard rocks; 2. Curve for all examined rocks.

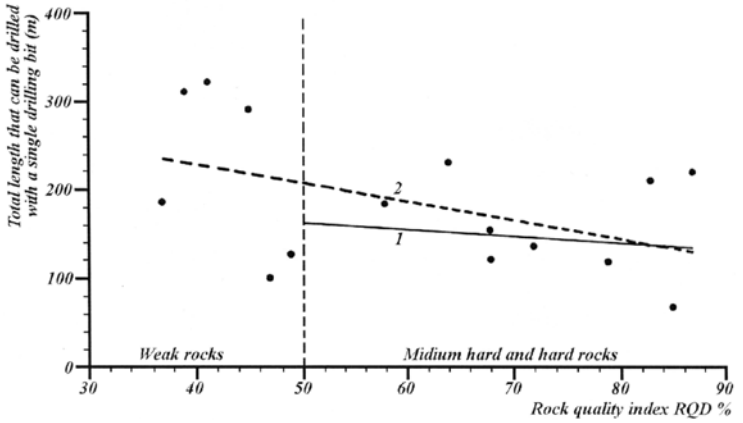

Figure 4. Correlation between the drilling bit endurance and the rock quality index according to DIR (*RQD*) 1. Curve for medium hard and hard rocks; 2. Curve for all examined rocks.

relation curve for medium hard and hard rocks was defined as follows:

$$L = 205{,}44 - 0{,}844\ (RQD) \qquad (7)$$

Correlation curve for all other examined rocks is defined as follows:

$$L = 313{,}30 - 2{,}103\ (RQD) \qquad (8)$$

Defining a correlation relationship between working environment parameters (f, E, f_1, RQD) and the drilling bit endurance

Using the linear regressive analysis, it was possible to define an equation of the correlation between the drilling bit endurance and a group of mechanical and structural characteristics of the rock mass for all examined parameters of a working environment and the drilling bit endurance.

Interdependence analysis was performed separately for medium hard and hard rocks and separately for examined rock masses. Based on such an analysis, the correlation interdependences were established as follows:

- For medium hard and hard rocks:

$$L = 166{,}09 - 24{,}93\,f + 1{,}21 \cdot 10^{-4} E + \\ + 4{,}48\,f + 1{,}28\,(RQD) \qquad (9)$$

- For all examined rock masses:

$$L = 286{,}0 - 13{,}45\,f + 1{,}96 \cdot 10^{-4} E + \\ + 8{,}91 f_1 + 0{,}56\ (RQD) \qquad (10)$$

Conclusions

The obtained results and their analysis has shown that it is possible to define the interdependencies, not only between one parameter of the rock mass and the drilling bit endurance, but also among a large number of various parameters, and to obtain high-level correlation relationships.

References

[1] Savić, Lj. (1993): Effects of technical parameters on the percussion drilling speed in various rock types. *Doctoral thesis*, Faculty of Mining and Geology, Belgrade, 150 p.

[2] Jovanović, P. (1980): Mechanical process of rock blasting during mining works. Faculty of Mining and Geology, Belgrade.

[3] Jovanović, P. (1990): Construction of mine workings. *Book I*, Faculty of Mining and Geology, Belgrade.

[4] Redžić, Lj., Savić, Lj., Ristović, I. (1995): Studying the influence of a cut type on the rate and costs of tunneling in the conditions of Trepca Mine – Stari Trg. *Jurnal of Underground Mining Engineering*, ISSN 0354-2904, N^0 4, Faculty of Mining and Geology, Belgrade, Serbia, pp. 23–30.

[5] Ristović, I., Živančević, D., Milisavljević, V. (1995): Maintainance of drilling machines in the Stari Trg Mine. *Proceedings of 1st Yugoslav Symposium with International Participation Drilling and Blasting*, Faculty of Mining and Geology, Belgrade, Serbia, pp. 389–405.

Surveying drill holes

Branko Leković[1], Aleksandar Ganić[1], Milivoj Vulić[2]

[1]University of Belgrade, Faculty of Mining and Geology, Đušina 7, 11000 Belgrade, Serbia, E-mail: blekovic@rgf.bg.ac.yu, aganic@rgf.bg.ac.yu
[2]University of Ljubljana, Faculty of Natural Sciences and Engineering, Aškerčeva 12, SI-1000 Ljubljana, Slovenia, E-mail: milivoj.vulic@ntf.uni-lj.si

Received: December 16, 2008 **Accepted:** February 17, 2009

Abstract: The determining bore hole course is very important in drilling, and even more so in geologically complex, small oil and gas deposits, and high angle/horizontal wells in which bottom hole location becomes necessary for successful drilling. Due to the high costs of drilling, rough drilling conditions and demands in a trajectory well control the use of modern technology, and can provide more data for the driller about the state of the borehole, the formation properties and the drill string in real time. This is provided by measuring while drilling (MWD) toll in drill string above the bit. These geological and engineering measurements are transmitted via mud pulses through the mud and to the surfacing operators' console.

Key words: drilling, measuring, trajectory, well, drill string.

Introduction

A driller's ability to optimize drilling performance increased with knowledge conditions on hole bottom in real time. MWD systems achieved great contribution to this, providing real time data, increasing safety and enhancing the financial aspect of drilling.

The most significant advantage of MWD technology is that it provides down hole measurements and their interpretations in real time. Furthermore these measurements are made before any substantial damage to the formation arises from invasion. As down hole measurements such as weight on bit, torque and temperature have never been available before, these capabilities result in better, faster drilling operations.

Highly deviated holes producing difficulties in logging operations and often only MWD tools can obtain formation properties.

Measured values from downward borehole are:

- Direction related data, inclination, and azimuth and tool face angle.
- State of the borehole, hydrostatic pressure, formation pressure, temperature.
- Drilling parameters, rotating speed, weight on bit, torque and condition of

Review paper

the bit.

- Formation properties, density, formation resistance, natural radioactivity and type of contents in the formation.

The impact that the MWD has on the safety of drilling is most significant. In addition to making provisions of the reliable detection of the pressure in formations by using the resistivity measurement method, the MWD measurement may also be used for the detection of the initial operating problems such as differential sticking. The use of the MWD affects the efficiency of drilling in several ways. Faster testing of the direction of the well enables more time for drilling, and more frequent measuring reduces the risk to turn away from the course (Vukelič, 2004).

At some wells with large angle of deflection, measuring of characteristics formation can even be the only measurement that can be obtained.

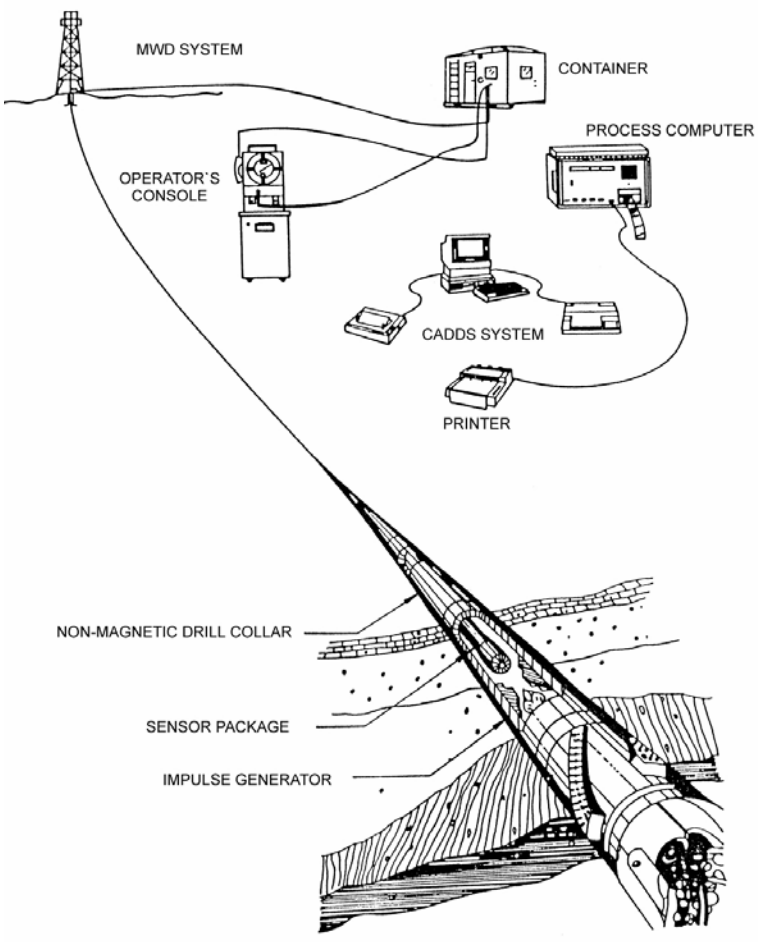

Figure 1. Measuring while drilling

DESIGN OF THE MWD MEASURING SYSTEMS

The MWD down hole tool consist of three main parts: measuring instruments with sensors, transmission element and surface equipment for receiving and manipulating the down hole data.

Measuring instrument in the drill string

The measuring instrument is located in the drill string, inside a special non-magnetic drill collar, close above the bit and/or the down hole motor and consist of the parts:

- Sensor or measured value receiver,
- Measured value processor which control system and codes the values and »telemeters« them to the surface by means of a transmission medium,
- Energy part, which provide power for the system from the batteries (lithium) or turbine generator driven by mud.

Surface equipment

In general, the surface recording equipment consists of device, which receives signals from the transmitter and converts them into electric pulses, and the decoder which provides representation of the measured values. Peripherals devices - such as digital computer, terminal, plotter and line printer - are usually connected to the system, ensuring analysing and storage of measured values.

The signal transmission systems

Depending on the type of a transmission medium and/or method used for transmission of data up to the surface, it is possible to classify the MWD systems in a clear and logical way. In most cases, they consist of electromagnetic wave system and the pulsating drilling fluid system. The type of the basic transmission is also crucial for the duration of transmission and/or frequency of data as well as for the quality of the obtained measured values. This is generally the result of the fact that the noise encountered in the transmission channel may reduce the efficiency of the transmission, sometimes resulting in the data interruption.

THE ELECTROMAGNETIC TRANSMISSION SYSTEM

The electromagnetic system for the transmission of the obtained data up to the surface emits electromagnetic waves through the surrounding formations or through drilling tools. Due to the large transmission losses, it is possible to transmit only small frequency signals, so that it is very difficult to filter them. Electromagnetic waves tend to disappear in the formations with the resistance smaller than 1 Ω/m. The current commercial electromagnetic systems are suitable only for the land operations where the resistance is larger than 1 Ω/m and if the formation is not too deep.

The impulse transmission system by pulsation of the drilling mud

Two primary means of transmitting data, trough a fluid column inside drill pipes, to the surface exist:

- Pulse telemetry, encodes data in binary format and sends it to the surface by positive or negative pressure pulses generated by means of valve in the fluid;
- Continuous-wave telemetry employs

rotating device that generates a fixed frequency signal which sends binary information encoded on pressure wave to the surface.

The description of the signal transmission by drilling mud pulsation

During the pulsation process, the drilling mud pressure within drill collars near bit alters due to the effect of valves, so that the pressure drop or build-up of pressure occurs. Those impulses enable the signals transmission, because the impulses, made at the bottom, are spreading within the column of drilling mud at the speed of the sound, 1200 to 1500 m/s, all the way to the surface. This pulsation of pressure represents, in digital form, a coded group of analogously measured data. The speed of data transmission is from 1 to 3 bits per second (limited by pulsation valves and by the speed at which the valve actuation system is being shut down).

The positive pulse system

It represents the pulsation process, which causes the build-up of pressure within the drilling mud column by activating valve by means of the hydraulic system, which is controlled electronically.

- It enables every value of the pressure within practical limits and the pulsation can easily be detected.
- There is no direct communication between the inner space and annular.
- Currently, with the existing technique, higher rate of transmission is possible.

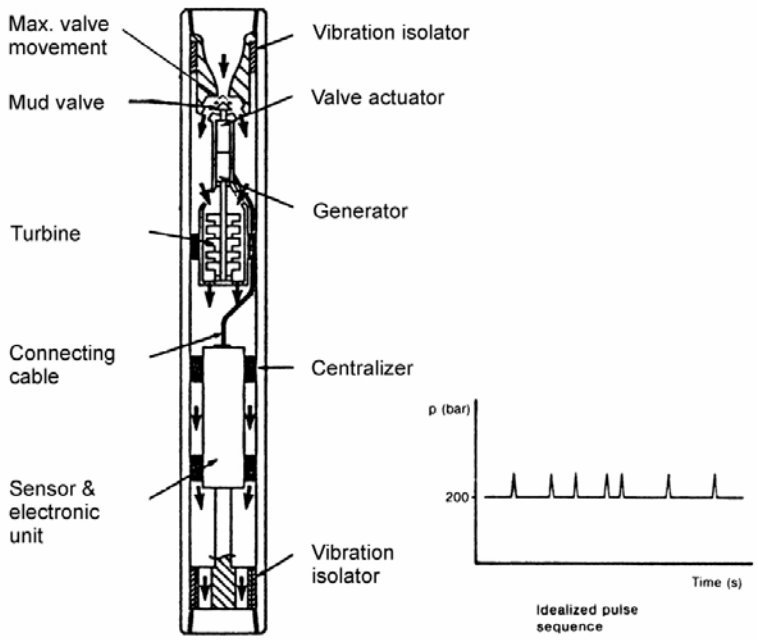

Figure 2. Positive pulse system

The negative pulse system

The principle of negative pulsation is based on the use of differential pressure, which exists inside and outside drill collars. The valve allows the discharge of drilling mud from the interior into the annular in a short time, and thus pressure drop noted on the surface occurs. The negative pulse system may cause permanent communication between the interior and the annular if the valve fails while closing.

- The pressure drop is possible up to approximately 10–15 % of the drilling mud pressure with complicated recognition of pulses.
- During the pulsation process, 5–20 % of drilling mud passes through the opening on the instrument into the annular.
- By using the existing technology, lower transmission rate is achieved than by using the positive system.

There is also another coding system in use, where the value of data is displayed by means of the interval between two pulses. The advantage of this system is higher speed for processing smaller value data.

Each pulse system is susceptible to noise made by drilling mud pump, and the filtration is made more difficult due to the wide range of frequencies contained in pulses. The drive system differs, and depending on the type of the valve used, it can be direct or with hydraulic servo valves.

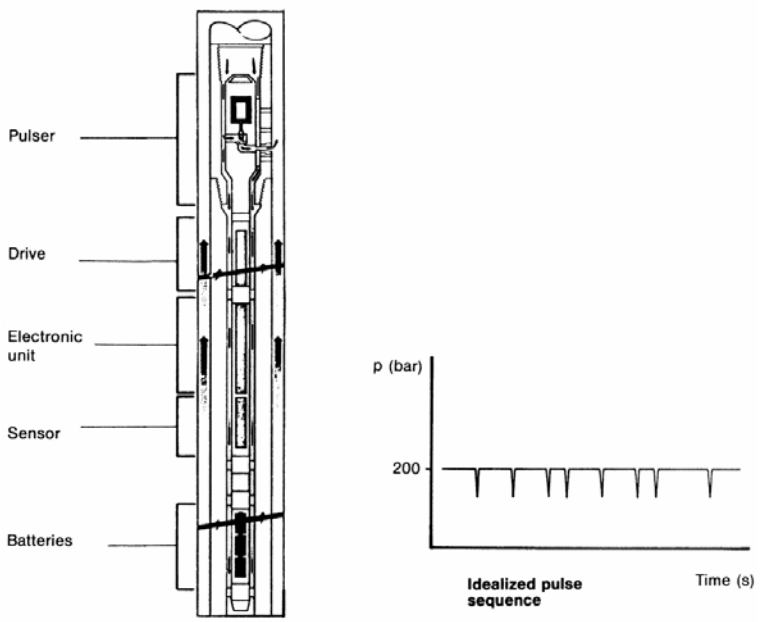

Figure 3. Negative pulse system

The continuous wave system

The drilling mud impulse generating system, the so called continuous wave system, uses the vortex pulsation valve, which, through fluid damping, produces the signal of pressure traveling through fluid within drilling pipes up to the surface at the speed of sound.

The most often wave frequency is 12 Hz and the alteration of phase is used more often than the frequency modulation.

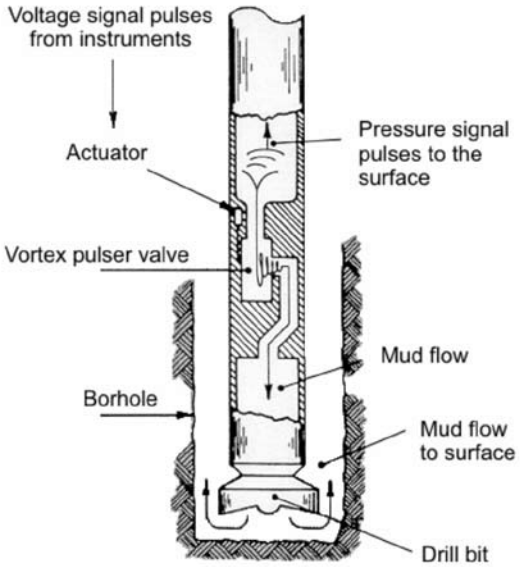

Figure 4. Continuous wave system

The pulsation transmission rate

The rate and weakening of drilling mud pulses depends on the drilling mud density, compressibility, as well as on the characteristics of drilling rods. It varies from 1500 m/s for light drilling mud to 1200 m/s for heavy drilling mud based on water. The speed within the drilling mud based on oil shall vary from 1200 m/s for light drilling mud to 1000 m/s for heavy drilling mud. Pressure impulse damping becomes increasingly intensive with the depth and compressibility of drilling mud. Even more expressed pressure reduction was observed at oil based drilling mud, which is mainly used at deep wells.

Reliability of the system

As the MWD systems are comprised of sensors, power supply sources, and pulsating unit and detecting system on the surface, it is probable that the system might fail.

In addition, the pulsating system contains elements with moving parts, so therefore is generally to expect larger tendency toward failing than with other components. Failing of MWD instruments results in premature pulling out of tools, which extends working time of the rig and directly affects the cost increase.

In the past, MWD tools were criticized because of their unreliability and poor durability. Today, the reliability is increased and the majority of producers guarantee more than 250 working hours between malfunctions.

By applying measurements of tool vibrations at the bottom, reliability of the MWD systems is improved and the lifetime of the bit and drilling tools is increased. Working energy of the probe is provided with batteries (lithium batteries – whereby it is necessary to provide approximately 200

working hours) or with generators. Turbine driven generator systems allow higher temperature than the systems with batteries.

All elements of the system are usually foreseen for the following conditions:

Temperature:	up to 150°C
Pressure:	up to 1500 bar
Shock:	up to 1000 G
Vibration:	up to 40 G

Large values of the resistance to impact and vibrations do not arise only from the conditions in the well during drilling; they are also necessary for the manipulation during transport and assembling. The majority of systems is susceptible to foreign objects in drilling mud (lost circulation material), so that it is necessary to put protective sieves at the inlet of the instrument.

The accuracy of the measurement is for the following:

Azimuth	± 1,5 º
Inclination	± 0,1 º
Face angle	± 1,5 º

THE APPLICATION OF MWD SYSTEMS

In general, the system consists of adequate sensors for analog or digital recording of the desired measured values, which can be divided into four groups of basic data:

Directing and guiding of drilling tools
- Tool face orientation
- Azimuth
- Inclination

Safety factors – conditions at the bottom of the well
- Hydrostatic pressure
- Mud flow
- Temperature

The optimization of drilling – drilling parameters
- Weight on bit
- Torque
- Rotating speed

Formation characteristics – geological correlation
- Natural radioactivity
- Formation resistivity
- Density
- Porosity

Directing and guiding of drilling tools

The first commercial application of MWD systems was for the directed drilling. The MWD testing lasts for 32 seconds compared with approximately one hour for the conventional measurement (*single-shot*). This leads to time savings and significant reduction of risks against the sticking of tools. Measurements made more often, which are enabled with MWD systems, allow better control of the direction and inclination during drilling. With modern accelerometers and magnetometers, complete data for inclination, orientation of the tool face and azimuth, including the magnetic correction are available. The inclination can be calculated with the equation (1). Gravitational angle of the tool face is the angle between vertical plane, which contains the well axis and planes of the mud motor, i.e. well axes. The term tool face refers only to drilling with mud mo-

tor. In case of housing with bent sub, lower part of the housing is to be considered as the tool face. Figure 5 shows the orientation of the tool face.

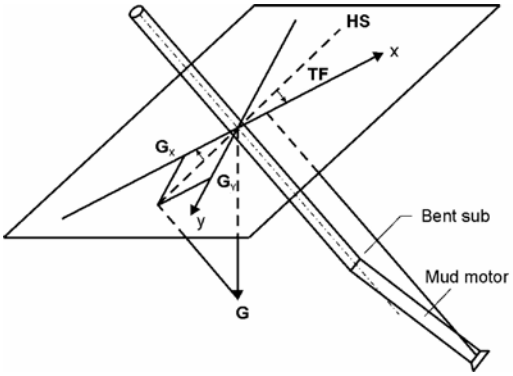

Figure 5. Planes defining the tool face angle

The angle TF is to be calculated with the following equation:

$$TF = \arctan\left(-\frac{G_y}{G_x}\right) \quad (1)$$

Where:
G_x = acceleration of gravity connected with the engine or the bit face in a plane normal to the axis of the well;
G_y = a normal to G_x in the same plane.
If $TF > 0$, well turns right, if $TF = 0$, well goes straight and if $TF < 0$, the well turns left. The angle TF is not defined if the inclination is zero. The drilling stage, in which the deflection begins, is called "*kickoff*". It is achieved by using bent sub and down hole motor to orient the tool face toward the angle of vertical plane, in which is the sub or the motor housing located in relation to the north.

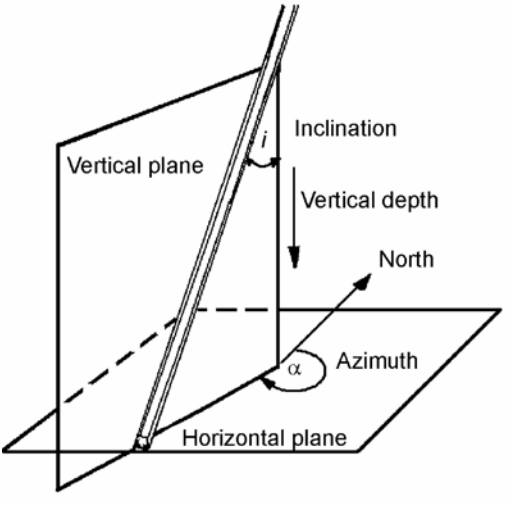

Figure 6. Planes defining the azimuth angle

The azimuth (α) is the angle between the direction of the north and the direction of the well in horizontal plane in clockwise direction (Figure 6).

The MWD sensors are positioned in the non-magnetic part of drill collars; however, magnetic pipes, which are distant, nevertheless have the impact by making perturbation in the direction of the well axis. This causes the error in measurement, which must be corrected. Those perturbations may arise from the points within the non-magnetic drill collars, where magnetism developed or due to the external factors such as the existence of casing in the vicinity.

With MWD system, an expert for directional drilling is able to determine the point of deflection precisely and to control operations for the correction of direction during process of reaching the geological aim.

Safety factors – conditions at the bottom of the well

The detection of high pressure and the appropriate maintenance of primary hydrostatic control of formation fluids is the most important safety problem affecting the drilling operations. Many methods for the detection and prediction of pore pressure are used, and the most frequently used is the method by which the resistance trends to predict overpressure zones and its comparison with the tendency of the pressure gradient determined in this area. By using values of pore pressure resulting from the MWD measurement in real time, the appropriate density of drilling mud can be chosen in order to maintain hydrostatic control and therefore to reduce the risk of kick. The indirect benefit of the use of MWD for determination of pore pressure is also the fact that drilling mud of minimum density can be used for appropriate pressure control, due to which the risk of losing the circulation is reduced and the drilling speed is increased.

The optimization of drilling – drilling parameters

The weight on bit at the bottom and torsion are significantly different from the surface measuring. The difference is especially characteristic at wells with deflection or while using stabilizer in the drilling tools column near bit. The difference between weight measured on the surface and the weight measured with MWD sensors may be used to determine the transfer of the efficiency ratio. The effectiveness depends on many factors such as well inclination, type of formation, drilling mud, lubricant used in circulation system etc. Sensors for measurement of weight at the bottom are also used to measure torsion on the bit during drilling. Sudden changes of torsion at the bottom signal the change of bit weight, types of formation or blocked bit cone. By using data from the surface and by using weight on bit at the bottom and torsion at the bottom for early detection of friction at the bottom in real time, a driller can take preventive action to avoid stuck pipe, to optimize bit performances and to avoid unnecessary trip with the tool.

Formation characteristics – geological correlation

Values obtained by MWD measurements and by conventional wire line logging measurements do not have to be identical (sensors do not measure absolutely the same condition of the layer); however, general compatibility is quite good and enough to permit the use of MWD chart for geological correlations and in some cases also quantitative calculations for evaluation of the formation. The advantage of MWD instruments is also the fact, that they are positioned in a rotating housing, which moves a relatively small logging speed. At inclined (with inclination larger than 50 º) and especially at horizontal wells, difficulties while making wire line logging measurements are quite often so that the MWD measurement represents the only solution.

DATA OF MEASUREMENT FOR A WELL "ORMOŽ G-1"

On the basis of the exploratory drilling results, for suitable geological interpretation of a deposit, it's necessary to define

Table 1. Survey data at every 10 m and coordinate of survey points

Survey Point	Measured Depth d_m/m	Inclination *i*/°	Azimuth *A*/°	True Vertical Depth d_v/m	Coordinate of Points			
					±	N/m	±	E/m
1	993,0	14,5	144,5	983,58	-	61,52	+	28,10
2	1003,0	14,5	144,7	993,26	-	63,56	+	29,55
3	1013,0	14,5	144,5	1002,94	-	65,60	+	31,00
4	1023,0	14,5	145,0	1012,62	-	67,65	+	32,44
5	1033,0	14,5	146,8	1022,31	-	69,75	+	33,81
6	1043,0	14,4	146,8	1031,99	-	71,83	+	35,17
7	1053,0	14,4	146,8	1041,68	-	73,91	+	36,53
8	1063,0	14,4	147,8	1051,36	-	76,01	+	37,86
9	1073,0	14,3	149,3	1061,05	-	78,14	+	39,12
10	1083,0	14,4	150,7	1070,74	-	80,31	+	40,33
11	1093,0	14,4	152,2	1080,43	-	82,51	+	41,49
12	1103,0	14,4	153,3	1090,11	-	84,73	+	42,61
13	1113,0	14,4	154,4	1099,80	-	86,97	+	43,69
14	1123,0	13,2	151,1	1109,53	-	88,97	+	44,79
15	1133,0	13,2	159,0	1119,27	-	91,10	+	45,61
16	1143,0	13,2	167,1	1129,00	-	93,33	+	46,12
17	1153,0	13,2	174,1	1138,74	-	95,60	+	46,35
18	1163,0	13,2	180,6	1148,48	-	97,88	+	46,33
19	1173,0	13,2	186,0	1158,21	-	100,15	+	46,09
20	1183,0	13,2	193,2	1167,95	-	102,38	+	45,57
21	1193,0	13,2	200,8	1177,68	-	104,51	+	44,76
22	1203,0	13,2	208,8	1187,42	-	106,51	+	43,66
23	1213,0	13,2	215,6	1197,15	-	108,37	+	42,33
24	1223,0	13,3	221,9	1206,89	-	110,08	+	40,79
25	1233,0	13,3	227,6	1216,62	-	111,63	+	39,09
26	1243,0	13,3	234,1	1226,35	-	112,98	+	37,23
27	1253,0	13,3	240,6	1236,08	-	114,11	+	35,23
28	1263,0	13,4	249,8	1245,81	-	114,91	+	33,05
29	1273,0	13,4	258,5	1255,54	-	115,37	+	30,78
30	1283,0	13,4	265,2	1265,27	-	115,57	+	28,47
31	1293,0	13,5	272,2	1274,99	-	115,48	+	26,14
32	1303,0	13,5	279,9	1284,71	-	115,08	+	23,84
33	1313,0	13,6	286,5	1294,43	-	114,41	+	21,58
34	1323,0	13,6	294,6	1304,15	-	113,43	+	19,45
35	1333,0	13,6	301,6	1313,87	-	112,20	+	17,44
36	1343,0	13,7	308,8	1323,59	-	110,71	+	15,60
37	1353,0	13,7	315,8	1333,30	-	109,02	+	13,95
38	1363,0	13,7	324,5	1343,02	-	107,09	+	12,57
39	1373,0	13,7	332,5	1352,73	-	104,99	+	11,48
40	1383,0	13,7	338,6	1362,45	-	102,78	+	10,61
41	1393,0	13,7	344,4	1372,16	-	100,50	+	9,98
42	1403,0	13,7	350,2	1381,88	-	98,17	+	9,57
43	1413,0	13,7	355,9	1391,60	-	95,80	+	9,40
44	1423,0	13,6	1,2	1401,31	-	93,45	+	9,45
45	1433,0	13,6	7,1	1411,03	-	91,12	+	9,74
46	1443,0	13,5	12,5	1420,76	-	88,84	+	10,25
47	1453,0	13,4	24,9	1430,49	-	86,74	+	11,22
48	1463,0	13,3	38,4	1440,22	-	84,94	+	12,65
49	1473,0	13,3	51,5	1449,95	-	83,50	+	14,45
50	1483,0	13,3	60,6	1459,68	-	82,37	+	16,46
51	1493,0	13,4	71,1	1469,41	-	81,62	+	18,65
52	1498,0	13,4	81,3	1474,27	-	81,45	+	19,80

location of a well in the space (VIŽINTIN, 2008). Measurements are being done in points along axes of a well on certain distances. It's been applicable the data of the well "Ormož G-1" (Table 1). The well was made until profundity of 1500 m, in order to exploitation of thermomineral water from the carbonate rock collector (VESELIČ, 1996). The measurements were done, with the instrument EASTMAN W – 120 SINGLE SHOT. That survey instrument is single shot, which enables measurement in one point only at what, the instrument is pulled up after each measurement, on surface in order to reading the data which are measured. The accuracy of the instrument is: ± 0,3 ° for Inclination and ± 0,5 ° for Azimuth.

For comparing the data from survey points of different distance (10 m and 30 m) is chosen a segment of hole at 1000 m until bottom, because the collector rocks are located in this section.

A calculation of coordinate in survey points is performed by equation (*ROŠER R., 2008*):

$$P_{\begin{bmatrix} I \\ J \end{bmatrix}} = \begin{bmatrix} P_I \\ P_J \end{bmatrix} = \begin{bmatrix} \begin{bmatrix} x_I \\ y_I \\ z_I \end{bmatrix} \\ \begin{bmatrix} x_J \\ y_J \\ z_J \end{bmatrix} \end{bmatrix} = \begin{bmatrix} x_I \\ y_I \\ z_I \\ x_J \\ y_J \\ z_J \end{bmatrix} = \begin{bmatrix} \begin{bmatrix} \cos\alpha_I \sin i_I \\ \sin\alpha_I \sin i_I \\ \cos i_I \end{bmatrix} \\ \begin{bmatrix} \cos\alpha_J \sin i_J \\ \sin\alpha_J \sin i_J \\ \cos i_J \end{bmatrix} \end{bmatrix} = \begin{bmatrix} \cos\alpha_I \sin i_I \\ \sin\alpha_I \sin i_I \\ \cos i_I \\ \cos\alpha_J \sin i_J \\ \sin\alpha_J \sin i_J \\ \cos i_J \end{bmatrix} \quad (2)$$

where:

x_I, y_I, z_I – coordinate of the point *I*/m
x_J, y_J, z_J – coordinate of the point *J*/m
α_I, α_J – azimuth at the points *I* and *J*/°
i_I, i_J – inclination at the points *I* and *J*/°

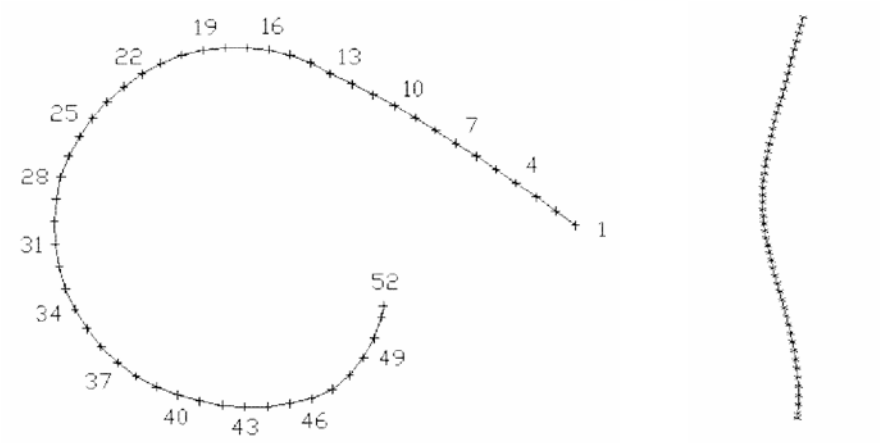

Figure 7. Trajectory of a well in horizontal surface and axonometric presentation (survey points on 10 m)

Table 2. Simulation of measurement in a well on 30 m and coordinates of the survey points.

Survey Point	Measured Depth d_m/m	Inclination *i*/°	Azimuth *A*/°	True Vertical Depth d_v/m	Coordinate of Points			
					±	N/m	±	E/m
1	993,0	14,5	144,5	983,58	-	61,52	+	28,10
4	1023,0	14,5	145,0	1012,62	-	67,67	+	32,41
7	1053,0	14,4	146,8	1041,68	-	73,92	+	36,49
10	1083,0	14,4	150,7	1070,74	-	80,42	+	40,14
13	1113,0	14,4	154,4	1099,80	-	87,15	+	43,37
16	1143,0	13,2	167,1	1129,00	-	93,83	+	44,90
19	1173,0	13,2	186,0	1158,21	-	100,64	+	44,18
22	1203,0	13,2	208,8	1187,42	-	106,64	+	40,88
25	1233,0	13,3	227,6	1216,61	-	111,30	+	35,78
28	1263,0	13,4	249,8	1245,80	-	113,70	+	29,26
31	1293,0	13,5	272,2	1274,97	-	113,43	+	22,26
34	1323,0	13,6	294,6	1304,13	-	110,49	+	15,85
37	1353,0	13,7	315,8	1333,27	-	105,40	+	10,89
40	1383,0	13,7	338,6	1362,42	-	98,78	+	8,30
43	1413,0	13,7	355,9	1391,57	-	91,70	+	7,79
46	1443,0	13,5	12,5	1420,74	-	84,86	+	9,31
49	1473,0	13,3	51,5	1449,93	-	80,56	+	14,71
52	1498,0	13,4	81,3	1474,25	-	79,69	+	20,44

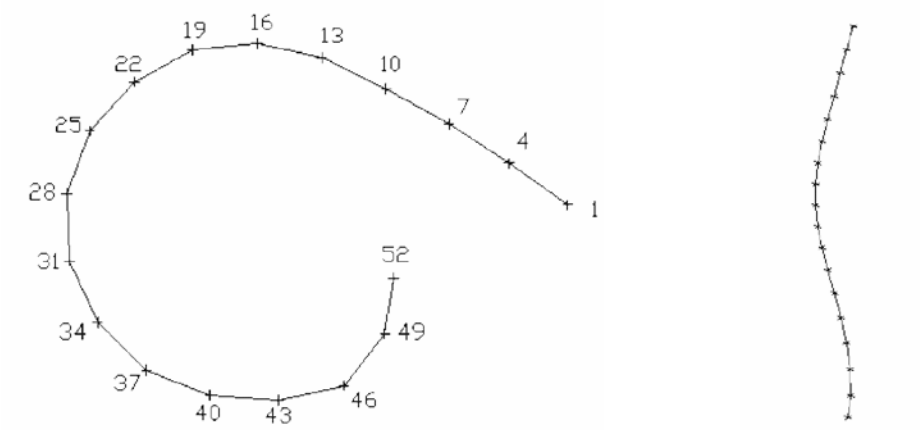

Figure 8. Trajectory of a well in horizontal surface and axonometric presentation (survey points on 30 m)

In order to comparing a trajectory of a well in a function of different sediment of survey points, the calculation of the coordinates were made, as though common measurement were simulated, on 100 ft, i.e. 30 m. The results of the coordinates of the survey points are presented on the table 2, whereas on the figure 8, the relevant trajectory of a well are presented in a horizontal surface and an axonometric presentation.

Comparing the coordinates of the same survey point either from Table 1 and Table 2, it's obvious that all linear deviation for survey point 52 amount to 1,87 m, but that all the greatest deviation for survey points 43 and amount to 4,40 m. Since her profundity 420 m in relation to adopted reference point 1, resulted that the deviation of a trajectory of a well in this point is a little more than 1% and only as a consequence of different sediment of survey points.

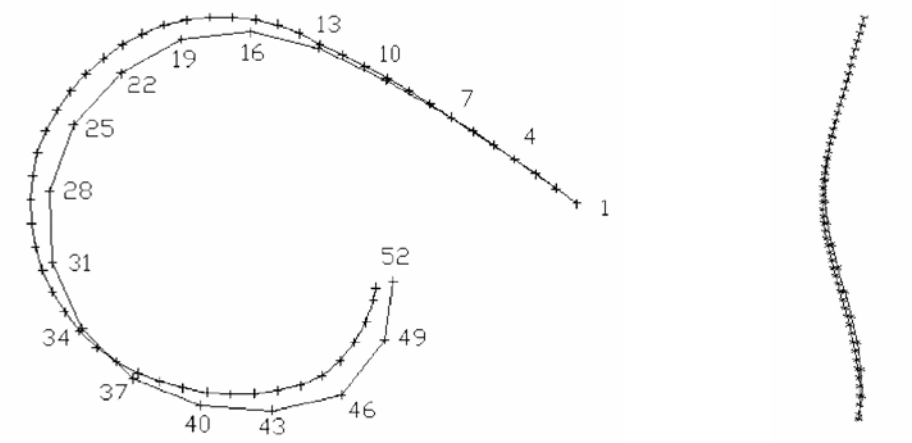

Figure 9. Comparative presentation of a well trajectory at different reciprocal distances of survey points

CONCLUSIONS

Measuring while drilling technology have increased drilling efficiency with obtaining direction related data, state of the borehole, drilling parameters and formation properties. This technology has become, in many cases an active part of the drilling operations. Future technological developments and improved measurement will make MWD essential part of drilling and formation evaluation.

At the example of the well "Ormož G-1" is presented indirectly advantage MWD in relation to conventional methods of measurement in a drill hole. Except of saving time, MWD allows greater profundity of measurement, by which the precision of controll the bore hole towards the desired target is going to increase. According to this it is obvious to pay attention that errors of measurement dimensions that are consequence of a precision of measuring device itself, are going to accumulate, so

it can be loosing on the precision because of much greatness of profudity of survey points.

Since that engaging of service companies with MWD devices increase the expenses of drilling substantially, their application can be proposed in cases of a high accuracy that is requirement of trajectory well controll, i.e. at the drilling of a directional–horizontal wells.

References

[1] Burgess T., Voisin B. (1992): Advances in MWD technology improve real time data. *Oil & Gas J.*; Vol. 90, No.7, Tulsa.

[2] Desbrandes R. (1988): Status Report: MWD Technology. *Pet. Eng. Itl.*; Vol. 61, No. 9–11, Houston.

[3] Eickelberg D., Rischmüller W. et al. (1982): Controlled Directional Drilling, Preussag AG, Peine.

[4] Rao M. V., Fontenot J. E. (1988): MWD poised for future. *Oil & Gas J.*; Vol. 90, No. 4–5, Tulsa.

[5] Rošer R. (2008): Usmerjanje vrtin pri raziskovanju nafte, plina in geotermalne energije, Diplomsko delo, Naravoslovnotehniška fakulteta, Ljubljana.

[6] Tsai C. R. (1992): MWD Sensors Improve Drilling Safety And Efficiency. *Pet. Eng. Itl.*; Vol. 65, No. 9, Houston.

[7] Veselič M., Božović M., Štancar J., Vižintin G. (1996): *Raziskave za zajetje termalne vode na območju Ormoža*. Ljubljana: IRGO, 14 f., 9 pril., načrti, zemljevidi.

[8] Vižintin G., Viršek S. (2008): Analitical surface water forecasting system for Republic of Slovenia. Analitičen sistem napovedovanja pretokov površinskih vod v Republiki Sloveniji. *RMZ;* Vol. 55, No. 2, str. 215–224.

[9] Vukelič Ž., Šporin J., Vižintin G. (2004): Pore pressure. *RMZ;* Vol. 51, No. 4, str. 2117–2125.

Analysis of self-declared environmental labels

Analiza samodeklariranih ekoloških oznak

Milana Ilić[1], Igor Budak[1], Branislava Crnobrnja[1], Janko Hodolič[1]

[1]University of Novi Sad, Faculty of Technical Sciences, Trg Dositeja Obradovića 6, Novi Sad, Serbia;
E-mail: milic@uns.ac.rs, budaki@uns.ac.rs, brcrnobrnja@uns.ac.rs, hodolic@uns.ac.rs

Received: January 13, 2009 **Accepted:** February 10, 2009

Abstract: Environmental labelling today presents one of the tools for environmental protection improvement. Expanse of eco-labelling is connected with the invention of firms that care for environment can make profit. Result was appearance of different declarations, claims and environmental labels on products and service. This trend, in the first phase influenced consumers in finding a way to act more environmentally advisedly through "green buying". In the next phase, by the appearance of large number of eco-labels, this trend caused confusion and scepticism of certain consumers.
In response to a number of misleading marketing claims in the late 1980s and early 1990s, in June 1993 a subcommittee of the International Organisation for Standardization (ISO) Technical Committee on Environmental Management began work on standards covering environmental marketing claims. The result was the standard ISO 14020 and the definition of three types of eco-labelling. In this article detailed analysis of eco-labelling fitting under the type II, according to ISO 14020 standard, is given.

Izvleček: Sedaj je okoljsko označevanje eno najpomembnejših orodij za dvig nivoja varovanja okolja. Širjenje okoljskega označevanja je povezano z dognanji podjetij, da skrb za varovanje okolja prinaša tudi dobiček. Rezultat tega je pojav različnih deklaracij, zahtev in okoljskih oznak za proizvode in storitve. Ta naravnanost, je v prvi fazi vplivala na potrošnike v smislu iskanja načina za ekološko delovanje z „zelenim nakupovanjem". V naslednji fazi se je zaradi prevelikega števila ekooznak pojavljala zmedenost in skeptičnost med potrošniki.
Kot odgovor na številne nejasnosti marketinških trditev v poznih osemdesetih in začetku devetdesetih let prejšnjega stoletja je v juniju leta 1993 podkomite Mednarodne organizacije za standardizacijo (ISO) začel delo pri standardih, ki obsegajo ekološko-marketinške trditve. Rezultat njihovega dela je standard ISO 14020 in definicija treh tipov ekoozačevanja. V prispevku je podana detajlna analiza ekoloških oznak tipa II po standardu ISO 14020.

Key words: environmental labels, self-declaration, ISO 14020, type II, claims
Ključne besede: ekološke oznake, samodeklarirane, ISO 14020, tip II, trditve

Review paper

Introduction

More expressive environmental consciousness put the demand to manufacturers that they should offer marketplace products that are pleased by high ecological standards[1]. There is growing interest among consumers, governments, and businesses in the environmental aspects of products, such as product energy efficiency, product take back and recycling, and use of hazardous materials are increasingly a part of the buying decision[2]. This is particularly true in the more environmentally aware markets of northern and central Europe and Japan. This recognition for products with environmentally preferable attributes has prompted green procurement activities in markets around the world and created the need for systematic and standardized communications with respect to environmental claims for products[3].

Environmental labelling is one of results of concern for environment, on local, as on global level. On their expanse the most influence had "invention" of firms that through careness for environment can make profit. So different declarations, claims and environmental labels appeared on products and service (for example, natural, recycle, eco-useful, low-energetic, etc.). However, this trend by one side influenced on consumers to find a way to reduce damaging on environment choosing buying, but on the other side provoked confusion and scepticism of certain consumers.

In response to a number of misleading marketing claims in the late 1980s and early 1990s, in June 1993 a subcommittee of the International Organisation for Standardization (ISO)[4] Technical Committee on Environmental Management began work on standards covering environmental marketing claims[5]. This was in response to growing international concern about the lack of consistent guidance for environmental claims and for eco-labels. Result is defining three type of eco-labelling by ISO[6]:

- Type I - a voluntary, multiple-criteria based, third party program that awards a license that authorizes the use of environmental labels on products indicating overall environmental preferability of a product within a particular product category based on life cycle considerations,
- Type II - informative environmental self-declaration claims, and
- Type III - voluntary programs that provide quantified environmental data of a product, under pre-set categories of parameters set by a qualified third party and based on life cycle assessment, and verified by that or another qualified third party.

The basic of environmental self-declared claims is security of reliability. It is important properly conduction of verification, in the aim of interruption negative marketing consequences, such as marketing abutment or unfair practices, which can ensue from disputable and deceivable environmental claims. Method of prediction environmental self-declared claims have to be clearly, transparent, scientifically supported, so potential customer of product can be sure in validity of claims[7]. In the following part of this article, detailed analysis of eco-la-

belling fitting under the type II according to ISO 14020 standard, is given[8].

Basic principles, definitions and procedures of environmental labels type II

Significant phase of developing ISO standard about self-declared environmental claims is evolution of ISO 14021, international standard that defines type II ecolabelling - self-declared environmental claims, issued in 1999.

A self-declared environmental claim is a declaration, a label or a symbol which draws attention to a certain element of the organisations activities, products or services and which can influence the environment. It is a special type of advertising. It is related to the product, its component or packaging. It can take the form of a statement, a label or a symbol placed on the product or on the products packaging, in the products documentation, in technical bulletins, in advertising and promotion, in TV marketing or possibly by means of digital and electronic media, such as the Internet. It can be issued by producers, importers, distributors, retailers or any other people that might benefit from such declarations. The parameters, environmental aspects which are intended to prove the products environmental friendliness, are chosen by the company-claimant themselves.

Environmental claims allow consumers to more easily differentiate between products in the market, so consumers can make better purchasing decisions in relation to the environment. In turn, consumer's purchasing power for such products is a market driver for business - to invest in more sustainable environmental practices[9]. The main advantage of the self-declared environmental claim is the opportunity to attract the attention of all target groups in a simple way, at a very low cost. Other advantages include:

- reducing the uncertainty in the market (credible information for consumers),
- facilitating international trade, and
- wider opportunities for customers, potential customers and users of the product to make a better informed decision when choosing a product.

Procedure for obtaining environmental labels

Before manufacturer decides to use self-declared environmental label, it is important to ascertain if there is some specific law or convention in which is requested how that environmental information need to be issued. Conventions are used for better understanding of minimal postulation, and to assure that claim/label is used properly by potential user.

Since Type II eco-labelling is more liable to an abuse, international standard ISO 14021 are proscribed exact directions for giving this declaration about product[7]. There are three main elements to be taken into account when considering making a self-declared environmental claim:

- the quality of the actual information being communicated (content),
- the way in which the information is presented (presentation), and
- the steps and methods taken to verify its accuracy (assurance of accuracy).

The content of the claim should be:
- correct and truthful,
- relevant,
- specific and unambiguous – especially when making a comparison.

The presentation of the claim should ensure that:
- the claim uses plain language,
- all relevant information is presented together,
- the meaning of any symbols or pictures is clear and relevant.

To ensure accuracy all claims should be:
- substantiated and verifiable,
- reassessed and updated as necessary,
- based on the best agreed standards available,
- supported by information needed to verify its accuracy.

Basic demands for correct and true environmental claims

While it might appear obvious that any environmental claim ought to be correct and truthful, this is not always easy to achieve. In particular, an environmental claim can be literally true, but still capable of being widely misunderstood or misinterpreted. This can be sold:
- consider how an ordinary member of the public, not an expert, might understand the claim;
- don't make claims, even when they are literally true, if they are likely to be misinterpreted;
- avoid claims indicating an environmental benefit that, while literally true, is unlikely to happen in practice,
- make sure a single environmental benefit isn't restated using different terminology to infer multiple benefits,
- if a claim relates to a pre-existing, but previously undisclosed aspect, don't make a claim inferring a recent improvement or enhancement,
- make sure that any claim indicating that a product is free of a specified substance contains no more of that ingredient than would be found as an acknowledged trace contaminant or background level. The threshold level used should be specified.

Basic demands for relativity of environmental claims

Relevance is about enabling customers to understand the context within which the claim is made. Environmental claims:
- make sure the claim is relevant to that particular product,
- make sure the claim is relevant to the place where the corresponding environmental impact occurs,
- clearly indicate whether the claim refers to the whole product, or just part of it, or just the packaging,
- do not make claims that imply that a product is exceptional when in fact all products in the marketplace share the same characteristic. The exception to this rule is where significant levels of consumer concern exist and consumers do not realise that it is a legislative requirement that all products share the same characteristic. In this scenario, the claim should be qualified, for example by the statement "in line with similar products …" or "as required by law …",
- don't make a claim based on the absence of ingredients or features which have never, or have not for some time,

been associated with the product category;
- regularly review and update all claims to ensure that they remain relevant in view of changes such as new legislation being enacted, improvement in the environmental performance of competing products and technological advances,
- make sure that any claim is used only in circumstances where there is a net environmental benefit associated with the product.

Basic demands for specific and unambiguouing of environmental claims

Ensuring that environmental claims are specific and unambiguous will help ensure that customers fully appreciate their intended meaning. The worst examples of this kind of labelling are those that are highly generalised, such as "environmentally friendly" or "nature's friend". It is this kind of poor quality labelling which has, in the past, discredited all forms of environmental labelling. This can be anticipating as:
- Make clear what environmental impact or improvement the claim relates to. A claim should identify exactly why a product is better for the environment and make a specific statement to that effect. Vague or non-specific environmental claims should never be used.
- Make clear the level of environmental improvement or performance achieved.
- If the claim involves a comparative assertion:
  - make clear the basis for the comparison
  - quantify the claim using either percentages or absolute values as appropriate
  - always make a comparison against a comparable product serving similar functions, either currently or recently in the same marketplace
  - only make a claim against: your own prior products or processes or/ and another organisation's products or processes.

Basic demands about understanding of environmental claims

It is possible for the information associated with a product to meet all the criteria referred to above, and yet still be unhelpful to customers as a result of the way that it is presented. To be sure that none of these cases appear, it is need to:
- make sure that any further information needed to understand an environmental claim is not buried in the small print,
- do not use language that exaggerates the advantages of the environmental feature the claim refers to,
- make sure that any symbols or logos are used in a way that their intended meaning is clear, if necessary by adding an explanatory statement,
- symbols used for environmental claims should be easily distinguishable from any other symbols found on products,
- natural objects such as trees, flowers or animals, should only be used if there is a direct and verifiable link between the product, the object and the environmental benefit being claimed. This link should be clearly explained.

Basic demands tied up with exact of environmental claims

There is no requirement to use third party verification or certification before an environmental claim is made, but it should be substantiated and verifiable. A business' own internal procedures may very well be able to perform this function. In addition, information should be retained by the person making the claim and supplied to anyone seeking justification of it.

In the aim of prevention arising of problem in relation with the previous need to be observed by next instructions[9]:

- check that the claim is fair and truthful, whether by testing the product or otherwise,
- don't make a claim if it could only be verified through access to confidential business information,
- document and retain information that others may need to verify any claims made,
- if the claim is a comparative claim, this should include data relating to the product with which the comparison is made.

Symbols of self-declared environmental labels

Symbols that are used for needs of self-declared claims need to be simple, easily reproducible and by position and size liable to product.

Usage of environmental labels and symbols serve as important source of information about product and producer. Usage need to be avoided in case they provoke wrongly interpreted definition and meaning of symbol by consumer. If company decides to announce this symbol, need to obligated (itself) that symbol owns an advantage qualities over similar products, services and companies. To avoid confusion, should avoid similarity with current official symbols. Explaining of environmental labels, with the definition and meaning need to be on package, promoting and other marketing material, and also instruction where can be find detailed information about label. More details can be found on web site, too. Possibility of checking and verification of evidences that support usage of environmental label must exist. Usage label/symbol to marketing causes must be in accordance with national marketing law, also in advancing defined criteria about ecological environmental claims. „Official labels" need to be mentioned here. Their usage is regulated and observed by competent organs, with advancing defined criterions[10].

Evaluation and verification procedures of self declared environmental claims

A person stating an environmental claim has to be responsible for evaluation and gathering of data necessary for verification of self declared claims. Prior to designing a environmental claim, additional evaluation measures have to be implemented in order to come to reliable results necessary to verify the statement. Evaluation has to be documented in detail, and person that voices the environmental claim has to adopt documentation in order to make the information public. This has to be applied to a period while the product was present in the market and to a realistic period after that, taking into account products shelf life.

Methods for verification and evaluation of environmental labels have to be supported by chronologically ordered following documents:

- international standards,
- standards easily identified and recognizable as well as internationally accepted (this also applies to regional and international standards), and
- industrial and merchandizing methods to which the same examination method will be applied.

In cases where the methods are not in place, the person putting forward an environmental claim can suggest a method, providing that the method is in line with other requests and that it is possible to examine it. Environmental labels are certified only in cases when classified business information has not been used. The labels shouldn't be shown if the only way to verify them is through classified business information. Environmental labels can voluntarily offer to the public information necessary to verify it. Otherwise, information which is necessary to verify the symbol has to be, at request and at reasonable expense, made public (which are covering the administrative expenses), time and place, to each individual wishing to check stated environmental labels.

The minimum information necessary, which are documented and adopted, should include the following[7]:

- identification of standards or methods used,
- proof in a form of a document if marking a environmental label cannot be checked on final product,
- results of the checking which are necessary to verify a environmental claims,
- name and address of an independent party, should the checking be implemented by an independent party,
- if self declared environmental claim cover comparison with other product, it has to exist highlighted description of applied method, results of any examination of these products and all potential assumptions,
- proof (statement) that evaluation of environmental claim by individuals pronouncing it offers guarantees on continuity of self declared environmental claim accuracy while the product is in the market and within particular period after, taking into account the product's shelf life.

The most applying environmental labels

There has been a number of type II environmental labels developed and actively used. However, among them, according to how often are they used and to which extent they are being recognized globally, there are several which are widely known. They are as follows: Mobius loop (environmental label for recycling), Green dot, Energy star, Pitch in, and Ozone friendly[9].

Self-declared environmental labels used for recycling

The original recycling symbol was designed in 1970 by Gary Anderson from L.A. University. He was sent to an International Design Conference as a part of

a wider competition between university students. The competition was a result of an increasing interest of consumers in environmental protection.

The symbol represents Mobius loop which is consisted of three interconnected arrows shaped as a triangle with somewhat rounded angles. Each arrow is being backwards bended and all three are connected to each other which in a way represents recycling cycles.

RE + CYCLE = repeated circulation: There is a common opinion that this is a recycling symbol, but that is only a partial answer. Originally the meaning of this symbol was a much broader one. That is a symbol for three "R" related to environment[11]: Reduce, Re-Use and Recycle.

Reduce - Re use - Recycle are the basic postulates of total waste management, in the first place the emphasis on avoiding waste, reduce it's amount, intention for its re use, it's repeated use, recycle and process giving new purposes to products and only in the end, what cannot be used will disposed in a way that will not be harmful for both the environment and our health. The reason why there is a common opinion that this is only a sign that symbolizes recycling, has been formed, according to many independent environmental movements and associations, because out of its three components, recycling is the most profitable ones. Mobius loop is a self declared environmental label whose use is not charged, but its use has been technically regulated. The label cannot be used in any modified shape and companies will adopt it as it is, as their logo or another brand. Specific requests that regulate the use of Mobius loop can be found in ISO standards. Having in mind that the consumers might not be fully aware of exact meaning of the symbol when it is presented in a different form, it is considered to be a good practice if it is published along a short explanation.

This symbol hasn't been protected and it is used in various ways and in different versions. In its most general sense it points out to the following facts[6]: that the product (or one of its parts) could be recycled or that recycled material has been used for the production of that particular item.

Recyclability is the most frequent sense of using the Mobius loop. It is being applied to products made out of recyclable materials.

Graphic design of the label is in Figure 1. The original Mobius loop graphic has been given in Figure 1 a), but the variation of the original symbol – in colour, which is used first of all because of the need to fit it with the design of the product or its emphasis (Figure 1b) and - *generic* (Figure 1c) derived from the original symbol that is used in cases when it is necessary to simplify the design for the applied production technology (for example in cases of tools for plastic, processing when cutting is used etc.). To generic version often some specific sign and markings are added pointing to the material from which they are made of: steel – made out of steel, alu - aluminium, pap - paper, special marking of plastic etc.[12].

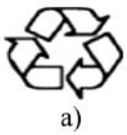

Figure 1. Mobius loop – variations of graphics used for term "recyclable"

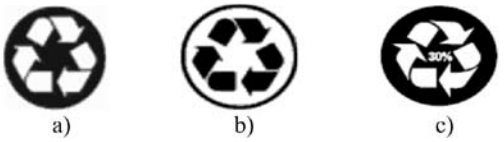

Figure 2. Versions of Mobius loop graph with application to products produced out of recycled material

This symbol is used to mark products which can be recycled e.g. those that can be recycled if the local community secured suitable conditions for collection and separation of waste.

The term "recyclable" can be used when there is evidence that[13]:

- the collection, sorting and delivery systems to transfer the materials from the source to the recycling facility are conveniently available to a reasonable proportion of the purchasers, potential purchasers and users of the product,
- the recycling facilities are available to accommodate the collected materials,
- the product for which the claim is made is being collected and recycled.

Recycled – when recycling material is used in producing a certain product to a certain extent, Mobius loop in a circle is being used. (Figure 2 a and b) and similar to previous case there are variations of graphic solution depending on the need. The most frequent ones are paper and cardboard products and nowadays more and more plastic products. In many cases a percent is placed in the centre of the symbol which tells us what is the percentage of recyclable material contained in the product (Figure 2 c)[12].

Environmental protection symbol – „Green dot"

Symbol „Green dot" started to be used in Germany within "Grüne Punkt" programme which is considered a prerun of the European programme. The original of this symbol (Figure 3) was presented in 1991 by „Duales System Deutschland" a non profit organization. Since 1994, it has been accepted by EU member states as well as some other European countries.

Figure 3. The original image of environmental symbol „Green dot"

The licence to use „The Green dot" has been transferred to an organization PRO Europe (Packaging Recovery Organisation) whose seat is in Brussels, Belgium and who is today a general representative of the Green dot. The Green dot is also an umbrella association that gathers several national organized industries that are successfully dealing with wrapping material waste in over 27 states of European Union[6].

By joining the green dot programme, the manufacturers are free of any commitment to take back the wrapping material of their products. The green dot is a registered symbol that is allocated to a wrapping and not to the product itself. The trade mark of the green dot could be placed on the package only once the product becomes licensed. The price of the license varies from state to a state and producers have to register individually with the programme in each of the countries to which they want to export their goods to. Payment is based on a principle „the producer pays" and it takes into account all expenses of gathering, sorting and recycling of various wrapping materials. The price depends on the state and material type that is used to produce the wrapping material. The system contributes to decreasing the level of waste as the producers that shrink their packaging are paying less. After the registering once in a month, tree month or on annual level, the companies have to submit the reports to the national programme of the green dot on waste creation. Only those companies that are doing their business in Europe can gain the green dot licence. Non European companies, therefore, often depend on their distributors in the process of getting a hold of the licence. This may result with the loss of control over finance or administration, conflict of interest if the cooperation is with several distributors in one state, in the loss of multiple reports from various distributors or confusion and additional work once the distributor is changed.

The green dot is one of today's most used symbols on environmental protection in the world. Currently, the standard of the return programme in 23 EU states and Canada and it is applied by over 130.000 companies that cover 460 billion packages[14].

Environmental label - "Energy star"

The global warming and the other global problems regarding environment are closely connected to the use of energy. In the last years, the energy consumption in the offices and especially in the households has been drastically increased, which in developed countries, this became a focus problem. Under such circumstances, at the end of 1992, the International program "Energy Star"[14] has started as a result of an agreement between Japan and the USA, which represented the collection of criteria for the decrease of the energy consumption, concerning office equipment with the major goal – the environmental protection. Later the other countries (Australia, New Zeeland, Taiwan Canada, etc.) supported and joined the program, and the process of EU countries joining to the program is ongoing.

Figure 4. Graphic presentation of the environmental label "Energy Star"

The program is applied in the market by placing the label "Energy Star"(Figure 4) on the products, which have shown that such products satisfy the program special criteria for the energy saving, and to, regardless their price, point out the advantage of the products to the consumers,

which is the environmental protection through saving of the energy. The label could be placed on the product, its wrappings or in the product documentation. By supporting this program the consumers are in the position to directly influence the environmental protection and to save their budget, by saving the energy, while the manufacturers, traders and the distributors are stimulated to produce, sell and promote such products, even more.

The Energy Star program was created in 1992 by the United States Environmental Protection Agency in an attempt to reduce energy consumption and greenhouse gas emission by power plants. The program was developed by John S. Hoffman (inventor of the Green Programs at EPA), and implemented by Cathy Zoi and Brian Johnson. The program was intended to be part of a series of voluntary programs that would demonstrate the potential for profit in reducing greenhouse gases and facilitate further steps to reducing global warming gases.

Since 1992 "Energy Star" becomes an international standard for energy efficiency of electronic equipment, and represent, perhaps, the most recognized type II labels. A recent agreement between the U.S. government and the European Union on development and use of the Energy Star label opens the way for further international acceptance of the logo. While the U. S. EPA along with the EU now establishes Energy Star criteria, manufacturers are allowed to self-certify compliance[14]. Organizations which are interested in connection with "Energy Star" are necessary to predict next steps if they want their products bee allowed by this programme:

- consider producer terms,
- consider product specifications, legal criteria, and partnership documents (which are on website www.energystar.gov),
- define the area of interests in this partnership, and describe its products filling in obliged form,
- review, complete, and sign agreement about partnership,
- register agreement about partnership and obliged form to "Energy Star".

Environmental label "Pitch-in"

Environmental label "Pitch-in" (Figure 5), which symbolizes a person who cleaning environment, is accepted in 1976 by non-profit international organization "Clean World International".

Figure 5. Format of eco-label "Pitch-in"

Unlike the other recycling symbols, this symbol is not primarily used to identify materials for separation, but it is widely used in the context of public education and outreach for anti-littering efforts. The use of this symbol is not limited to one country and therefore makes it a good candidate for inclusion in an international standard[12].

Environmental labels in conjunction with ozone protection

The labels and statements that certain

product is "Ozone Friendly", as it is often formulated falls under the so called, general statements, which means that there is no legal frame, or standards, that would regulate such type of label. Therefore the manufacturers decide themselves whether to use this statement or not, which tells us that such type of label could easily be misused for the interest of a manufacturer.

Ozone friendly is a claim that implies that the product or packaging has some kind of environmental benefit or that it causes no harm to the environment[15].

Figure 6. The environmental labels regarding ozone protection

"Ozone friendly" label can be found in most cases on deodorants and refrigerators. It means that the product does not contain CFC [Chlorofluorocarbons] gas (Figure 6), that contributes to the ozone layer depletion. There are German - "Ozon freundlich", "FCKW-frei", and French lection – "Preserve la couche d'ozone"[16].

All products have some environmental impact. Some manufacturers may cite specific reasons why they consider a product to be "ozone-friendly," while others may not. Some chemicals, like chlorofluorocarbons (CFCs) can damage the ozone layer. CFCs were banned in nearly all consumer products in 1978. Without more specific information, there is no way to determine whether products labelled "ozone friendly" is in any way better for the atmosphere than other products. To learn more about what is meant by this term, consumers must contact the manufacturer.

The International Standards Organization (ISO) considers this claim to be too vague to be meaningful to consumers. To comply with the ISO standard for environmental claims companies must not use "ozone-friendly" on their products.

Conclusions

In the European Union and the other developed countries, the programs of the ecolabeling are acting in large and the products without environmental label have difficult passage to the global market or are disabled in some cases.

Very important aspect is, however, a responsible use of environmental labels, otherwise, their use would have little sense, and therefore, the good organization and the efficiency of the system and the institutions are more than necessary.

Important problem is also the development of the infrastructure that should pro-

vide the sustainability of the application of these programs. As an example, we can again use the recycling label and green dot, which among the rest include the existence of the recycling machine of the satisfying capacities.

There is an urgent need to give great attention to:

- The education of the manufacturers about their benefits if they apply this sort of eco-labels and about the obstacles they can have if they do not apply it, and
- The education of the consumers for better understanding of the meaning of certain eco-labels and the influence of the labelled products on the environment.

Uplifting of the educational level of the mentioned subjects, regarding above cited, will have a synergetic effect to both, rising of the level of ecological consciousness and environmental protection in our country.

Acknowledgement

The results presented in this article have been obtained in the frame of Tempus project JEP_41156(2006), "Training of Institutions in Modern Environmental Approaches and Technologies – TIMEA".

References

[1] R. Nowosielski, A. Kania, M. Spilka: Indicators of technological processes environmental estimation, Journal of Achievements in Materials and Manufacturing Engineering, 22 (2007) 2, pp. 99–102.

[2] B. Kosec, M. Soković, L. Kosec, M. Bizjak, Z. Kampuš: Case of introduction of new ecologically safe material, Journal of Achievements in Materials and Manufacturing Engineering, 17 (2006) 1-2, pp. 85–88.

[3] J. Hodolič, M. Badida, M. Majernik, D. Šebo: Mechanical engineering in environmental engineering, University of Novi Sad, Faculty of Technical Sciences, Novi Sad, 2003.

[4] S. Senčič, B. Kosec: Sistem ravnanja z okoljem SIST EN ISO 14001, Univerza v Ljubljani, 2005 (in Slovene).

[5] W. Whitelaw: ISO 14001 – Environmental System Handbook, Elsevier, London, 2004.

[6] Hodolič, I. Budak: Prilazi označavanju proizvoda sa aspekta zaštite životne sredine, Festival kvaliteta 2004, JUSK-Jugoslovensko udruženje za standardizaciju i kvalitet, Zbornik radova, pp. IV-35 do IV-42, Kragujevac, 2004 (in Serbian).

[7] ISO 14021: Environmental labels and declarations - Self-declared environmental claims (Type II environmental labelling), 1999.

[8] A. J. Edwards: ISO 14001 Environmental Certification Step by Step, Elsevier, Amsterdam, 2007.

[9] I. Budak, B. Kosec: Environmental labelling of products and services, Teaching material, Tempus project JEP_ 41156(2006) "Training of Institutions in Modern Environmental Approaches and Technologies – TIMEA", 2009 (in print).

[10] A. P. Borštnik, M. Zarnik, T. Žagar:

Odgovorno okoljsko ravnanje – Sistemi ravnanja z okoljem, SIQ, Ljubljana, 2004 (in Slovene).

[11] M. Kutz: Environmentally conscious mechanical design, John Wiley & sons, New Jersey, 2007.

[12] Green Claims – Practical Guidance, www.defra.gov.uk/environment/consumerprod/pdf/growingmediaguid.pdf

[13] H. F. Lund: The McGraw-Hill Recycling Handbook, McGraw-Hill, New York, 2001.

[14] Energy Star, www.energystar.gov

[15] Environmental Label Claims and Advertising of Pest Control Products, www.pmra-arla.gc.ca/english/pdf/dir/dir9602-e.pdf

[16] The "OZONE FRIENDLY" labels, www.earth-conservation.org/index-english.php

Applicability of two different methods for determining particle shape

Uporabnost dveh različnih metod za določevanje oblike delcev

Damjan Hann[1]

[1]University of Ljubljana, Faculty of Natural Sciences and Engineering, Aškerčeva cesta 12, SI-1000 Ljubljana, Slovenia; E-mail: damjan.hann@ntf.uni-lj.si

Received: January 20, 2009 **Accepted:** February 24, 2009

Abstract: This report presents two methods for determining the shape of coarse aggregate grains with grain size ranging from 4 mm to 8 mm, and describes the shape index and shape factor. The method for determining the shape index according to SIST EN 933-4:2000 standard and the method for determining shape factor in two-dimensional space using computer software Leica Image Manager IM 50, used for processing of digital images, are presented. Particle shape plays a significant role in using rock aggregates for various purposes, both in terms of quality management and product price. Due to their isometric shape and consequently relatively high strength, cubic-shaped particles are often favoured. In this study we used three samples from different surface excavation sites in Slovenia. Each sample consisted of 80 randomly selected grains of coarse rock aggregate. The purpose of the research was to determine the advantages and disadvantages of both methods for determining the particle shape and to suggest the optimal method for quick and objective quality control in production with regard to particle shape.

Izvleček: Članek govori o določevanju oblike delcev grobega kamenega agregata frakcije velikosti delcev 4–8 mm oz. o indeksu in faktorju oblike, ki sta bila določena po dveh med seboj različnih metodah. Predstavljena je metoda določevanja indeksa oblike po evropskem standardu SIST EN 933-4:2000 ter metoda določevanja faktorja oblike v dvodimenzionalnem prostoru s pomočjo računalniške programske opreme Leica Image Manager IM 50, ki je bila uporabljena pri obdelavi digitalnih posnetkov. Oblika delcev ima sicer velik pomen pri uporabi kamenih agregatov za različne namene, opredeljuje lahko tudi kakovost in ceno nekega proizvoda. Zaradi svoje izometrične oblike in posledično relativno visoke trdnosti so najpogosteje zaželena kubična zrna. V raziskavo so bili vključeni trije vzorci iz različnih slovenskih površinskih kopov. V vsakem vzorcu je bilo 80 naključno izbranih delcev grobega kamenega agregata. Cilj raziskave je bil določiti prednosti in pomankljivosti izbranih metod za določanje oblike delcev oz.

Review paper

določiti ustrezno metodo za hitro in objektivno kontrolo kakovosti proizvodnje z ozirom na obliko delcev.

Key words: particle shape, shape index, shape factor, isometricity of particles
Ključne besede: oblika delcev, indeks oblike, faktor oblike, izometričnost delcev

Introduction

Rocks appear in different particle shapes in nature. For example, particles which have been formed by the process of physical weathering of rocks are much more angular than the particles which have been subjected to the activity of water, glaciers or waves, which are more round-shaped. Particles of rock aggregates, obtained by crushing or milling of the excavated material also produce a specific shape[1].

Particle shapes play a significant role in processes and influence the quality of the product and hence its price. In crushing rocks it is necessary to select a suitable crusher. Some crushers produce large amounts of unwanted shapes, i.e. elongated and flat grains[2]. The most desirable shapes are cubic grains due to their isometric form and relatively high strength.

Almost all processing industries require cubic grain forms. In road construction, for example, elongated and flat grains will crush after first rolling. Such grain shapes cause problems in bituminizing, leaving faults in the coating which are further exposed to weather impacts. If we use cubic-shaped grains for making concrete, we can achieve better and more even strength of cubes, use less cement and achieve better shapability of concrete.

In our project we focussed on determining the shape of particles in coarse rock aggregate which is usually incorporated in the material for making road fundations and as an aggregate in making concrete. The objects of research were the shape index and shape factor of particles in coarse rock aggregate (fractions with particle size ranging from 4–8mm), which were determined by two different methods.

We present the method for determining the shape index according to the European standard SIST EN 933-4:2000[3] and the method for determining the shape factor in two-dimensional space, using computer software Leica Image Manager IM 50[4] for digital image processing.

Materials and methods

Determining the shape index of particles following the European SIST EN 933-4:2000 standard

The European SIST EN 933-4:2000 standard describes the method of determining the shape index in coarse aggregates. This testing method is useful for fractions with particle size between 4–63 mm, or fractions $D_i \leq 63$ mm and $d_i \geq 4$ mm, where:

D_i/mm	maximum particle size,
d_i/mm	minimal particle size.

The shape index, obtained by the standard above, classifies particles based on the ratio between the particle length and its thickness, and gives two categories of particle shape: cubic in non-cubic particles. Individual particles in the sample of coarse aggregate are classified based on the ratio between the length of the particle *L* and its thickness *E* using a particle slide gauge for determining category (Figure 1).

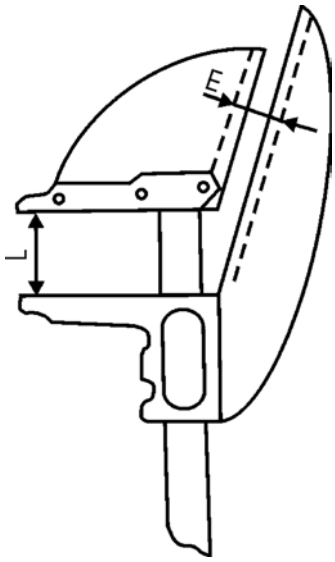

Figure 1. Scheme of the slide gauge
Slika 1. Skica pomičnega merila

The particle length *L* represents the maximum dimension of the particle, which is defined as the gratest distance between two parallel planes, tangential to the surface of the particle. The thickness of particle *E* represents the minimum dimension of the particle, as defined by the least distance between two parallel planes, tangential to the surface of the particle. Slide gauge has two openings: one is used for measuring the length *L*, and the other for measuring the thickness of the particle *E*.

Prior to analysing the shape index of particles it is necessary to prepare a sample. The sample must be passed through sieves with mesh sizes of 4 mm, 8 mm, 11,2 mm, 16 mm, 22,4 mm, 31,5 mm, 45 mm, and 63 mm. This allows for suitable separation of particles, i.e. larger than 4 mm and smaller than 63 mm. According to the standard, minimum quantities of sample are required considering the upper size limits of particles (Table 1).

Table 1. Minimum mass of the sample with regard to the maximum size of the aggregate
Tabela 1. Minimalna masa vzorca glede na maksimalno velikost agregata

Maximum size of aggregate D_i/mm	Minimum mass of the sample m/kg
63	45
32	6
16	1
8	0,1

Non-cubic particles are those in which the ratio between the length and the thickness is $L/E > 3$. The shape index is calculated as a mass of particles with the ratio of dimensions $L/E > 3$ against the total dry mass of the particles tested and is expressed in percentage.

The shape index is defined by the following equation:

$$SI = \frac{M_2}{M_1} \cdot 100 \qquad (1)$$

where:

SI/%	shape index
M_1/g	mass of the sample
M_2/g	mass of non-cubic particles

Determining the shape of particles in two-dimensional space using computer supported image processing

Computer processing of images has greatly contributed to the development of determining the shape of particles. The method for determining the shape of particles in two-dimensional space using computer software Leica Image Manager IM 50 is a method by which geometrical parameters of individual particles are determined by computer processing of digital images.

The shape factor of the particle in two-dimensional space can be determined using the following equation[5, 6]:

$$F = \frac{4 \cdot \pi \cdot A}{P^2} \quad (2)$$

Where the symbols mean:

F	shape factor
A/m^2	surface of particle
P/m	circumference of particle
π	constant

Shape factor F denotes the roundness of the sample: it tells how close the shape of the particle is to the shape of a regular circle. In particles with spherical shape F = 1, while for all other shapes $FO < 1$. For easier presentation, the shape factors for some basic shapes are given:

- CIRCLE
  1.0
- SQUARE
  0.785
- RECTANGLE (a/b = 1/2)
  0.698
- EQUILATERAL TRIANGLE
  0.605
- TRIANGLE (base/altitude = 1/3)
  0.376

Selection of samples

In our study we used samples from three surface excavations sites in Slovenia. Each sample consisted of 80 randomly selected particles of coarse rock aggregate fractions 4–8 mm in size, which we obtained by quartering. The first sample contained well-rounded gravel, the second sample consisted of crushed dolomite, and the third of crushed limestone.

According to SIST EN 933-4:2000 standard the mass of the sample should be minimum 100 g for the fraction with particle size range 4–8 mm. Since the same sample was also tested by computer method for determining particle shape, the scope of research would be much too large. For this reason we had to quarter the samples until we obtained only 80 grains in each sample. Using the slide gauge we determined the particles with non-cubic shapes and calculated the shape index.

Digital images of coarse rock aggregate particles of fractions with particle size of 4–8 mm were obtained by using a Canon Power Shot S70 digital camera. The images were then transferred and processed by the Leica Image Manager IM 50 computer

Table 2. Results of determining the shape index according to SIST EN 933-4:2000 standard
Tabela 2. Rezultati določanja indeksa oblike po standardu SIST EN 933-4:2000

Sample	Mass of the sample M_1/g	Mass of non-cubic particles M_2/g	Mass of cubic particles M/g	Shape index SI/%
1	23.1	0.8	22.3	3.46 ≈ 4
2	16.6	3.0	13.6	18.07 ≈ 18
3	14.4	2.9	11.5	20,14 ≈ 20

program, where we manually encircled the particles to obtain the information on two geometrical parameters i.e. the surface area and circumference of the particles. This allowed for calculating the shape factor.

RESULTS AND DISCUSSION

Results of determining the particle shape according to SIST EN 933-4:2000 standard

The samples from all three surface excavations were weighed and the mass (M_1 in grams) of each sample was recorded (Table 2). Using a slide gauge we determined the length L and the thickness E for each particle in the sample. The particles with dimension ratio $L/E > 3$ were classified as non-cubic particles. Non-cubic particles in samples were then weighed and the mass of each sample was recorded (M_2 in grams).

Results of determining the particle shape in two-dimensional space using Leica Image Manager IM 50 computer program

Average shape factor (F) for sample No. 1:
$F_{(\text{sample No.1})} = 0.9$

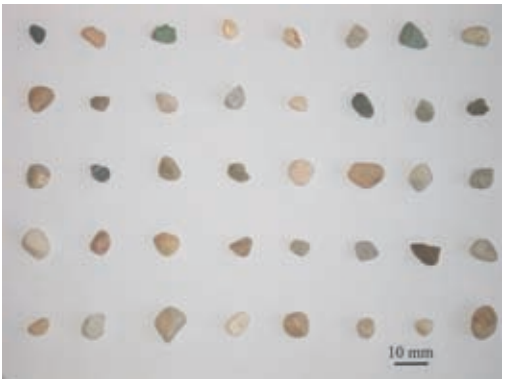

Figure 2. Sample No. 1 – gravel
Slika 2. Vzorec št. 1 – prod

Average shape factor (F) for sample No. 2:
$F_{(\text{sample No. 2})} = 0.84$

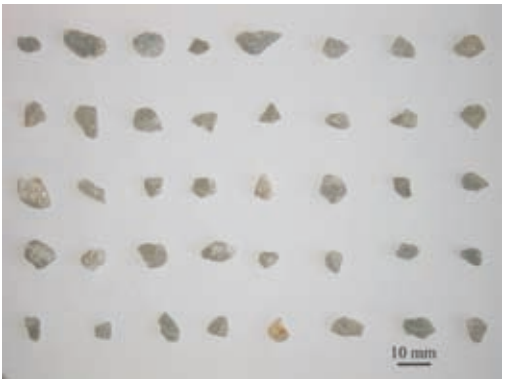

Figure 3. Sample No. 2 – dolomite
Slika 3. Vzorec št. 2 – dolomit

Average shape factor (F) for sample No. 3: $F_{(\text{sample No.3})} = 0.83$

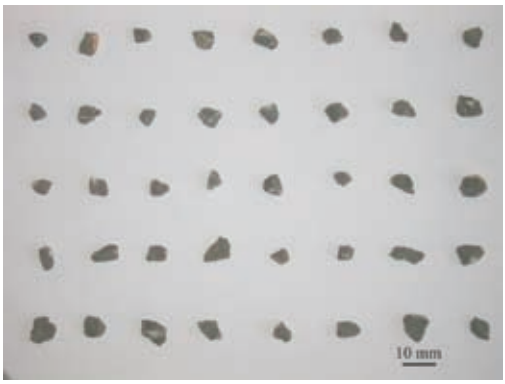

Figure 4. Sample No. 3 – limestone
Slika 4. Vzorec št. 3 – apnenec

Table 3. Research results
Tabela 3. Rezultati raziskave

Sample	Shape index *SI*/%	Shape factor *F*
1	4	0.90
2	18	0.84
3	20	0,83

The shape index for sample No. 1 was 4 % (Table 3), meaning that the share of non-cubic particles in the sample was 4 %, while there were 96 % particles with relatively regular shape and these were considered as cubic particles. The average shape factor for sample No. 1 was 0.90.

The shape index for sample No. 2 accounted for 18 %, meaning that there were 18 % of particles in the sample which were considered as non-cubic and the remaining 82 % were cubic particles. The average shape factor for sample No. 2 was 0.84. The same analogy applies to sample No. 3: there were 20 % of non-cubic particles and 80 % of cubic particles. The average shape factor for this sample was 0.83.

Conclusions

Using the SIST EN 933-4:2000 standard for determining the shape index is an easy and quick method for separating cubic and non-cubic particles from a coarse rock aggregate. This method allows for a rapid and reliable quality control in production. However, this method is not automated; measurements must be done manually, and for this reason the results may be subjective. The downside of this method is that it can be applied only for characterising particles larger than 4 mm and smaller than 63 mm. This method has been developed for determining the particles shape in coarse rock aggregates which are used in the production of asphalt mixtures, production of concrete and construction materials. For these purposes this method for determining particle shape is quite suitable.

The method of determining the shape factor in two-dimensional space using computer processed images is also applicable at micrometer particle size range, which all greatly contributes to the developments in cement, chemical and pharmaceutical industries. This method provides an easy way for measuring geometrical parameters, e.g. surface area, circumference, the length and the width of particles. The weakness of this method is that particles are presented in two dimensions only while the third dimension remains hidden. Therefore, it depends on the position of particles

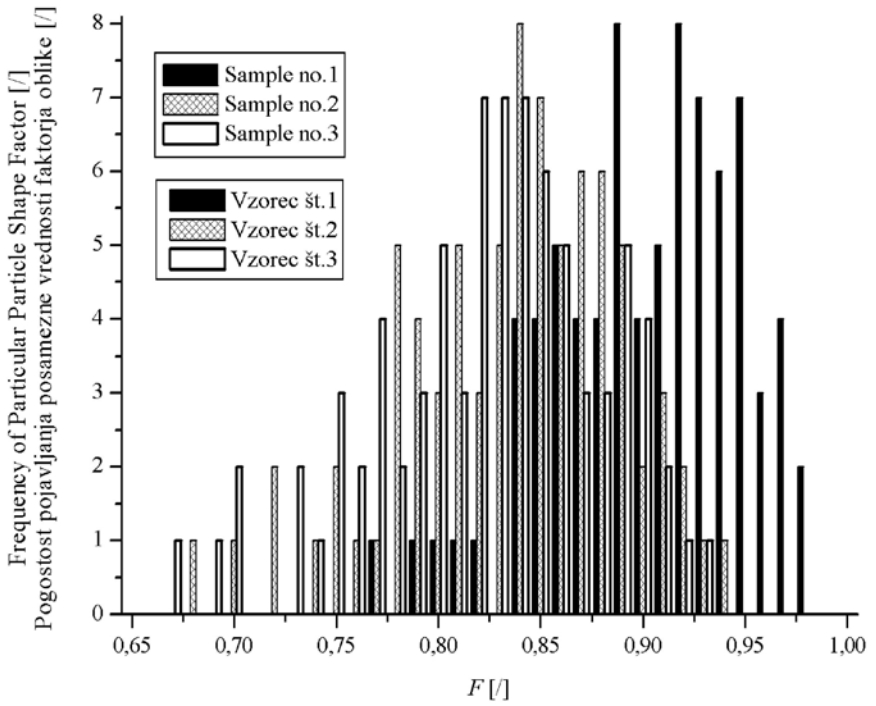

Figure 5. Frequency of particular particle shape factor
Slika 5. Pogostost pojavljanja posameznih vrednosti faktorja oblike

which dimension will be shown. However, this method proved to be quite time-consuming since we had to »manually encircle« every particle. Even though there is a market available software, which allows for automated capturing and processing of data, we found this software of no use in our study.

Both methods are comparable, since both can show the isometricity of particles, as shown by our results. The method according to SIST EN 933-4:2000 standard is faster, while the method of determining the shape factor in two-dimensional space using Leica Image Manager IM50 computer software was more accurate in determining the shape of particles, i.e. the differences in particle shapes were shown more precisely. The shortcoming of this method, however, is that it is time-consuming and limited only to two-dimensional presentation.

POVZETEK

Oblika delcev lahko ima velik pomen pri poteku nekega procesa ter opredeljuje kakovost nekega proizvoda in njegovo ceno. Zaradi svoje izometrične oblike in posledično relativno visoke trdnosti so v industriji običajno najbolj zaželena kubična zrna.

Članek govori o določevanju oblike delcev

grobega kamenega agregata, ki se uporablja za vgradnjo v cestne podlage in kot agregat pri izdelavi betona. Predmet raziskav sta bila indeks in faktor oblike delcev grobega kamenega agregata (frakcije velikosti delcev 4–8 mm), ki sta bila določena po dveh med seboj različnih metodah. Predstavljena je metoda določevanja indeksa oblike po evropskem standardu SIST EN 933-4:200 ter metoda določevanja faktorja oblike v dvodimenzionalnem prostoru s pomočjo računalniške programske opreme Leica Image Manager IM 50, ki je bila uporabljena pri obdelavi digitalnih posnetkov.

Indeks oblike, pridobljen s pomočjo pomičnega merila po navedenem standardu klasificira delce na osnovi razmerja med dolžino delca L in debelino delca E in nam podaja dve kategoriji oblike delcev, kubične in nekubične delce. Nekubični delci so tisti delci, za katere velja, da je razmerje $L/E > 3$. Indeks oblike je izračunan kot masa delcev z razmerjem dimenzij $L/E > 3$ proti celotni suhi masi preskušanih delcev in je izražen v odstotkih.

Metoda določanja oblike delcev v dvodimenzionalnem prostoru s pomočjo računalniške programske opreme Leica Image Manager IM 50 je metoda, kjer s pomočjo računalniške obdelave digitalnih posnetkov določimo geometrične parametre posameznega delca.

Faktor oblike F opisuje okroglost delca oz. sporoča, kako blizu ali daleč je oblika delca od oblike pravilnega kroga. Za delce okrogle oblike velja $F = 1$, za vse ostale oblike pa je $FO < 1$.

V raziskavo smo vključili vzorce iz treh slovenskih površinskih kopov. Vsak vzorec je vseboval 80 naključno izbranih delcev grobega kamenega agregata frakcije velikosti delcev 4–8 mm, ki smo jih pridobili s četrtinjenjem. V primeru prvega vzorca je šlo za dobro zaobljene prodnike, v drugem za dolomitne drobljence, v tretjem pa za drobljeni apnenec.

Digitalne slike delcev smo pridobili s pomočjo digitalnega fotoaparata Canon Power Shot S70. Slike smo nato prenesli v računalniški program Leica Image Manager IM 50, kjer smo na podlagi ročnega obkrožanja delcev pridobili informacijo o dveh geometričnih parametrih (površini delca in obsegu delca), s katerima smo lahko izračunali faktor oblike.

Rezultati so pokazali, da sta metodi med seboj primerljivi, ker sta obe sposobni prikazati izometričnost delcev. Metoda po standardu SIST EN 933-4:2000 je hitrejša, metoda določevanja faktorja oblike v dvodimenzionalnem prostoru s pomočjo računalniške programske opreme Leica Image Manager IM50 pa je bolj natančno določila obliko delcev oz. je bolj dosledno razlikovala med posameznimi oblikami delcev. Pomankljivost slednje metode je poleg zamudnosti tudi ta, da gre za dvodimenzionalni prostor, kar prinaša določene omejitve.

References

[1] Stark, U., Mueller, A. (2004): Effective methods for measurement of particle size and shape. *Aufbereitungs*

Technik; Vol. 45, No. 6, pp. 6–16.

[2] KUYUMCU, H. Z., PETERSSON, E., ROLF, L. (2005): Studies on the Influence of Comminution Mechanisms on the Particle Shape of Comminuted Products. *Aufbereitungs Technik;* Vol. 46, No. 11, pp. 4–13.

[3] European Standard EN 933-4:2000 – *Tests for geometrical properties of aggregates – Part 4: Determination of particle shape – Shape index*, European Committee for Standardization, 2000.

[4] Leica Image Manager IM 50, manual (CD-version).

[5] KALIŠNIK, M., ERŽEN, I., SMOLEJ, V. (2002): *Temelji stereologije*, 3rd ed. Ljubljana: DSKAS, 133 p. (In Slovene).

[6] HANN, D. (2007): *Vpliv nekaterih lastnosti na tečenje sipkih snovi: doktorska disertacija*. Ljubljana, 108 p.

Author`s Index, Vol. 56, No. 1

Budak Igor	budaki@uns.ac.rs
Crnobrnja Branislava	brcrnobrnja@uns.ac.rs
Ganić Aleksandar	aganic@rgf.bg.ac.yu
Glavaš Zoran	glavaszo@simet.hr
Gusković Dragoslav	
Hann Damjan	damjan.hann@ntf.uni-lj.si
Hodolič Janko	hodolic@uns.ac.rs
Ilić Milana	milic@uns.ac.sr
Kobe S.	
Kovačič Miha	miha.kovacic@store-steel.si
Leković Branko	blekovic@rgf.bg.ac.yu
Mačkošek Katja	
Manasijević Dragan	
Marjanović Saša	smarjanovic@tf.bor.ac.yu
Markoli B.	bostjan.markoli@ntf.uni-lj.si
Marolt Tomaž	
Mcguiness P. J.	paul.mcguiness@ijs.si
Mihevc Andrej	
Minić Duško	
Okunlola Olugbenga A.	o.okunlola@mail.ui.edu.ng
Oyedokun Matthew O.	
Podmiljšak B.	beno.podmiljsak@ijs.si
Ristović Ivica	ivica@rgf.bg.ac.yu
Savić Ljiljana	
Savić Ljubinko	
Škulj I.	
Terzić Katarina	terzicka@simet.hr
Unkić Faruk	unkic@simet.hr
Vulić Milivoj	milivoj.vulic@ntf.uni-lj.si
Živković Dragana	

INSTRUCTIONS TO AUTHORS

RMZ-MATERIALS & GEOENVIRONMENT (RMZ- Materiali in geookolje) is a periodical publication with four issues per year (established 1952 and renamed to RMZ-M&G in 1998). The main topics of contents are Mining and Geotechnology, Metallurgy and Materials, Geology and Geoenvironment.
RMZ-M&G publishes original Scientific articles, Review papers, Technical and Expert contributions (also as short papers or letters) **in English**. In addition, evaluations of other publications (books, monographs,...), short letters and comments are welcome. A short summary of the contents in Slovene will be included at the end of each paper. It can be included by the author(s) or will be provided by the referee or the Editorial Office.
**** Additional information and remarks for Slovenian authors:***
English version with extended "Povzetek", and additional roles (in Template for Slovenian authors) ***can*** *be written. Only exceptionally the articles in the Slovenian language with summary in English will be published. The contributions in English will be considered with priority over those in the Slovenian language in the review process.*

Authorship and originality of the contributions. Authors are responsible for originality of presented data, ideas and conclusions as well as for correct citation of data adopted from other sources. The publication in RMZ-M&G obligate authors that the article will not be published anywhere else in the same form.

Specification of Contributions

Optimal number of pages of full papers is 7 to 15, longer articles should be discussed with Editor, but 20 pages is limit.
Scientific papers represent unpublished results of original research.
Review papers summarize previously published scientific, research and/or expertise articles on the new scientific level and can contain also other cited sources, which are not mainly result of author(s).
Technical and Expert papers are the result of technological research achievements, application research results and information about achievements in practice and industry.
Short papers (Letters) are the contributions that contain mostly very new short reports of advanced investigation. They should be approximately 2 pages long but should not exceed 4 pages.
Evaluations or critics contain author's opinion on new published books, monographs, textbooks, exhibitions...(up to 2 pages, figure of cover page is expected).

In memoriam (up to 2 pages, a photo is expected).
Professional remarks (Comments) cannot exceed 1 page, and only professional disagreements can be discussed. Normally the source author(s) reply the remarks in the same issue.

Supervision and review of manuscripts. All manuscripts will be supervised. The referees evaluate manuscripts and can ask authors to change particular segments, and propose to the Editor the acceptability of submitted articles. Authors can suggest the referee but Editor has a right to choose another. **The name of the referee remains anonymous.** The technical corrections will be done too and authors can be asked to correct missing items. The final decision whether the manuscript will be published is made by the Editor in Chief.

The Form of the Manuscript

The manuscript should be submitted as a complete hard copy including figures and tables. The figures should also be enclosed separately, both charts and photos in the original version. In addition, all material should also be provided in electronic form on a diskette or a CD. The necessary information can conveniently also be delivered by E-mail.

Composition of manuscript is defined in the attached Template

The original file of Template is temporarily available on E-mail addresses:
peter.fajfar@ntf.uni-lj.si,
barbara.bohar@ntf.uni-lj.si

References - can be arranged in two ways:
- first possibility: alphabetic arrangement of first authors - in text: (Borgne, 1955),
or
- second possibility: [1] numerated in the same order as cited in the text: example[1]

Format of papers in journals:

Le Borgne, E. (1955): Susceptibilite magnetic anomale du sol superficiel. *Annales de Geophysique*, 11, pp. 399-419.

Format of books:

Roberts, J. L. (1989): Geological structures, *MacMillan*, *London*, 250 p.

Text on the hard print copy can be prepared with any text-processor. The electronic version on the diskette, CD or E-mail transfer should be in MS Word or ASCII format.
Captions of figures and tables should be enclosed separately. **Figures (graphs and photos)** and tables should be original and sent separately in addition to text. They can be prepared on paper or computer designed (MSExcel, Corel, Acad).
Format. Electronic figures are recommended to be in CDR, Al, EPS, TIF or JPG formats. Resolution of bitmap graphics (TIF, JPG) should be at least 300 dpi. Text in vector graphics (CDR, Al, EPS) must be in MSWord Times typography or converted in curves.
Color prints. Authors will be charged for color prints of figures and photos.
Labeling of the additionally provided material for the manuscript should be very clear and must contain at least the lead author's name, address, the beginning of the title and the date of delivery of the manuscript. In case of an E-mail transfer the exact message with above asked data must accompany the attachment with the file containing the manuscript.
Information about RMZ-M&G:
Editor in Chief prof. dr. Peter Fajfar (tel. ++386 1 4250-316) or
Secretary Barbara Bohar Bobnar, un. dipl. ing. geol. (++386 1 4704-630),
Aškerčeva 12, Ljubljana, Slovenia

or at E-mail addresses:
peter.fajfar@ntf.uni-lj.si,
barbara.bohar@ntf.uni-lj.si

Sending of manuscripts. Manuscripts can be sent by mail to the **Editorial Office** address:

- RMZ-Materials & Geoenvironment
  Aškerčeva 12,
  1001 Ljubljana, Slovenia

or delivered to:

- **Reception** of the Faculty of Natural Science and Engineering (for RMZ-M&G)
  Aškerčeva 12,
  1001 Ljubljana, Slovenia
- E-mail - addresses of Editor and Secretary
- You can also contact them on their phone numbers.

These instructions are valid from September 2003

TEMPLATE

The title of the manuscript should be written in bold letters (Times New Roman, 14, Center)

Name Surname[1], …. , & Name Surname[X]
(Times New Roman, 12, Center)

[x]Faculty of ... , University of ... , Address…, Country, e-mail: ...
(Times New Roman, 11, Center)

THE LENGTH OF FULL PAPER SHOULD NOT EXCEED TWENTY (20, INCLUDING FIGURES AND TABLES) PAGES (OPTIMAL 7 TO 15), SHORT PAPER FOUR (4) AND OTHER TWO (2) WITHOUT TEXT FLOWING BY GRAPHICS AND TABLES.

Abstract (Times New Roman, Normal, 11): The text of the abstract is placed here. The abstract should be concise and should present the aim of the work, essential results and conclusion. It should be typed in font size 11, single-spaced. Except for the first line, the text should be indented from the left margin by 10 mm. The length should not exceed fifteen (15) lines (10 are recommended).

Key words: a list of up to 5 key words (3 to 5) that will be useful for indexing or searching. Use the same styling as for abstract.

Introduction (Times New Roman, Bold, 12)

Two lines below the keywords begin the introduction. Use Times New Roman, font size 12, Justify alignment.
There are two (2) admissible methods of citing references in text:

1. by stating the first author and the year of publication of the reference in the parenthesis at the appropriate place in the text and arranging the reference list in the alphabetic order of first authors; e.g.:
   "Detailed information about geohistorical development of this zone can be found in: Antonijević (1957), Grubić (1962), ..."

"… the method was described previously (Hoefs, 1996)"

2. by consecutive Arabic numerals in square brackets, superscripted at the appropriate place in the text and arranging the reference list at the end of the text in the like manner; e.g.:
   "... while the portal was made in Zope[3] environment."

Materials and methods (Times New Roman, Bold, 12)

This section describes the available data and procedure of work and therefore provides enough information to allow the interpretation of the results, obtained by the used methods.

Results and discussion (Times New Roman, Bold, 12)

Tables, figures, pictures, and schemes should be incorporated in the text at the appropriate place and should fit on one page. Break larger schemes and tables into smaller parts to prevent extending over more than one page.

Conclusions (Times New Roman, Bold, 12)

This paragraph summarizes the results and draws conclusions.

Acknowledgements (Times New Roman, Bold, 12, Center - optional)

This work was supported by the ****.

References (Times New Roman, Bold, 12*)*

In regard to the method used in the text, the styling, punctuation and capitalization should conform to the following:

FIRST OPTION - in alphabetical order
Casati, P., Jadoul, F., Nicora, A., Marinelli, M., Fantini-Sestini, N. & Fois, E.

(1981): Geologia della Valle del'Anisici e dei gruppi M. Popera - Tre Cime di Lavaredo (Dolomiti Orientali). *Riv. Ital. Paleont.*; Vol. 87, No. 3, pp. 391-400, Milano.

Folk, R. L. (1959): Practical petrographic classification of limestones. *Amer. Ass. Petrol. Geol. Bull.;* Vol. 43, No. 1, pp. 1-38, Tulsa.

SECOND OPTION - in numerical order

[1] Trček, B. (2001): *Solute transport monitoring in the unsaturated zone of the karst aquifer by natural tracers.* Ph.D. Thesis. Ljubljana: University of Ljubljana 2001; 125 p.

[2] Higashitani, K., Iseri, H., Okuhara, K., Hatade, S. (1995): Magnetic Effects on Zeta Potential and Diffusivity of Nonmagnetic Particles. *Journal of Colloid and Interface Science 172*, pp. 383-388.

Citing the Internet site:

CASREACT-Chemical reactions database [online]. Chemical Abstracts Service, 2000, updated 2.2.2000 [cited 3.2.2000]. Accessible on Internet: http://www.cas.org/CASFILES/casreact.html.

Povzetek (Times New Roman, 12)

A short summary of the contents in Slovene (up to 400 characters) can be written by the author(s) or will be provided by the referee or by the Editorial Board.

TEMPLATE for Slovenian Authors

The title of the manuscript should be written in bold letters (Times New Roman, 14, Center)

Naslov članka (Times New Roman, 14, Center)

Name Surname[1],…. , & Name Surname[X] (Times New Roman, 12, Center)
Ime Priimek[1], …, Ime Priimek[X] (Times New Roman, 12, Center)

[X]Faculty of ... , University of ... , Address…, Country; e-mail: ...
(Times New Roman, 11, Center)
[X]Fakulteta…, Univerza…, Naslov…, Država; e-mail: …
(Times New Roman, 11, Center)

THE LENGTH OF ORIGINAL SCIENTIFIC PAPER SHOULD NOT EXCEED TWENTY (20, INCLUDING FIGURES AND TABLES) PAGES (OPTIMAL 7 TO 15), SHORT PAPER FOUR (4) AND OTHER TWO (2) WITHOUT TEXT FLOWING BY GRAPHICS AND TABLES.
DOLŽINA IZVIRNEGA ZNANSTVENEGA ČLANKA NE SME PRESEGATI DVAJSET (20, VKLJUČNO S SLIKAMI IN TABELAMI), KRATKEGA ČLANKA ŠTIRI (4) IN OSTALIH PRISPEVKOV DVE (2) STRANI.

Abstract (Times New Roman, Normal, 11): The text of the abstract is placed here. The abstract should be concise and should present the aim of the work, essential results and conclusion. It should be typed in font size 11, single-spaced. Except for the first line, the text should be indented from the left margin by 10 mm. The length should not exceed fifteen (15) lines (10 are recommended).

Izvleček (TNR, N, 11): Kratek izvleček namena članka ter ključnih rezultatov in ugotovitev. Razen prve vrstice naj bo tekst zamaknjen z levega roba za 10 mm. Dolžina naj ne presega petnajst (15) vrstic (10 je priporočeno).

Key words: a list of up to 5 key words (3 to 5) that will be useful for indexing or searching. Use the same styling as for abstract.

Ključne besede: seznam največ 5 ključnih besed (3-5) za pomoč pri indeksiranju ali iskanju. Uporabite enako obliko kot za izvleček.

Introduction – Uvod (Times New Roman, Bold, 12)

Two lines below the keywords begin the introduction. Use Times New Roman, font size 12, Justify alignment. All captions of text and tables as well as the text in graphics must be prepared in English and Slovenian language.
Dve vrstici pod ključnimi besedami se začne Uvod. Uporabite pisavo TNR, velikost črk 12, z obojestransko poravnavo. Naslovi slik in tabel (vključno z besedilom v slikah) morajo biti pripravljeni v slovenskem in angleškem jeziku.

Figure (Table) X. Text belonging to figure (table)
Slika (Tabela) X. Pripadajoče besedilo k sliki (tabeli)

There are two (2) admissible methods of citing references – obstajata dve sprejemljivi metodi navajanja referenc:

1. by stating the first author and the year of publication of the reference in the parenthesis at the appropriate place in the text and arranging the reference list in the alphabetic order of first authors; e.g.:
1. z navedbo prvega avtorja in letnice objave reference v oklepaju na ustreznem mestu v tekstu in z ureditvijo seznama referenc po abecednem zaporedju prvih avtorjev; npr.:
   "Detailed information about geohistorical development of this zone can be found in: Antonijević (1957), Grubić (1962), ..."
   "… the method was described previously (Hoefs, 1996)"

or/ali

2. by consecutive Arabic numerals in square brackets, superscripted at the appropriate place in the text and arranging the reference list at the end of the text in the like manner; e.g.:
2. z zaporednimi arabskimi številkami v oglatih oklepajih na ustreznem mestu v tekstu in z ureditvijo seznama referenc v številčnem zaporedju navajanja; npr.;
   "... while the portal was made in Zope[3] environment."

Materials and methods (Times New Roman, Bold, 12)

This section describes the available data and procedure of work and therefore provides enough information to allow the interpretation of the results, obtained by the used methods.
Ta del opisuje razpoložljive podatke, metode in način dela ter omogoča zadostno količino informacij, da lahko z opisanimi metodami delo ponovimo.

Results and discussion – Rezultati in razprava (Times New Roman, Bold, 12)

Tables, figures, pictures, and schemes should be incorporated (inserted, not pasted) in the text at the appropriate place and should fit on one page. Break larger schemes and tables into smaller parts to prevent extending over more than one page.
Tabele, sheme in slike je potrebno vnesti (z ukazom Insert, ne Paste) v tekst na ustreznem mestu. Večje sheme in tabele je potrebno ločiti na manjše dele, da ne presegajo ene strani.

Conclusions – Sklepi (Times New Roman, Bold, 12)

This paragraph summarizes the results and draws conclusions.
Povzetek rezultatov in zaključki.

Acknowledgements – Zahvale (Times New Roman, Bold, 12, Center - optional)

This work was supported by the ……..
Izvedbo tega dela je omogočilo ……

References - Viri (Times New Roman, Bold, 12)

With regard to the method used in the text, the styling, punctuation and capitalization should conform to the following:
Glede na uporabljeno metodo citiranja referenc v tekstu upoštevajte eno od naslednjih oblik:

FIRST OPTION (recommended) – PRVA MOŽNOST (priporočena) – in alphabetical order (v abecednem zaporedju)

Casati, P., Jadoul, F., Nicora, A., Marinelli, M., Fantini-Sestini, N. & Fois, E. (1981): Geologia della Valle del'Anisici e dei gruppi M. Popera – Tre Cime di Lavaredo (Dolomiti Orientali). *Riv. Ital. Paleont.*; Vol. 87, No. 3, pp. 391-400, Milano.

Folk, R. L. (1959): Practical petrographic classification of limestones. *Amer. Ass. Petrol. Geol. Bull.;* Vol. 43, No. 1, pp. 1-38, Tulsa.

SECOND OPTION – DRUGA MOŽNOST - in numerical order (v numeričnem zaporedju)

[1] Trček, B. (2001): *Solute transport monitoring in the unsaturated zone of the karst aquifer by natural tracers.* Ph.D. Thesis. Ljubljana: University of Ljubljana 2001; 125 p.

[2] Higashitani, K., Iseri, H., Okuhara, K., Hatade, S. (1995): Magnetic Effects on Zeta Potential and Diffusivity of Nonmagnetic Particles. *Journal of Colloid and Interface Science 172*, pp. 383-388.

Citing the Internet site:
CASREACT-Chemical reactions database [online]. Chemical Abstracts Service, 2000, updated 2.2.2000 [cited 3.2.2000]. Accessible on Internet: http://www.cas.org/CASFILES/casreact.html.

Citiranje Internetne strani:
CASREACT-Chemical reactions database [online]. Chemical Abstracts Service, 2000, obnovljeno 2.2.2000 [citirano 3.2.2000]. Dostopno na svetovnem spletu: http://www.cas.org/CASFILES/casreact.html.

Povzetek – Summary (Times New Roman, 12)

An extended summary of the contents in Slovene (from one page to approximately 1/3 of the original article length).
Razširjeni povzetek vsebine prispevka v Angleščini (od ene strani do približno 1/3 dolžine izvirnega članka).

Skupina GEN

PREMOGOVNIK VELENJE

PREMOGOVNIK VELENJE

je pomemben in zanesljiv člen
v oskrbi Slovenije
z električno energijo.

Zavedamo se odgovornosti do
lastnikov, zaposlenih in okolja.

ČUT ZA PRIHODNOST

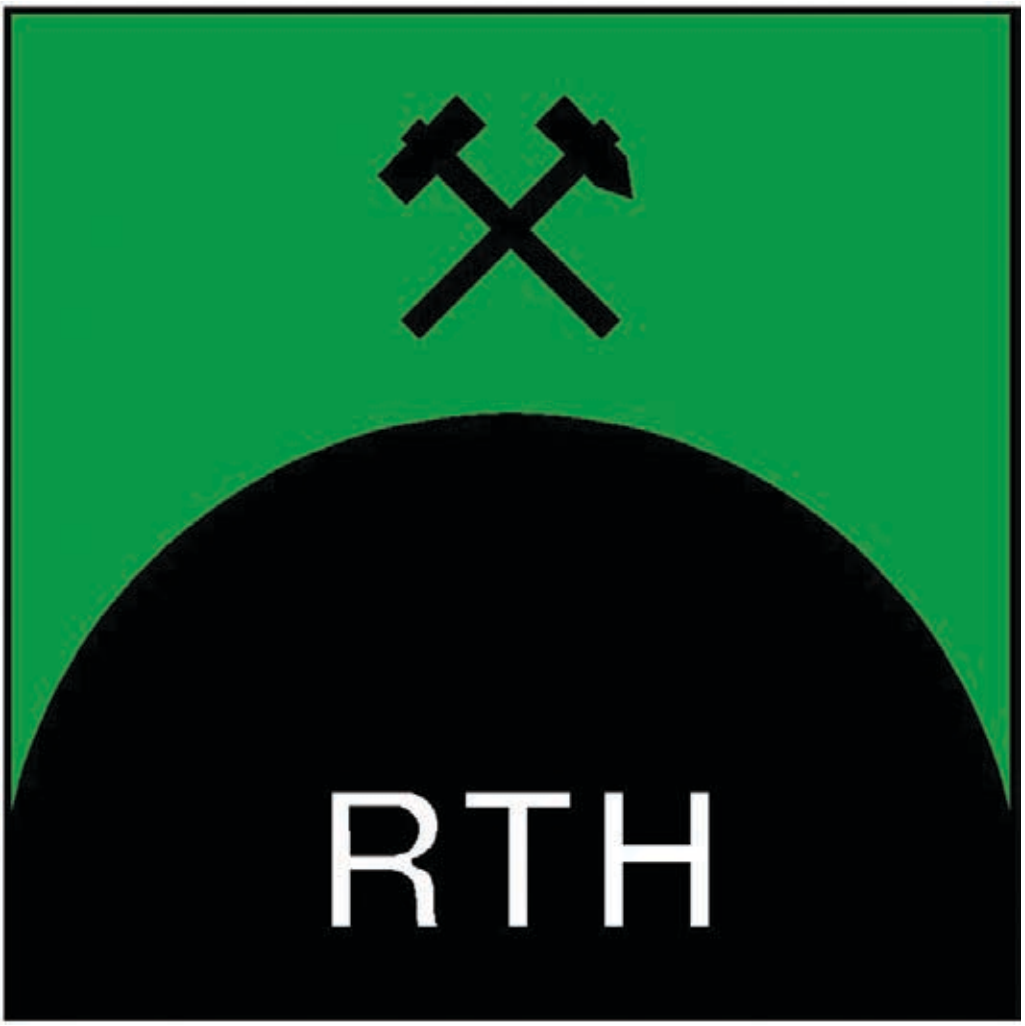
RTH

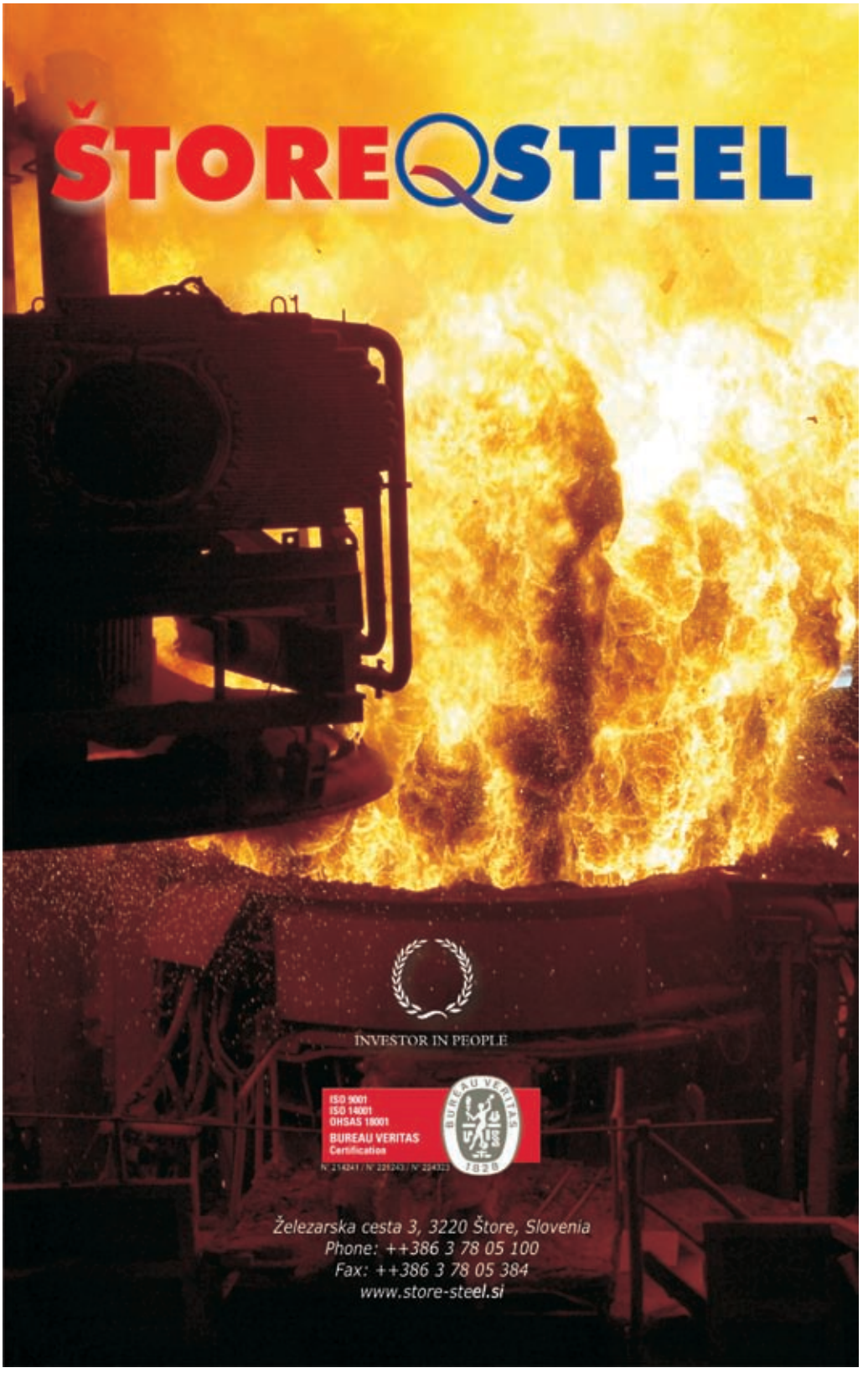
ŠTOREQSTEEL
INVESTOR IN PEOPLE
ISO 9001
ISO 14001
OHSAS 18001
BUREAU VERITAS
Certification
Železarska cesta 3, 3220 Štore, Slovenia
Phone: ++386 3 78 05 100
Fax: ++386 3 78 05 384
www.store-steel.si

prof. dr. Andrej Paulin

Tehniški metalurški slovar *(CD-ROM za WINDOWS)*

slovensko - angleško - nemški

Technical metallurgical dictionary *(CD-ROM for WINDOWS)*

Slovenian - English - German

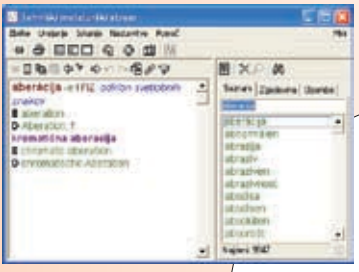

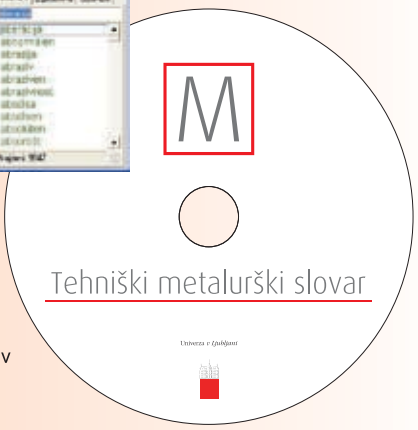

Več kot 10.000 gesel s področij:
- metalurgije,
- tehniških materialov,
- tehnike površin,
- analiznih metod,
- strojništva,
- kemije,
- elektrotehnike,
- ekologije,
- standardizacije,
- predpisov,
- ekonomike in
- uporabe računalništva pri tehnoloških postopkih.

Osnovne značilnosti oz. prednosti elektronske različice slovarja so preprost in izjemno hiter dostop do iskanega gesla, besede ali zveze, tudi pri zahtevnejših pogojih, ter velika prilagodljivost vmesnika uporabnikovim potrebam in željam. Slovar uporablja pregledovalnik ASP32 in je združljiv s številnimi drugimi slovarji v tem sistemu.

Cenik elektronskega slovarja:
Enouporabniška lokalna verzija - 58,00 EUR
5 licenc mrežna verzija - 390,00 EUR
10 licenc mrežna verzija - 535,00 EUR
20 licenc mrežna verzija - 680,00 EUR
30 licenc mrežna verzija - 825,00 EUR
40 licenc mrežna verzija - 970,00 EUR
50 licenc mrežna verzija - 1.115,00 EUR

Leto izdaje: 2007
Issued in 2007

Prices for the electronic dictionary:
Single user local version - 58,00 EUR
5 users network version - 390,00 EUR
10 users network version - 535,00 EUR
20 users network version - 680,00 EUR
30 users network version - 825,00 EUR
40 users network version - 970,00 EUR
50 users network version - 1.115,00 EUR

More than 10 000 technical terms on:
-metallurgy
-technical materials
-surface engineering
-analytical methods
-mechanical engineering
-chemical engineering
-electrical engineering
-environmental engineering
-standardization
-technical regulations
-economics, and
-computer engineering in technological processes

Basic characteristics or advantages, respectively, of electronic version of the dictionary is simple and very fast access to sought term, word or to complex term, also in more demanding conditions, and a great adaptability of the interface to user's needs and wishes. The dictionary uses ASP32 search system that is compatible to numerous other dictionaries in this system.

Za naročila in dodatne informacijenas kontaktirajte preko e-pošte:
For orders and additional information please contact us by e-mail: ***omm@ntf.uni-lj.si***

Slovenčeva 93
SI 1000 Ljubljana

tel.: +386 (1) 560 36 00
fax: +386 (1) 534 16 80
www.irgo.si

IRGO

Inženirska geologija
Hidrogeologija
Geomehanika
Projektiranje
Tehnologije za okolje
Svetovanje in nadzor

Univerza v Ljubljani, Naravoslovnotehniška fakulteta

Oddelek za materiale in metalurgijo

Aškerčeva cesta 12
1000 Ljubljana

Telefon: (01) 470 46 08,
E-pošta: omm@ntf.uni-lj.si

internetni naslov:
http://www.ntf.uni-lj.si/